REDOX ACTIVE LIGANDS TO FACILITATE NOVEL REACTIVITY FROM REDOX RESTRICTED METALS

by

Matt Hewitt

A Dissertation

Submitted to the Faculty of Purdue University

In Partial Fulfillment of the Requirements for the degree of

Doctor of Philosophy

Department of Chemistry

West Lafayette, Indiana

August 2021

THE PURDUE UNIVERSITY GRADUATE SCHOOL

STATEMENT OF COMMITTEE APPROVAL

Dr. Suzanne C. Bart, Chair

Department of Chemistry

Dr. Christopher Uyeda

Department of Chemistry

Dr. Herman O. Sintim

Department of Chemistry

Dr. Arun Ghosh

Department of Chemistry

Approved by:

Dr. Christine Hyrcyna

To Mel.

ACKNOWLEDGMENTS

I would first like to thank Professor Suzanne Bart, who trusted me and gave me the opportunity to finish my degree and advance my career in synthetic chemistry. You have been a great mentor and I greatly appreciate your time and patience as I adapted to organometallic chemistry, as well as your support for my professional development both at Purdue and through the application processes for internships, postdocs, and jobs. You have given me the information and honest assessment needed for me to set myself up for success. You have been a large, positive force for my career and development, and I cannot thank you enough. I would also like to thank the group for your support and help, teaching me the skills and supporting me through the last chapter in the Ph.D. You have all been immensely helpful and I thank you all dearly. I would like to thank my support network, starting with those as Purdue. I would not have gotten through to my Ph.D. without Rob Reason and the ear you gave when I was going through the most tumultuous times here at Purdue. Your support and advice are the foundation for the mental health foundation I implemented to overcome and persevere through the unique circumstances I encountered. Aside from advice, I greatly appreciated our casual chats, especially about family and scouting. Our chats when I first found out about Mel and being a father were immensely valuable to adapting and adjusting. Your desire to generate memories has been a cornerstone to my relationship with Mel, particularly balancing being a graduate student and father, along with the issues associated with the time and distance. To my family and friends, who were the backbone of my support, I cannot thank you enough. There are too many conversations and situations to mention them all, but I want to thank everyone: Charli Bupp and Abriti Sharma, Sarah Desroches, Blane Evans, Aristide Gumyusenge, Steven Kerchmar, Ethan Kiser, Miran Mavlan, Asanka Nanayakkara, Yuicihiro Watanabe, Danny Weskstein. Thank you to all my friends who have been there for me the last few years. Lastly, and most importantly, I want to thank my family, Mike, Mom and Dad. You are why I have been successful. Your support and help have given me the skills and perseverance to get to this point and I would not be here without you.

TABLE OF CONTENTS

LIST OF TABLES 7
LIST OF FIGURES 8
LIST OF ABBREVIATIONS 10
ABSTRACT 11
CHAPTER 1. COPPER IMINOQUINONE COMPLEXES 12
1.1 Introduction 12
1.1.1 Experimental 12
1.1.2 General Considerations 12
1.2 Copper Iminoquinone Chemistry 14
1.2.1 Introduction - Our Work[13] 14
1.2.2 Characterization Analysis 15
1.2.3 Iminoquinone Reactivity 16
1.3 Copper Iminosemiquinone 19
1.3.1 Introduction – Our Previous Work[13] 19
1.3.2 Data Analysis 21
1.4 Copper Amidophenolate 25
1.4.1 Intro Copper Nitrene 25
1.4.2 Intro-our previous work[13] 26
1.4.3 Data Analysis 28
1.4.4 Reactivity of copper bis(amidophenolate) complex 31
1.4.5 Validation of copper NTs species 35
CHAPTER 2. SYNTHESIS TOWARDS AN YTTERBIUM IMIDO 37
2.1 Rare earth elements and their redox active ligands and imido complexes 37
2.2 Experimental 37
2.2.1 General Considerations 37
2.3 Rare Earth Metals and Redox Active Ligand 39
2.3.1 Introduction 39
2.3.2 Introduction: Transition Metal Tetrazenes 40
2.4 Our Previous Work[8] 40

2.5 Data Analysis 43
2.6 Reactivity 47
2.6.1 Introduction to Rare Earth Imido 47
2.6.2 Reactivity of $Yb(ap)_2K$ 47
CHAPTER 3. ORGANIC SYNTHESIS 53
3.1 Potential Antibiotic Synthesis 53
3.2 Experimental 53
3.2.1 Non-Polar Tail 53
3.2.2 Platensimycin head 55
3.2.3 Linking 56
3.2.4 Synthetic Route 57
3.3 Cyclopropene Synthesis 58
3.3.1 Experimental 59
3.3.2 Reactivity 60
REFERENCES 64
VITA 72
PUBLICATIONS 74

LIST OF TABLES

Table 1-1: Cu(II) bis(iminosemiquinone) complexes and selected bond distances. 21
Table 1-2: Electrochemical properties of previously synthesized Copper complexes. 22
Table 1-3: Comparing reduction potentials for related Cu(II) iminosemiquinone complexes. 23
Table 1-4: Selected bond metrics for copper complexes. 29
Table 2-1: Selected bond distances for Yb-^{Dipp}ap and Yb-^{Dipp}isq complexes..... 42
Table 2-2: Magnetic susceptibility and Evan's Method data 46
Table 2-3: Selected bond angles for Yb-^{Dipp}ap and Yb-^{Dipp}isq products. 46
Table 3-1: Hydrolysis methods attempted for desired product deprotection. 58
Table 3-2: Krapcho decarboxylation conditions. 61
Table 3-3: Substituted dimethyl malonate conditions. 62

LIST OF FIGURES

Figure 1-1: Diisopropylphenyl iminoquinone ligand and its reduction series. 12

Figure 1-2: Synthesis of Cu iminoquinone complex. 15

Figure 1-3: Reaction of **1-iq** with various hydride sources, and the effect of adding an electrophile. 16

Figure 1-4: Effect of electrophiles on the reaction of **1-iq** with dimethylphenylsilane. 17

Figure 1-5: Reaction of **1-iq** with pinacol borane. 17

Figure 1-6: Crystal structures of **[1-iq]**$_2$ (left) and pinacol borane-^{Dipp}ap complex (right). 18

Figure 1-7: Reaction of **1-iq** with various reagents. 19

Figure 1-8: Synthesis of Cu iminoquinone. 19

Figure 1-9: Cyclic voltammagram of **2-isq** in THF solution with 0.1M $TBABF_4$. 20

Figure 1-10: Cyclic voltammagram of **2-isq** in DCM solution with 0.1M $TBABF_4$. 24

Figure 1-11: Synthesis of Cu(II) bis(amidophenolate) and its potassium ion sequestered analog. 26

Figure 1-12: UV-Vis absorbance spectra of the copper iminoquinone reduction series in toluene. 27

Figure 1-13: UV-Vis absorbance spectra of copper complexes in toluene (left) and in THF (right). 28

Figure 1-14: Reactions of **3-ap** with nitrene precursors. 32

Figure 1-15: Reaction to generate **5-NTs**. 33

Figure 1-16: IR absorption spectrum of **5-NTs**. 34

Figure 1-17: UV-Vis spectra of **5-NTs** and **3-ap crown** in toluene. 35

Figure 1-18: Reactivity of **3-ap crown** with N_3Ts in DCM. 36

Figure 2-1: Potential electronic configurations for metal-tetrazene complexes. 40

Figure 2-2: Synthesis of Yb tetrazene. 41

Figure 2-3: Synthesis of ^{Dipp}ap ring-inserted product. 43

Figure 2-4: Catechol nitrogen ring insertion. 43

Figure 2-5: UV-Vis of the Yb ligand compounds. 44

Figure 2-6: Synthetic route to Yb imido via DMAP steric hindrance. 50

Figure 2-7: Decomposition pathways of Yb-imido complex. 51

Figure 2-8: Reactivity of Yb-imido complex with azide. 51
Figure 3-1: Desired HMG CoA reductase inhibitor. 53
Figure 3-2: Synthetic strategy for inhibitor tail. 57
Figure 3-3: Synthetic strategy for the inhibitor head. 57
Figure 3-4: Final coupling and deprotection. 58
Figure 3-5: Initial synthetic strategy for ethylene antagonist handle. 61
Figure 3-6: Current synthetic strategy for cyclopropene handle. 62
Figure 3-7: General future plans. 63

LIST OF ABBREVIATIONS

Dipp	2,5 diisopropylphenyl group
^{Dipp}iq	N-(Diisopropylphenyl)-3,5-Di-*tert*-butyl-*o*-iminoquinone
^{Dipp}isq	N-(Diisopropylphenyl)-3,5-Di-*tert*-butyl-*o*-iminosemiquinone
^{Dipp}ap	N-(Diisopropylphenyl)-3,5-Di-*tert*-butyl-*o*-amidophenolate
C_6D_6	Deuterated Benzene
Pyr	Pyridine
THF	Tetrahydrofuran
Et_2O	Diethyl Ether
DCM	Dichloromethane
Tol	Toluene
18c6	18-crown-6
OTf	Triflate anion
Ts	Tosyl group
N_3	Azide group
*p*Tol	Para tolyl group
^{t}Bu	Tert-butyl group
nBu	n-butyl group
iBu	Iso-butyl group
^{i}Pr	Iso-propyl group
UV-Vis	Ultraviolet-visible light
NMR	Nuclear Magnetic Resonance
EPR	Electron paramagnetic Resonance
CV	Cyclic Voltammetry
PhI=NTs	*N*-(*p*-toluenesulfonyl)imino-λ^3-iodane
PFN_3	Pentafluorophenylazide
$PFNH_2$	Pentafluoroaniline
*p*TolN_3	Para-Toluene azide
DMAP	4-Dimethylaminopyridine
TEMPO	(2,2,6,6-Tetramethylpiperidin-1-yl)oxyl

ABSTRACT

The synthesis of metal-redox active ligand complexes is described, along with reactivity studies aimed at facilitating novel C-N bond forming reactions. A copper bis(iminosemiquinone) structure is and its reduction series are characterized, analyzed, and the reactivity of the Cu(II) bis(amidophenolate) analog is investigated with tosyl azide. The identification of the major reaction product and its characterization is detailed, with reaction sensitivities and heavily distorted x-ray diffraction single crystal structure generating a complex data set. The characterization of the isolated product is ongoing, with EPR studies aimed at identifying the radical nature of the complex. Unusual solvent effects and solubility issues have been noted with these initial EPR studies and more data is necessary before complete analysis. An ytterbium bis(amidophenolate) complex was synthesized and its reactivity studied with aryl azides. Initial reactivities generate the first documented lanthanide tetrazenes in-lieu of the targeted ytterbium imido. Reactivities and characterization of these complexes support a stable, heavily ionic tetrazene-metal complex with no observed redox nature, UV light sensitivities, or imido azide-tetrazene equilibrium observed in various tetrazene transition metal complexes. Synthesis of a sterically blocked ytterbium imido was attempted, utilizing DMAP. Initial isolation was achieved with characterization and reactivity studies supporting the imido nature of the complex. The imido could not be confirmed due to decomposition caused by DMAP ligand dissociation. Initial reactions using alternative ligands triphenylphosphine oxide and pyridine N-oxide prove promising to increasing the stability of the presumed ytterbium imido. Organic synthesis was performed generating a potential antibacterial agent. The synthesis of cyclopropenes was initiated as antagonists for ETR proteins in fruits and plants. The intermediates proved highly sensitive to harsh chemical conditions, which was overcome utilizing a tin-mediated Barbier allylation. The cyclopropene alcohol synthon was synthesized, though protecting group optimization is necessary.

CHAPTER 1. COPPER IMINOQUINONE COMPLEXES

1.1 Introduction

Research into biomimicry of metalloenzymes started growing in the mid-1990s, with new organometallic products based on the enzymatic, organic radical promoted, metal driven electron transfer.[1] Galactose oxidase and its tyrosine phenoxyl radical driven oxidation was the standard for studying copper based metalloenzymatic activity. This enzyme, along with others, such as pterin-dependent hydroxylases[2] with their related quinone-like cofactor, were the basis for the iminosemiquinone promoted, copper facilitated redox chemistry. The initial focus was replicating the biomolecular activity of aerobic oxidation,[3-7] but the system's unique three spin structure facilitates typically spin-forbidden reactions expanding its reactivity into the aziridination of styrene and its derivatives.[8] The copper and iminosemiquinone system, with its precedence for copper nitrene reactivity and known unique method of stabilization[8] made it a good choice to expand the chemistry of copper and related redox restricted metals and to isolate rare or novel catalytically important intermediates targeting C-N bond formation. The ligand's crystallographic bond distances also facilitate easy ligand oxidation state determination, aiding in compound characterization.

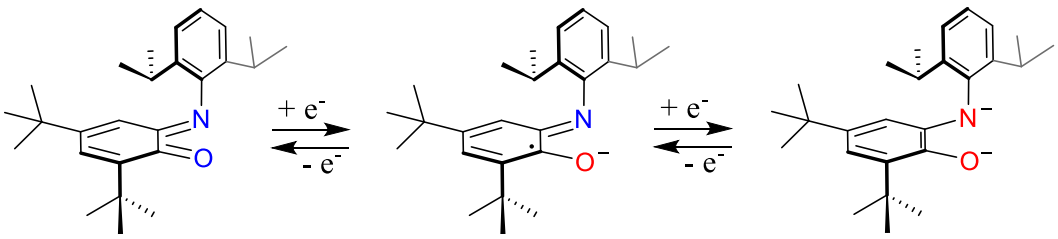

^{Dipp}**iq** ^{Dipp}**isq** ^{Dipp}**ap**

Figure 1-1: Diisopropylphenyl iminoquinone ligand and its reduction series.

1.1.1 Experimental

1.1.2 General Considerations

All reactions are air- and moisture-sensitive and were performed in an MBraun inert atmosphere drybox with an atmosphere of liquid nitrogen off-gas equipped with a -35°C freezer.

Pentane, toluene, diethyl ether, and tetrahydrofuran were purchased anhydrous and without stabilizers, dried in a Seca solvent purification system (SPS) and stored over 4 Å molecular sieves and $Na^0_{(s)}$. All other proteo solvents and compounds were purified, dried, and deoxygenated according to literature procedures, and dried overnight under vacuum on a Schlenk line prior to use in the drybox.[9]

^1H NMR spectra were recorded on either a Varian Inova 300 instrument operating at 300 MHz or a MBraun instrument operating at 400 MHz. The chemical shifts for ^1H spectra are reported relative to $SiMe_4$, with the residual solvent peak chemical shift as secondary standard. The chemical shifts for ^{31}P spectra are reported relative to H_3PO_4. All voltametric data were obtained under inert atmosphere in an MBraun drybox. All samples were collected with 0.1 M $[nBu_4N][PF_6]$ as supporting electrolyte and referenced to Fc/Fc+ as the internal standard under experimental conditions. The solutions were analyzed with a 3 mm glassy carbon working electrode, Ag^0 wire quasi-reference electrode, and Pt wire counter electrode, with the analysis performed by either Ezra Coughlin or Jerod Kieser. UV-Vis spectra were recorded in a sealed 1 cm quartz cuvette at room temperature with a Cary 100 Scan UV-Visible spectrophotometer.

Single-crystals suitable for X-ray diffraction were isolated and coated with (poly)isobutylene oil in a drybox. Their transfer to a goniometer and subsequent data processing and analysis was aided or performed by Ezra Coughlin, or Dr. Matthias Zeller, though not data analysis.

Synthesis of $[iqCu^ICl]_2$ (1-$[iq]_2$)

To a 20 mL scintillation vial was added CuCl (50 mg, 0.505 mmol), a magnetic stirring bar and Et_2O (8 mL). To this slurry was added dropwise a solution of ^{Dipp}iq (192 mg, 0.505 mmol) in Et_2O (10 mL). The combined solution changes from deep brown to a dark teal color over the reaction of up to 7 h. The volatiles were removed by high vacuum and the crude washed with pentane until the wash turns teal (2 x 1.5 mL), yielding **1-[iq]**$_2$ (226 mg, 0.236 mmol, 94% yield, 957.14 g/mol). Single-crystals were grown from a saturated solution in THF at -35°C.

Synthesis of $[(^{Dipp}isq)Cu^{II}(^{Dipp}ap)][K(THF)_6]$ (4-isq ap)

To a 20 mL scintillation vial was added **3-ap** (25 mg, 0.0239 mmol), a magnetic stirring bar, and THF (4 mL). While stirring at room temperature, a deuterated benzene solution of I_2

(0.548 M, 22 μL, 0.0120 mmol) was added dropwise. The solution was stirred at room temperature for 2 h before the volatiles were removed by high vacuum. The crude green solid was dissolved in deuterated benzene and decanted from the solid precipitate yielding the desired compound which was analyzed solely through ^{1}H NMR spectroscopy and X-ray diffraction.

Synthesis of [(^{Dipp}isq)Cu^{II}(^{Dipp}ap)][(K*18c6)$_2$(NTs)] (5-NTs)

To a 20 mL scintillation vial was added **3-ap crown** (71 mg, 0.041 mmol, 1745.33 g/mol as the pyridine solvate), a magnetic stirring bar, and Et_2O (3 mL). This slurry was cooled to -35 °C along with a solution of N_3Ts (8 mg, 0.04 mmol) in Et_2O (1 mL). After cooling, the N_3Ts solution was added to the **3-ap crown** slurry dropwise and the combined slurry solution was stirred at -35°C for 1.5 h. The volatiles were removed by high vacuum and the crude solid washed with pentane (5 x 1.5 mL) and Et_2O (3 x 1.5 mL), filtering through a pipet filter. The remaining solid was dissolved in THF (1.5 mL), filtering off a brown-orange precipitate which was subsequently washed with THF (2 x 1.5 mL). The volatiles of the combined THF solution were removed by high vacuum, yielding **5-NTs** (51 mg, 0.0305 mmol, 75 % yield, 1671.84 g/mol). Single crystals were generated from a saturated solution of C_6D_6 at room temperature.

1.2 Copper Iminoquinone Chemistry

With most of the chemistry of the copper iminosemiquinone system focusing on oxidation chemistry, the oxidized iminoquinone complexes were the initial target for use as precursors in the synthesis of a monomeric copper hydride. A related iminosemiquinone system was used to synthesize a Cu-CF_3 adduct[10-11], but due to the significantly smaller size of a hydride moiety, a more sterically bulky ligand was employed, as steric protection has been shown to be very important in related chemistry.[12]

1.2.1 Introduction - Our Work[13]

Studies were commenced by targeting a copper diisopropylphenyl iminoquinone (^{Dipp}iq) complex featuring two neutral ligands. Treating cuprous triflate was with two equivalents of ^{Dipp}iq caused a darkening of the solution to red. After workup, a reddish-black solid was obtained in good yield (74%). ^{1}H NMR spectroscopic analysis revealed 8 diamagnetic resonances corresponding to

the iminoquinone ligand, consistent with a Cu(I) formulation. ^{19}F NMR confirmed the presence of a triflate ion with a resonance at -78 ppm.

This Cu(I)-^{Dipp}iq product was probed with X-ray crystallography using crystals obtained from a concentrated toluene solution. Analysis shows a five-coordinate copper complex, as shown in Figure 1-2, in a pseudo-trigonal bipyramidal geometry (τ_5=0.61) with two ^{Dipp}iq ligands and one triflate anion completing the coordination sphere (**1-iq**). The interaction of the triflate anion with the copper atom is weak, as demonstrated by the relatively long bond distance of 2.1977(13) Å.

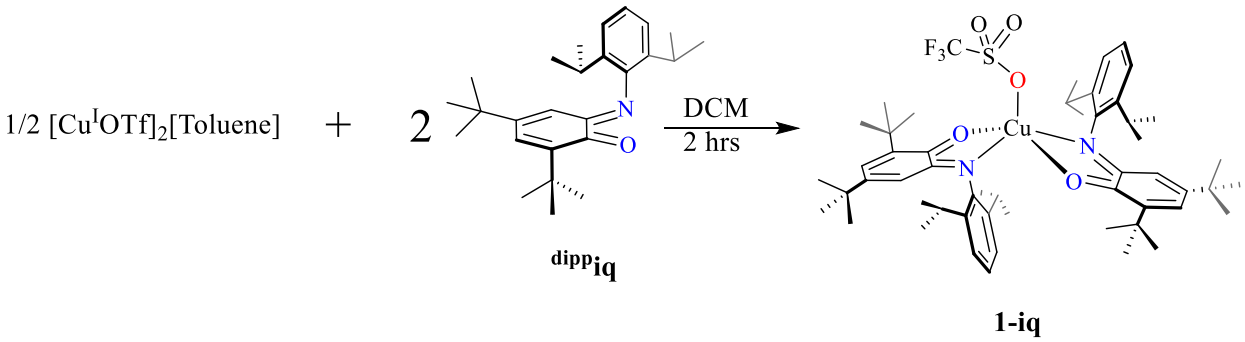

Figure 1-2: Synthesis of Cu iminoquinone complex.

The bond distances of **1-iq** around the copper center are indicative of dative interactions with Cu-O distances of 2.1688 Å and 2.1832 Å and Cu-N distances of 1.9345 Å and 1.9352 Å. This non-ionic interaction is supported by the intraligand bond distances in **1-iq**, making **1-iq** a rare example of a Cu(I) iminoquinone species, as Cu(II) species are more prevalent.[7, 14-16] The chemical reduction of the complex succeeding in forming the reduced, bis(diisopropylphenyl iminosemiquinone) (bis(^{Dipp}isq)) species, isqCu^{II}isq (**2-isq**).

1.2.2 Characterization Analysis

The UV-Vis spectrum of **1-iq**, seen in Figure 1-8, shows two strong absorptions. The absorbance at 452 nm was previously assigned as a π-π* transition of the Cu(I) coordinated iminoquinone intraligand charge transfer (ILCT)[17-18] at 734 nm.[18]

1.2.3 Iminoquinone Reactivity

Reactivity of the Cu(I)-^{Dipp}iq complex was investigated with various hydrides, silanes, and pinacol borane (HBpin) to synthesize a monomeric copper hydride. All reactions of **1-iq** with hydrides or related compounds evolved a gas (Figure 1-3, below), including triphenylsilane ($HSiPh_3$), pinacol borane (HBPin), lithium triethylborohydride ($LiHBEt_3$), diisobutyl aluminum hydride ($HAl(iBu)_2$), and tributyl tin hydride ($H\text{-}Sn(^nBu)_3$). The production of dihydrogen (H_2) and **2-isq** was identified in the reaction mixture through ^{1}H NMR spectroscopy, with degassing through three subsequent freeze pump thaw cycles of the C_6D_6 solution resulting in the disappearance of the H_2 resonance in the subsequent ^{1}H NMR spectra.

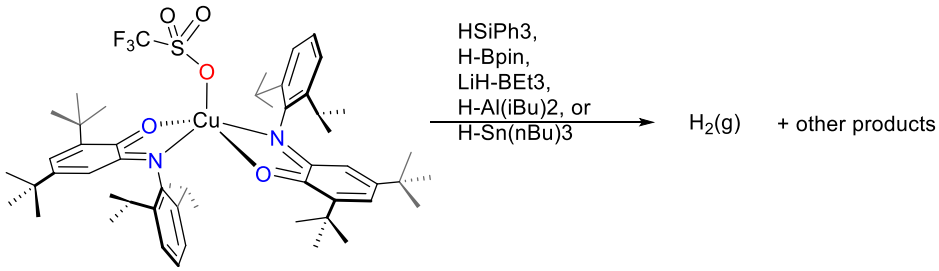

Figure 1-3: Reaction of **1-iq** with various hydride sources, and the effect of adding an electrophile.

To potentially trap a transient copper hydride generated *in-situ*, an electrophilic reagent was introduced to the reaction of **1-iq** with dimethylphenylsilane (Figure 1-3, below). When either phenylacetylene or benzaldehyde was added to the reaction, the carbonyl of the ligand was protonated cleanly as seen by ^{1}H NMR spectra, though at different reaction rates. The reaction with benzaldehyde took 1.5 hours while the reaction with phenylacetylene took up to 24 hours to complete, suggesting either reactant association or electrophilicity could be integral to the reaction rate.

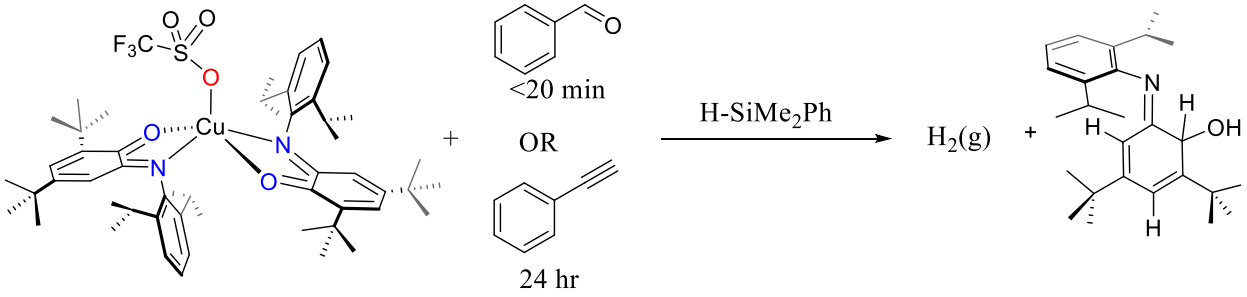

Figure 1-4: Effect of electrophiles on the reaction of **1-iq** with dimethylphenylsilane.

Dimeric ^{Dipp}iq Cu(I) chloride, [iqCu^{I}Cl]$_2$ (**1-[iq]$_2$**), was synthesized in the hope that with fewer iminoquinone ligands the complex would be less oxidizing. When **1-[iq]$_2$** was reacted with HBPin, single-crystals were obtained from the reaction solution and analyzed by x-ray crystallography. The structure revealed a free diisopropylphenyl amidophenolate (^{Dipp}ap) ligand bound to a ring opened pinacol borane, terminated with a second pinacol borate. The O-C bond distance of 1.385 Å, the N-C bond distance of 1.407 Å, confirm the single bond nature of the intraligand bonds, as well as the consistent C-C bond distance of the ring of 1.396 Å, confirming the reduced nature of the ligand. Similar reactivity has been shown in a transitive iridium hydride generated from pinacol borane.[19]

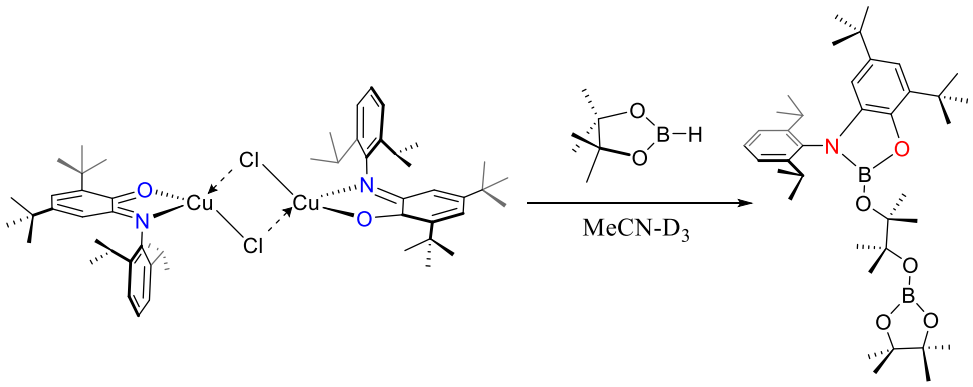

Figure 1-5: Reaction of **1-iq** with pinacol borane.

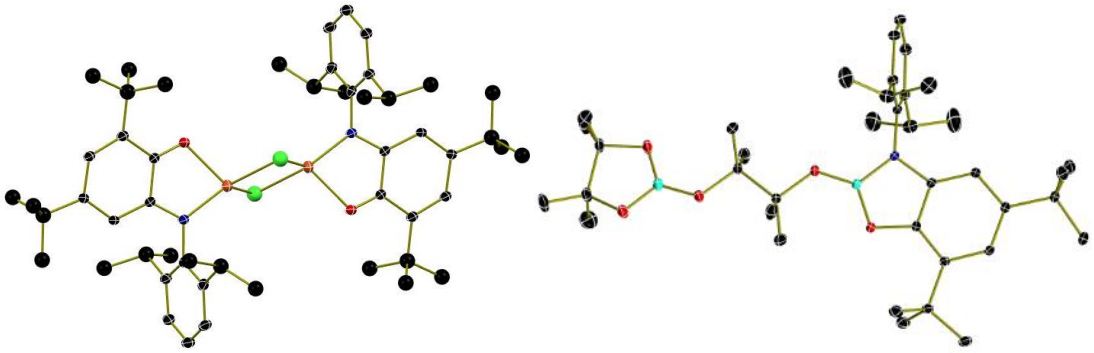

Figure 1-6: Crystal structures of **[1-iq]$_2$** (left) and pinacol borane-^{Dipp}ap complex (right).

Based on iminoquinone-Cu(I) complex reactivity with hydride donors and related compounds generating H_2 and complex decomposition products, the reactivity of the ligand ^{Dipp}iq with a pre-formed copper hydride was investigated. ^{Dipp}iq was titrated with Stryker's reagent, a stable hexameric copper hydride ($[(Ph_3P)CuH]_6$); both **2-isq** and H_2 were generated, as well as a potential triphenylphosphine coordination to **2-isq**, as well as potential reactivity with the ligand, as seen by ^{31}P NMR spectroscopy. With the instability of a copper hydride in the presence of ^{Dipp}iq established, alternative reactions with either **1-iq** or **1-[iq]$_2$** dimer were performed.

Reactions of **1-iq** or **1-[iq]$_2$** with strongly coordinating reagents generate **2-isq** (Figure 1-7, below), as seen in Figure 1-7. Dissolution of **1-iq** in pyridine or reacting with 1 equivalent of either potassium *tert*-butoxide or triphenylphosphine resulted in the synthesis of **2-isq.** When **1-iq** was reacted with triphenylphosphine, in addition to the synthesis of **2-isq**, side products were also observed. ^{1}H NMR spectroscopy and TLC-MS support the synthesis of a potential triphenylphosphine ^{Dipp}iq adduct and ^{31}P NMR spectroscopy indicates a potential equilibrium between both free and copper bound triphenylphosphine as seen by the broadening of the initial PPh_3 resonance. **2-isq** was also generated in the UV irradiated reaction of *p*-tolyl azide with **1-iq**. The coordination initiated intramolecular redox chemistry establishes a potential mechanism of reaction for reactivity. With no clear route to an isolable copper hydride, the focus was changed to the reactivity of the fully reduced, bis(^{Dipp}ap) copper complex, $[apCu^{II}ap][K(THF)]_2$ (**3-ap**) with azides, to generate an isolable copper nitrene.

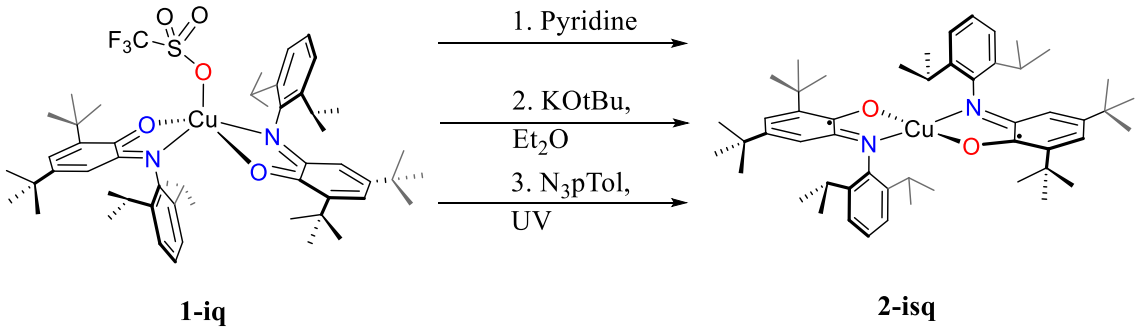

Figure 1-7: Reaction of **1-iq** with various reagents.

1.3 Copper Iminosemiquinone

1.3.1 Introduction – Our Previous Work[13]

Chemical reduction of the **1-iq** was attempted to form bis(^{Dipp}isq)Cu(II). Unfortunately, **1-iq** was not a suitable precursor for this chemistry; instead, a copper bis(^{Dipp}isq) complex was generated by reduction of a slurry containing copper iodide, or equivalent Cu(I) halide source, with two equivalents of ^{Dipp}iq, followed by the slow addition of one equivalent of KC_8. Upon addition of KC_8, the solution changed from brown/red to green, the color associated with ILCT of the one electron reduced ligand.[20] The ^{1}H NMR spectrum features broad, paramagnetic resonances ranging from -30 to +30 ppm.

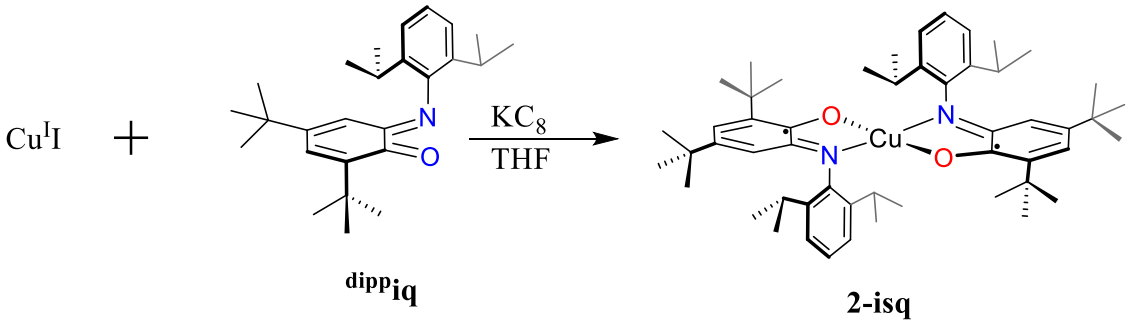

Figure 1-8: Synthesis of Cu iminoquinone.

Single crystals of **2-isq** grown from a concentrated toluene solution were analyzed using single crystal X-ray diffraction. The complex formed is a Cu(II) square planar coordination complex (τ_4'=0.04) with two iminosemiquinone ligands bound to the copper center with a *trans* arrangement of nitrogen atoms. This isomer is likely preferred due to the sterically favorable

positions of the large diisopropylphenyl substituents. The shorter Cu-O bond distances compared to **1-iq** signify anionic linkages at 1.909 Å and 1.905 Å, indicative of ligand reduction from inoquinone to iminosemiquinone. This ligand assignment is confirmed by the Cu-N bond distances, whose dative like those of **1-iq** with C-N distances of 1.938 Å and 1.933 Å.

Electrochemistry was employed to analyze the reduction potential of **2-isq**, with cyclic voltammograms of **2-isq** in THF acquired at ambient temperature. Analysis of cathodic scans revealed one irreversible oxidation at -0.51 V with rapid decay of signal after multiple scans. This is indicative of decomposition, likely stemming from iminosemiquinone ligand dissociation when bound only through dative interactions to the hard, Cu(II) center. Anodic scans showed two, quasi-reversible sequential reductions at -1.59 and -2.40 V (Figure 1-9, below), corresponding to the sequential reduction of the system by one electron. Only one previous example[18] has shown evidence for metal centered reduction of a bis(iminosemiquinone) species, based on the appearance of two new oxidations in subsequent scans. Absent these newly generated peaks, these two quasi-reversible reductions are assigned as ligand reductions, generating a Cu(II) bis(^{Dipp}ap) dianion complex.

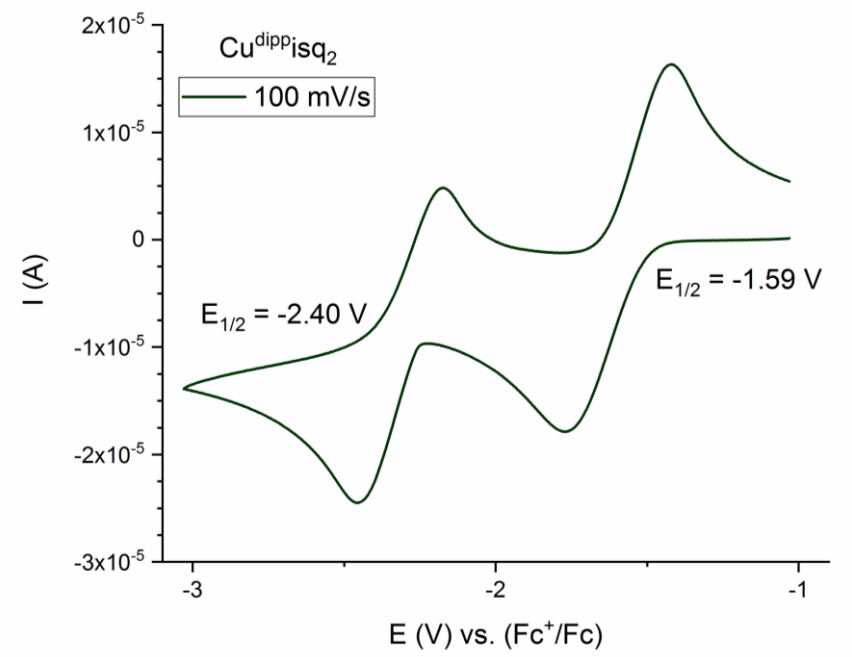

Figure 1-9: Cyclic voltammagram of **2-isq** in THF solution with 0.1M $TBABF_4$.

1.3.2 Data Analysis

A comparison of ^{Dipp}isq ligand and metal centered bond distances with previously synthesized Cu(II) bis(iminosemiquinone) complexes can be found in Table 1-1. Intraligand bond distances for **2-isq** compare well to literature precedence, with C-O and C-N distances generally falling within the error of the measurement and steric demand seemingly the source of any minor deviation. The Cu-O and Cu-N bond distances for **2-isq** also agree with previous Cu(II) iminosemiquinone complexes suggesting moderate steric differences have little impact on the iminosemiquinone complexation to copper.

Table 1-1: Cu(II) bis(iminosemiquinone) complexes and selected bond distances.

Complex	**2-isq**	$Cu^{II}(^{Ph}isq^{1-})_2$[21]	$Cu^{II}(^{biPh}isq^{1-})_2$[17]
Cu-O1	1.905(3), 1.909(3)	1.912	1.9083(11), 1.9046(11)
Cu-N1	1.938(3), 1.933(3)	1.936(2)	1.9267(13), 1.9307(13)
O1-C1	1.292(5), 1.294(5)	1.290(4)	1.2961(19), 1.2953(19)
N1-C6	1.345(5), 1.334(5)	1.335(4)	1.334(2), 1.336(2)

Table 1-2 compares the reduction potentials of literature Cu(II) bis(iminosemiquinone) complexes. Most complexes have similar reduction potentials in DCM solutions, with the first reduction potential ~ -1 V and a second reduction potential at ~ -1.4 V. When the two bidentate iminosemiquinone ligands are linked via the *N*,*N*'-(phenyl) moiety into a single, tetradentate ligand, the first reduction potential is shifted by ~ +400 mV, likely due to the increased delocalization of the ligand stabilizing the monoradical, iminosemiquinone-amidophenolate complex. The more negative reduction potentials for the *N*-substituted phenyl iminosemiquinone complexes can be attributed to the distortion of the copper-ligand plane either through a coordinating substituent or steric bulk.[17, 22]

Table 1-2: Electrochemical properties of previously synthesized Copper complexes.

Compound	$Cu^{I}(^{Ph}iq)CF_3$[11]	$Cu(^{Ph}biisq)_2$[6]	$Cu(^{Ph}isq)_2$[21]	$Cu(^{biPh}isq)_2$[17]	$Cu(^{SPh}isq)_2$[22]
E_{red2} (V)	-1.35 vs Fc	-1.42	-1.32	-1.480	-1.49
E_{red1} (V)	-1.04 vs Fc	-0.66	-1.02	-1.117	-1.07
Solvent	DCM	DCM	DCM	DCM	DCM
Electrolyte	0.1M $TBABF_4$	0.1 M $TBAPF_6$	0.10 M $TBAPF_6$	0.10 M $TBAClO_4$	0.1 M $TBAPF_6$
Reference	SCE	Fc	Fc	Fc	Fc

Red1 product: $[isqCu^{II}ap]^-$; Red2 product: $[apCu^{II}ap]^{2-}$

Electrochemical data was acquired for **2-isq** in DCM to compare to both literature and the previously acquired data obtained in THF solution. These comparisons are presented in Table 1-3. While both of the reduction potentials of previously synthesized Cu(II) bis(iminosemiquinone) complexes are within ~100 mV of each other, the **2-isq** reduction potentials in DCM show a significant perturbation of this trend, being more negative by ~ 200 mV and ~ 400 mV for the first and second reductions, respectively. While the lower reduction potentials seen in literature are from a bulkier aromatic system and from coordinating phenyl substitution, both of which distort the planarity of the complex. The strong perturbation of **2-isq** is likely due to the increased steric bulk of the *N*-(diisopropylphenyl) substitution in **2-isq**, which is unable to be distributed away from the copper coordination center like the biphenyl group.[17] This *ortho*-substituted steric bulk would reduce orbital overlap between the ligands and the copper center, particularly at higher negative charge that would create a closer ionic bond with the positive Cu(II) center.

The cyclic voltammagram of **2-isq** in a THF solution shows significantly more negative reduction potentials compared to when dissolved in a DCM solution, by ~300 mV and ~600 mV for the first and second reductions, respectively. This dramatic solvent-based change in reduction potential is hypothesized to be due to coordinating THF. This is supported by the quasi-reversible nature of the reduction potentials in THF which are shown to be reversible when in DCM, suggesting a solvent dependent, ligand rearrangement. The coordinating solvent's ability to shift the reduction potential for **2-isq** more negative can be explained by increased π backbonding to

the ligand aromatic system. This would destabilize the π system, increasing the energy necessary to reduce the ligands. Additionally, literature shows that changes in geometry are known to disrupt the orthogonality of the ligand-metal magnetic orbitals, so the addition of the coordinating THF could disrupt ligand-copper orbital overlap, leading to more pronounced degradation of intraligand orbital overlap, giving rise to stronger metal-ligand coupling and reducing the delocalization and stabilization of the intraligand system within the complex, increasing the energy of the system and therefore making the reduction potential more negative.[23]

Table 1-3: Comparing reduction potentials for related Cu(II) iminosemiquinone complexes.

Compound	**2-isq**	**2-isq**	$Cu(^{Ph}biisq)_2$[6]	$Cu(^{Ph}isq)_2$[21]
Ered2 (V)	-2.40	-1.82	-1.42	-1.32
Ered1 (V)	-1.59	-1.25	-0.66	-1.02
Solvent	THF	DCM	DCM	DCM
Electrolyte	0.1 M $TBAPF_6$	0.1 M $TBAPF_6$	0.1 M $TBAPF_6$	0.1 M $TBAPF_6$
Reference	Fc	Fc	Fc	Fc

This change in geometry and its effects on the iminosemiquinone-copper complexes has been studied extensively.[22, 24] When a coordinating functional group is added to the *N*-aryl group, such as a thioether, the subsequent S-Cu coordination perturbs the planarity of the complex. The shift in geometry alters the spin coupling, changing from ligand to ligand antiferromagnetic coupling to metal to ligand antiferromagnetic coupling.[22] This perturbation also increases the complex's second reduction potential by ~ 100 mV. This is comparable to that of a *N*-biphenyl substituted iminosemiquinone-copper complex which perturbs the planarity through steric bulk and bi-phenyl π-π stacking.[24] This complex also has a distorted square planar geometry (τ_4= 0.06) with a 9 degree dihedral angle between the planes of the two ligands. This is achieved without coordination, suggesting that these increases in reduction potential are due in greater part to the distortion of the geometry achieved through the coordination rather than the more electron rich nature the coordination imparts to the central copper. This loss of planarity breaks the magnetic coupling between the ligands and producing a more spin-isolated ligand based radical over the

metal based radical in a square planar geometry. The decreased magnetic coupling between ligands could be due to a reduction in orbital overlap, which would destabilize the ligand π system, making the reduction potential more negative. This change in spin and geometry could be the cause for the increased reduction potential.

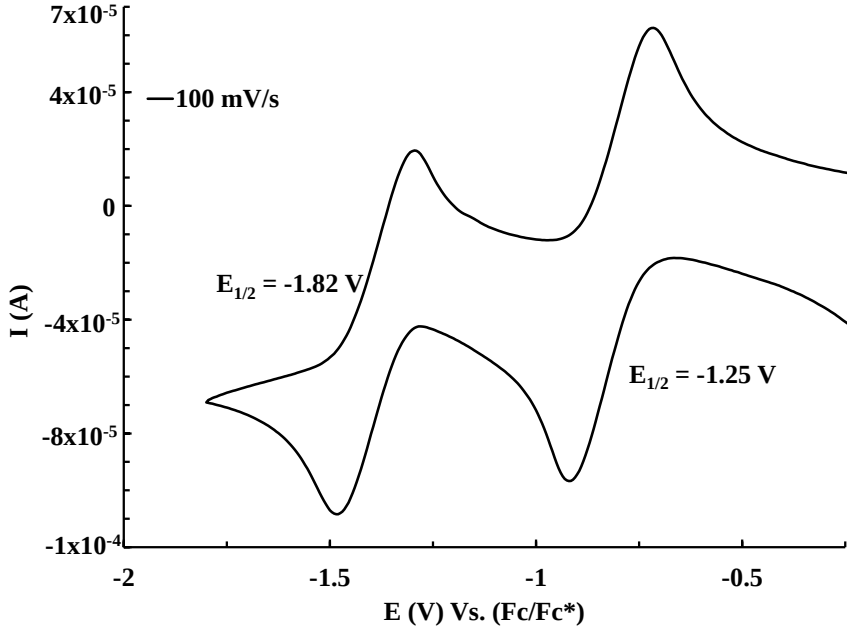

Figure 1-10: Cyclic voltammagram of **2-isq** in DCM solution with 0.1M $TBABF_4$.

Further support for transitive solvent ligation to $Cu^{II}(isq)_2$ complexes is shown in EPR spectra of $Cu(^{Ph}isq)_2$, which were taken in both THF and DCM at room temperature. In THF, ligand hyperfine splitting was simulated to be from 2 ^{14}N (I=1), predominately along the $g_\perp$ axes. This hyperfine splitting is absent in DCM, with copper hyperfine splitting dominating the EPR spectra.[21] This shows a coordination dependent change in frontier molecular orbitals of the complex which alters the electron coupling of the three spin system. Changing the solvent from non-coordinating to coordinating alters the EPR signal, presumably via changes in geometry affecting the spin-orbital coupling disrupting the orthogonality of the ligand-metal magnetic orbitals.[23], changing the electrons orbital occupation. Geometry changes altering spin coupling of copper complexes have been previously noted in literature,[17, 25-27] with planar complexes producing increased ligand to ligand coupling, leaving a Cu centered radical.[28] This delocalization

of the radicals across the aromatic system has been shown to lower the energy of otherwise spin-forbidden reactions.[8, 25]

The absorption spectroscopy of green **2-isq**, displays three absorbances in the visible region at 796 nm, 452 nm, and 415 nm. The absorption at 796 nm shows the highest molar absorptivity of the three, and has been previously assigned as a combination of metal to ligand (MLCT) and ligand to ligand (LLCT) charge transfer[17] and has been shown to be indicative of the presence of iminosemiquinone ligand. The absorptions between 400-500 nm were assigned as ligand to metal charge transfers (MLCT).

The ligand charge transfer absorbances of iminosemiquinone complexes have also been supported by the photoreactivity of related complexes. UV light has been shown to induce the reduction of DCM to 1,2 dichloroethane with by a Zn tetradentate diiminosemiquinone species, Zn(L3) cleanly generating the dicationic Zn species. $Zn(L3)^0$ has charge transfer bands at 506 nm and 405 nm and the one electron oxidized species, $Zn(L4)^+$, has absorbances at 411 nm and 385 nm. The copper equivalent complex, $Cu(L3)^0$ is also photoreactive, but produces both the one electron oxidized and two electron oxidized species as products.[6]

1.4 Copper Amidophenolate

1.4.1 Intro Copper Nitrene

Copper nitrenes have been utilized as proposed intermediates for the incorporation of nitrogen into a structure through the creation of C-N bonds via alkene aziridination and C-H amination. The reactivity of the proposed Cu-N intermediate is based in large part to the electronic structure of the Cu-N multiple bond, and the isolation of this species is important to understanding nitrene transfer chemistry for reaction specificity via targeted catalyst design.[29] Early first row transition metal-N multiple bonds are highly polarized, with electrophilic metals and nucleophilic dianionic imido ligands prone to 1,2 additions.[30] In contrast, softer late first row transition metals generate poor orbital overlap in combination with their high d-electron counts. This can generate an inverted ligand field, with the frontier molecular orbitals dominated the N ligand and a more reduced metal.[31-32] Utilizing a redox active ligand was hypothesized to help stabilize a potential copper nitrene intermediate through its low lying molecular orbitals, like the iminosemiquinone system, which has been shown to be a good catalyst for nitrene transfer.[8] The low lying redox

active ligand orbitals could facilitate an increased stability of a copper nitrene with more control over the desired reactivity through simple ligand tuning; this would facilitate an easy and expedited study of the effects of electronics through both ligand substitution and ligand redox chemistry. The bond distances within the iminosemiquinone ligand could also allow for easy ligand and metal oxidation state analysis.[2, 10, 16-18, 33-36] The redox non-innocent nature of both the nitrogen ligand and copper complex scaffold have been important in the most recent works of copper/nitrogen multiple bonds, whether a copper nitrene, imide, or iminyl.[29, 37]

1.4.2 Intro-our previous work[13]

With electrochemical evidence for the reducibility of **2-isq**, reduction of the green **2-isq** was facilitated using KC_8. Addition of two equivalents of KC_8 generated a purple solid in good yield after purification.

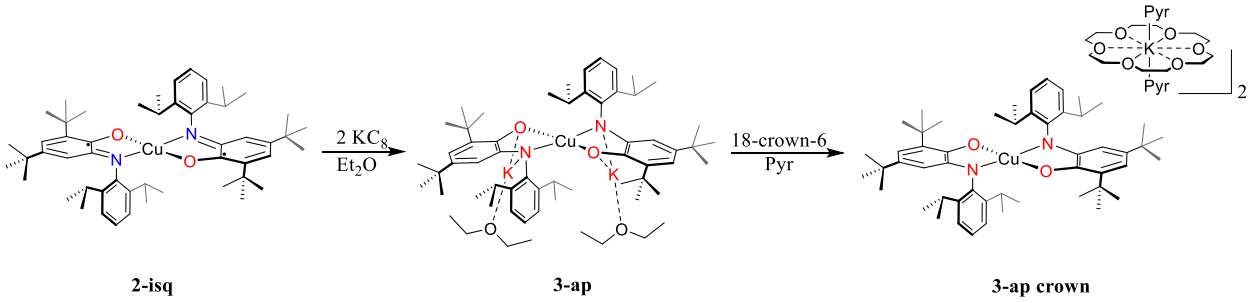

Figure 1-11: Synthesis of Cu(II) bis(amidophenolate) and its potassium ion sequestered analog.

This bis(^{Dipp}ap) Cu(II) complex (**3-ap**) crystallized readily from diethyl ether, with analysis by X-ray crystallography showing the copper center on a 2-fold rotation center, creating crystallographically symmetric ligands. The potassium counter-ions coordinate to the amidophenolate ligands, staying inner sphere to and distorting the geometry of the complex into a pseudo-tetrahedral geometry (τ_4=0.67, τ_4'=0.65).

In solution, **3-ap** displays a UV-Vis spectrum with three absorbances at 891, 569, and a shoulder at ~400 nm. The comparison of the UV spectra of **1-iq**, **2-isq**, and **3-ap** can be found in Figure 1-12, below.

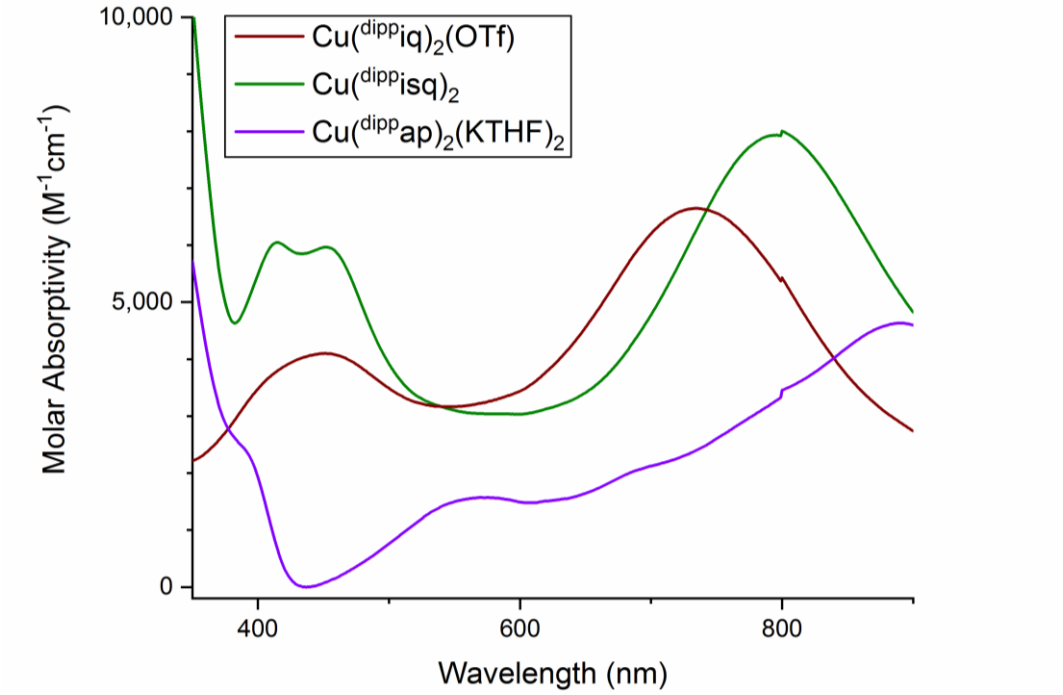

Figure 1-12: UV-Vis absorbance spectra of the copper iminoquinone reduction series in toluene.

Purple **3-ap** is insoluble in most non-polar solvents, but faintly red-colored in polar ones. Notably, as seen in Figure 1-13 below, the spectrum of **3-ap** in toluene is very different from that recorded in THF, featuring more absorptions that are higher in intensity This solvatochromism suggests that the potassium ions in **3-ap** are encapsulated with THF molecules. A bis(^{Dipp}ap) Cu(II) complex with outer-sphere potassium ions was targeted by encapsulating them with 18-crown-6, resulting in the tan solid **3-ap-crown**. The UV-Vis absorbance spectra of **3-ap** and **3-ap crown** in THF show nearly identical features with only one strong absorption at ~375 nm. In contrast, the spectrum of **2-isq** collected in THF retains its strong absorption features, indicating no interaction with THF solvent, supporting the potassium coordination hypothesis for the solvatochromism.

Sequestrating the potassium ions into the outer-sphere allows for a meaningful comparison of bond distances with the rest of the reduction series, **1-iq** and **2-isq**. **3-ap crown** crystallizes from a concentrated THF with the two potassium ions sequestered by crown ether and coordinating two tetrahydrofuran molecules each. The copper center is ligated by two amidophenolate ligands in a square planar geometry (τ_4'=0.00), similar to **2-isq**. The copper atom is located on an inversion center, producing crystallographically symmetric ligands, with nitrogen atoms *trans* to each other. The Cu-O and Cu-N bond distances of 1.940 Å and 1.923 Å, respectfully, are indicative of ionic bonds, and are shorter than **2-isq**. Furthermore, reduction of the ligand in **3-ap crown** lengthens

the C-O bonds to 1.328 Å and C-N bonds to 1.369(5) Å, consistent with single bond character as expected for the amidophenolate structures.

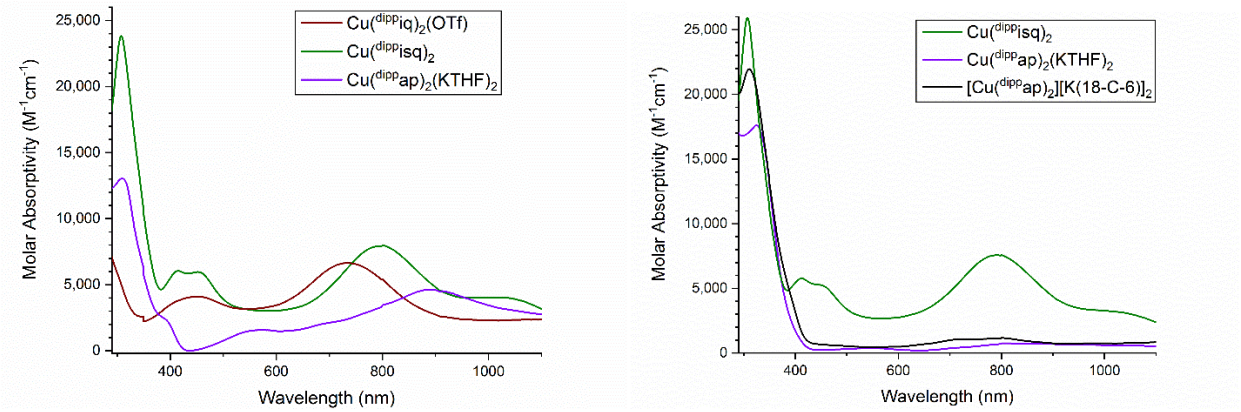

Figure 1-13: UV-Vis absorbance spectra of copper complexes in toluene (left) and in THF (right).

1.4.3 Data Analysis

This is the first known Cu(II) bis(amidophenolate) molecule to be isolated and fully characterized.[38] While other complexes have been characterized with amidophenolate ligands on Cu(II), either structural data was not obtained,[22] or the ligand radical is averaged over a singular multidentate ligand, changing ligand bond metrics of similar oxidation states.[6-7]

The one electron reduced, mixed iminosemiquinone-amidophenolate copper complex was synthesized to facilitate bond distance comparisons. Its synthesis can be achieved in THF through either reduction of **2-isq** with KC_8 or oxidation of **3-ap crown**. Oxidation of **3-ap** with I_2 proved amenable to the synthesis of the mixed ligand, Cu(II) ^{Dipp}isq/^{Dipp}ap complex, [isqCu^{II}ap][K] (**4-isq ap**) but proved troublesome to purify. The purity of **4-isq ap** is ensured before encapsulating with 18-crown-6, producing **4-isq ap crown**, due to the difficulties in separating it from **3-ap crown** due to their poor solubilities in most medium to low polarity solvents like diethyl ether and THF. Selected ligand bond distances for the reduced copper complexes found in Table 1-4.

Table 1-4: Selected bond metrics for copper complexes.

Complex	**2-isq** (Avg)	**5-NTs**	Avg(isq&ap)	**4-isq ap crown**	**3-ap crown**
Cu-O1	1.907	1.929	1.9235	1.939	1.940(3)
Cu-N1	1.9355	1.901	1.9293	1.910	1.923(3)
O1-C1	1.293	1.315(4)	1.311	1.323(3)	1.328(4)
N1-C6	1.3395	1.358(4)	1.3543	1.356(3)	1.369(5)

4-isq ap crown maintains the square planar geometry of both the **2-isq** and **3-ap crown** molecules. The Cu-O, O-C, and N-C bond distances of mixed ligand ^{Dipp}isq/^{Dipp}ap complexes, irrespective of the counter cation, fall between **2-isq** and **3-ap crown**, verifying the oxidation state of the ligands as between that of the bis(^{Dipp}isq) and bis(^{Dipp}ap) – indicating the ^{Dipp}isq and ^{Dipp}ap ligands are delocalized across both ligands.

When fully reduced to the bis(^{Dipp}ap), the copper is surrounded by four anions, including both nitrogens. This change explains the elongation of the Cu-N bond distance seen only in this fully reduced, **3-ap crown** compared to the mixed ligand complexes. This strong anionic character around a small dicationic copper facilitates the charge repulsion of the two nitrogen atoms. The less reduced ligand system has nitrogen atoms closer to the metal center, indicating that the sterics of the ligand are not a major factor in the N-C bond elongation observed in **3-ap crown**.

When **3-ap crown** is reacted with a tosyl nitrene precursor, a one electron oxidized, mixed ligand, ^{Dipp}isq/^{Dipp}ap Cu(II) complex is formed with a complex counter ion [isqCu^{II}ap][(K*18c6)$_2$(NTs)] (**5-NTs**). This reactivity is further elaborated upon in Section 1.4.4. The square planer geometry of the copper ion verifies the metal oxidation state as 2+, with the ligand bond metrics falling between that of **2-isq** and **3-ap crown**.

Interestingly, the counter ion to the Cu(II) mixed ligand, ^{Dipp}isq/^{Dipp}ap complex seems to influence bond distances both around the copper center and of the ligands. When paired with the outer sphere potassium ion, the mixed ligand bond distances in **4-isq ap** are closer to those of **3-ap crown**. In **4-isq ap crown**, the lone ligand radical is stabilized as if paired, as the distances around the oxygen are completely monoanionic in nature. Its Cu-O bond distance is within error

to that of **3-ap crown**, with the O-C bond distances overlapping within each other's error. The concomitant change of Cu-O and O-C bond distances suggests an effect related to the ligand oxidation state, and not of due to interactions with the copper.

This is not the case in **5-NTs**, when the cation consists of the bis potassium *N*-tosyl moiety. The copper complex still retains bond distances between that of **2-isq** and **3-ap crown**, giving the copper complex ion an overall -1 charge. The Cu-O, O-C, and N-C bond distances do not have the amidophenolate character seen with potassium counter cation. Instead, these bond distances are almost exactly the average between **2-isq** and **3-ap crown**, as would be expected of a fully delocalized ^{Dipp}isq/^{Dipp}ap ligand system.

Unfortunately, the extreme symmetry and disorder of **5-NTs** required manually solving for the bond distances around the bis(potassium crown), N-tosyl cation, making the bonds centered around the nitrogen in that complex ion artificial. By charge balance, the overall positive charge, with two potassium ions bound to the nitrogen suggests the nitrogen an overall 1^- charge.

The tan color associated with **3-ap** is intriguing. The nearly featureless UV-Vis absorption spectrum of **3-ap crown** makes chemical sense, as a d^9 system with two closed shell ligands there are none of the anticipated color causing charge transfer transitions that predominated the iminosemiquinone ligands. The purple coloration of **3-ap** is hypothesized to be based on the inner-sphere coordinating potassium ions, which is supported by the solvatochromism of **3-ap** seen in coordinating solvents that generates a featureless absorption spectrum like **3-ap crown**. Non-polar solvents such as pentane, toluene, and benzene gave purple solutions of **3-ap**, similar to the color of the powder, but solutions in THF are bleached of this color. The redox activation and charge transfer of copper(II) complexes mediated by ligating ions has been shown in literature,[17-18, 39] with the inner-sphere coordinating potassium ions generating the color causing charge transfer absorption observed in the UV-Vis spectra. With the ion facilitated charge transfer as the hypothesis for the color, analysis of **3-ap crown** was also performed.

The only other previously studied Cu(II) bis amidophenolate species was synthesized and characterized via spectroelectrochemistry. This *in situ* generated species, whose cations would have been derived from the noncoordinating $[Bu_4N][PF_6]$ electrolyte, was also found to have no intense absorptions above 450 nm.[22] When inner-sphere, the potassium ions facilitate charge transfer bands seen in the UV and visible spectrum, giving rise to its purple coloration. When these ions are forced outer sphere, either through solvent or crown ether chelation, the square planar

geometry returns to the copper complex and the charge transfer bands are dramatically reduced in intensity, bleaching the color of the compounds.

The geometry of the Cu complexes facilitates the observed characterization and reactivity of the reduction series. Highly planar complexes in the series have ligand to ligand electron spin coupling and charge transfer transitions. Distortion of this planarity whether by ancillary coordination of ligand, solvent, or presumably reagent, reduces orbital overlap and disrupting the interligand charge transfer. This, along with increased π backbonding into the π* ligand orbitals from a more electron rich metal, facilitates more negative reduction potential. With the closed shell ^{Dipp}ap ligands, charge transfer of the metal-based radical is facilitated to the ligands by the inner-sphere ion and the non-planar geometry they induce. When these ions are forced outer-sphere, either by solvent or other chelating agent, the planarity, and therefore interligand orbital overlap, is reestablished, isolating the radical to the metal surrounded by heavily reduced, highly charged ligands. [6, 8, 17, 21-22, 39]

The electronic structure of the copper complexes is currently being probed using EPR spectroscopy, given these species both contain an unpaired *d*-electron from the Cu^{2+}, d^9 species.

1.4.4 Reactivity of copper bis(amidophenolate) complex

3-ap proved unreactive with one equivalent of 1-azido-4-methylbenzene in benzene and toluene, even with UV irradiation. This can most likely be explained by the structure of **3-ap**, where the inner-sphere, bound potassium ions both sterically block reactivity as well as distort the interligand coupling, potentially reducing reactivity. A smaller, more reactive compound was reacted with **3-ap** and 18-crown-6 in C_6D_6, where one equivalent of methyl iodide (MeI) generated **4-isq ap crown** and ethane gas by ^{1}H NMR spectroscopy; subsequent degassing by three freeze-pump-thaw cycles removed the ethane peak. Two equivalents of MeI resulted in the generation of ethane with residual MeI remaining in solution.

Switching the azide reaction into a polar solvent, such as diether ether, resulted in the one electron oxidation of **3-ap** to **4-isq ap crown** with bond metrics between those of **2-isq** and **3-ap**. Utilizing two equivalents of azide did not result in the clean generation of **2-isq**, as expected, though switching to two equivalents of an alternative, hypervalent iodine nitrene precursor, *N*-(ptoluenesulfonyl)imino-λ^3-iodane (PhI=NTs), did cleanly yield **2-isq**. This was confirmed by both NMR and x-ray crystallography. With no isolated copper nitrene or nitrenoid species, **3-ap**

crown was used to help isolate the potassium ions during reaction, moving them outer sphere for more consistent reactivity due to the solvatochromism seen by UV-Vis spectroscopy. The necessity of encapsulating the potassium ions for improved reactivity was emphasized by the non-innocent reaction of adding 18-crown-6 to **3-ap**; encapsulating the potassium ions in weakly coordinating solvent produces free potassium iminosemiquinone ligand salt (K-isq) and is best achieved in either THF or pyridine.

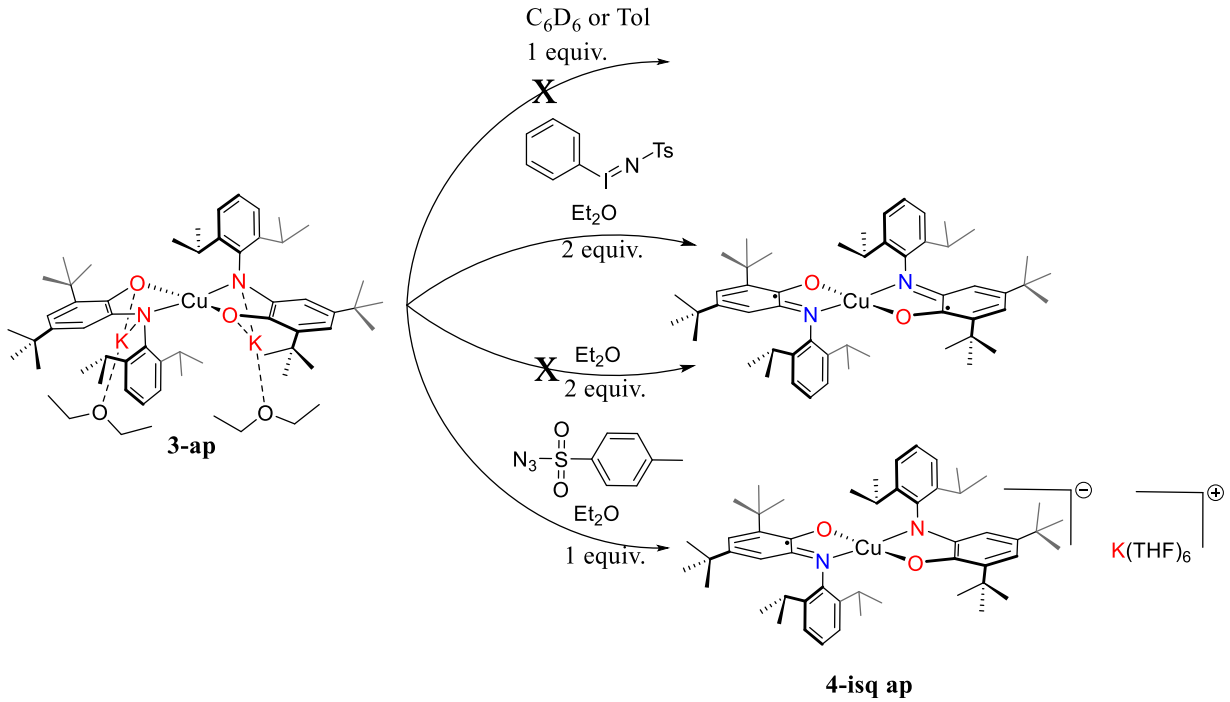

Figure 1-14: Reactions of **3-ap** with nitrene precursors.

Further attempts to isolate a copper nitrene proceeded, with 1 equivalent of PhI=NTs was reacted with **3-ap crown,** producing a product that was analyzed through X-ray diffraction. Single crystals were generated by layering pentane onto a saturated solution of benzene at room temperature, which were analyzed by X-ray diffraction. The structure was solved as **5-NTs**, though they were heavily disordered. Single crystals isolated from both pure benzene at room temperature and a vapor diffusion of pentane into a saturated solution of diethyl ether at -35 °C were similarly disordered. As described previously in Section 1.4.3, **5-NTs** consists of a monoanionic copper complex, whose oxidation state is confirmed by ligand bond distances, and a cation complex consisting of both encapsulated potassium ions from **3-ap crown** bound to a *N*-tosyl moiety. A

matching ^{1}H NMR spectrum was generated using the alternative nitrene precursor, tosyl azide, (N_3Ts).

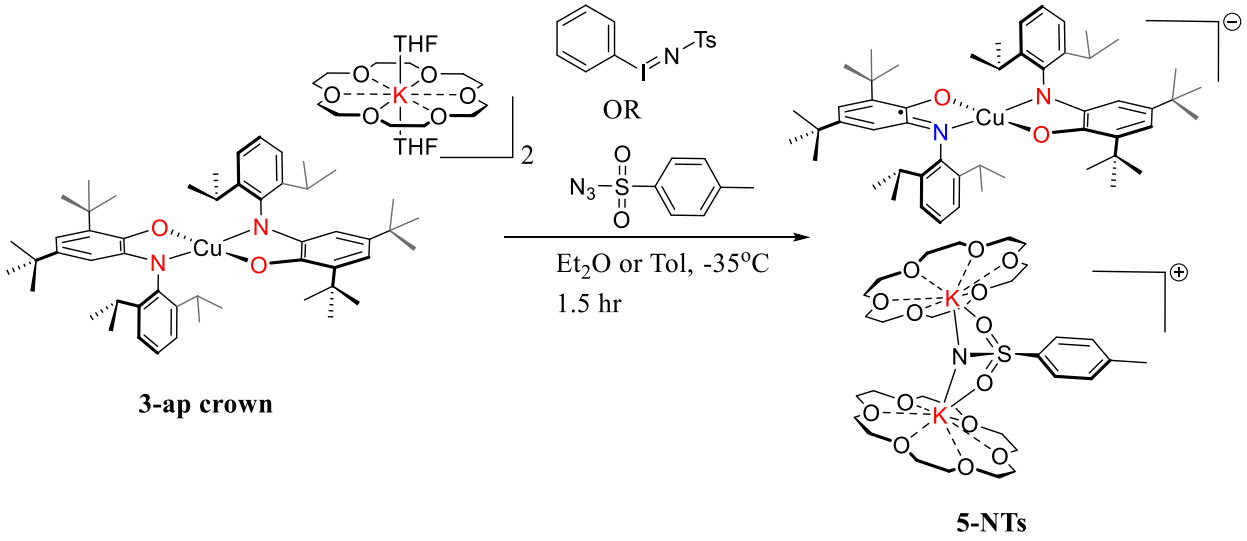

Figure 1-15: Reaction to generate **5-NTs**.

With initial yields close to 25%, X-ray diffraction was also performed on the impurities of the reaction between **3-ap crown** and PhI=NTs, yielding two products. The first is the monodeprotonated tosyl sulfonamide salt, [K(18c6)][HNTs]. The second product crystalized was **4-isq ap crown** complex, the one electron oxidation of **3-ap crown**. Yields improved to over 70% but were frequently inconsistent. With the crystal structure heavily disordered around the *N*-tosyl moiety the artifical bond metrics around the N atom is unable to provide either for or against N-H functionality, so IR spectroscopy of **5-NTs** was employed. The IR spectra showed a weak absorbance peak at 3334 cm^{-1}. While the wavelength of this absorbance suggests the prescence of an N-H peak, the weak strength suggests an assignment of a lone nitrogen, with minor

decomposition to N-H generated through adventitous water from transfering the IR sample from the drybox to the nitrogen gas purged IR chamber.

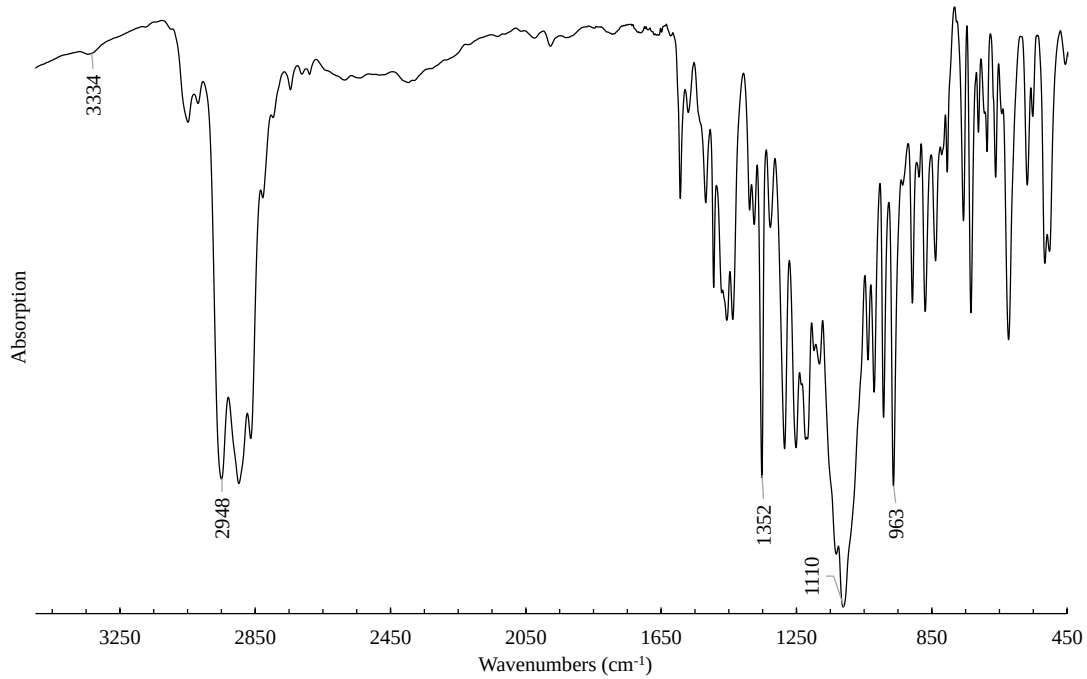

Figure 1-16: IR absorption spectrum of **5-NTs**.

This suggests a 3-coordinate nitrogen, with two bound encapsulated potassium ions and the sulfonyl moiety as an overall monocationic ion by charge balance with the unambiguous, overall monoanionic copper complex. This indicates the 3-coordinate nitrogen atom has an overall negative charge, suggesting some type of nitrenoid species.

The UV-Vis spectrum in toluene of **5-NTs** is shown below compared to **3-ap crown**. Broad features are visible around 430 nm and beyond 800 nm. The absorptions were assigned as MLCT and a combination of MLCT and LLCT, respectively.[17, 24]

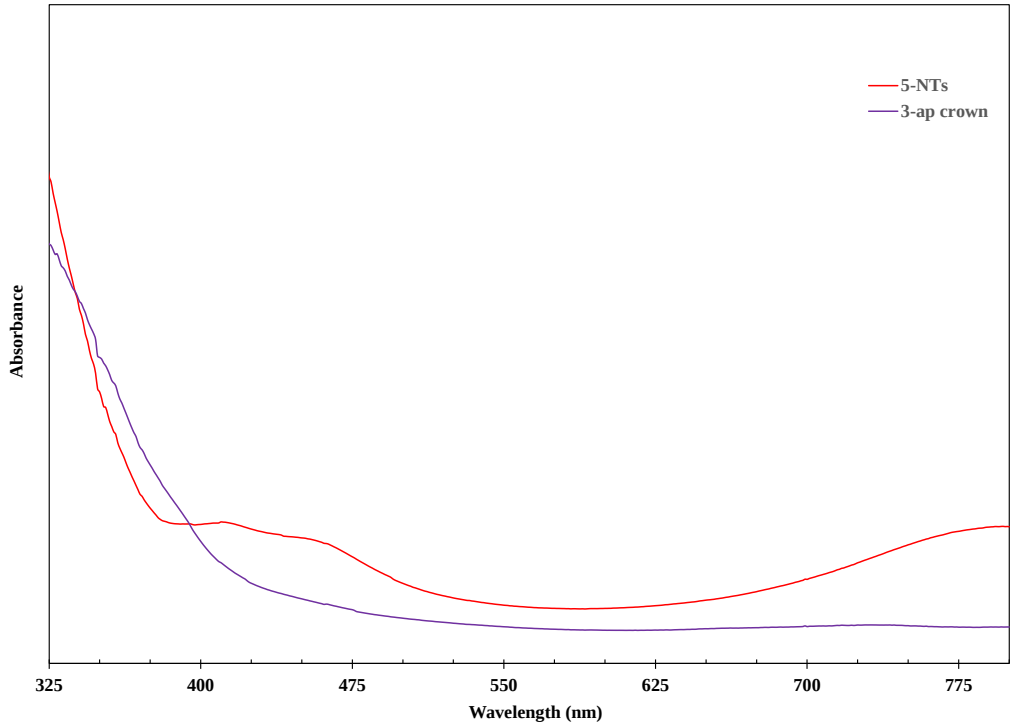

Figure 1-17: UV-Vis spectra of **5-NTs** and **3-ap crown** in toluene.

1.4.5 Validation of copper NTs species

This product can be generated with both PhI=NTs and N_3Ts, though with an altered purification. This reaction also shows immense sensitivity to water, with multiple reactions forming water generated decomposition products with anhydrous solvent (stored over 4 Å molecular sieves and Na^0) and reactions performed in a sealed vial, in a sealed freezer within a MBraun drybox. These side products were independently synthesized *in-situ* by adding water to solutions of both the isolated pentane and Et_2O washes in C_6D_6; The amount of pentane soluble product and THF precipitate also varies (between reaction, at the yield detriment of **5-NTs** (41%-75% yield); trace (K*18c6)HNTs is also generated during reaction, which occurs even when the reaction is performed from a thawing frozen solution of Et_2O. When the reaction is performed in toluene or at lower temperatures, **5-NTs** is still the major product, but the minor products change, including the generation of **2-isq** when the reaction is allowed to warm to room temperature. Solvents more polar than Et_2O cause a dramatic decrease in reaction yield and purity.

Initial reactivity and studies were performed on the water reacted product of **5-NTs** and is described below. Reactivity occurred instantaneously in C_6D_6 with lithium triethyl borohydride at

room temperature and at elevated temperatures overnight with (*n*-butyl)$_3$SnH (60 °C), as well as Ph_2P-PPh_2 and H_2PPh (90 °C). The unknown product was reactive with I_2 and PPh_3 in Et_2O at room temperature but, as with the reactions mentioned below, the anticipated product was not formed and the reactions suggest non-selective reactivity or decomposition by ^1H and ^{31}P NMR spectroscopy, likely due to reaction with both the reducing agent copper complex and the desired $(K(18c6))_2(NTs)$ cation. It was unreactive towards 1-hexene and TEMPO in Et_2O and THF up to 50 °C, approximately 15 °C under 1-hexene's boiling point. Its reactivity towards 1-hexene and TEMPO did not improve in THF, though it proved amenable to reaction with H_2PPh at 90 °C overnight.

DCM was shown to slowly oxidize over days **3-ap** to **2-isq** at -35 °C during an attempted crystallization. This slow oxidation used in an attempt to gently oxidize the reaction between **3-ap crown** with N_3Ts. When **3-ap crown** was reacted with N_3Ts in DCM, **2-isq** was identified by ^1H NMR spectroscopy, as well as a diamagnetic peaks assigned to **(K*18c6)HNTs**, shifted slightly by paramagnetic components in solution.

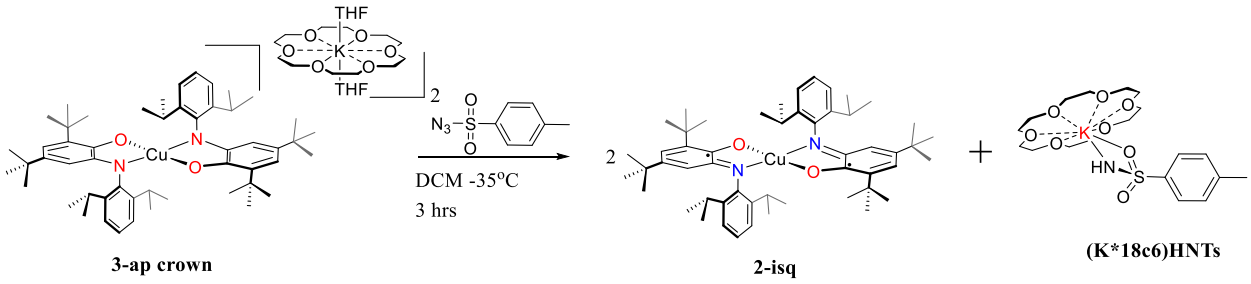

Figure 1-18: Reactivity of **3-ap crown** with N_3Ts in DCM.

5-NTs was reacted with excess TEMPO, generating **2-isq** and **(K*18c6)HNTs** by ^1H NMR spectroscopy. Further reactivity studies are ongoing to identify the nature of **5-NTs.**

CHAPTER 2. SYNTHESIS TOWARDS AN YTTERBIUM IMIDO

2.1 Rare earth elements and their redox active ligands and imido complexes

2.2 Experimental

2.2.1 General Considerations

All reactions are air- and moisture-sensitive and were performed in an MBraun inert atmosphere drybox with an atmosphere of liquid nitrogen off-gas equipped with a -35°C freezer. Pentane, toluene, diethyl ether, and tetrahydrofuran were purchased anhydrous and without stabilizers, dried in a Seca solvent purification system (SPS) and stored over 4 Å molecular sieves and $Na^0_{(s)}$. All other proteo solvents and compounds were purified, dried, and deoxygenated according to literature procedures, and dried overnight on a Schlenk line prior to use in the drybox.[1]

^1H, ^{19}F, and ^{31}P NMR spectra were recorded on either a Varian Inova 300 spectrometer operating at 300 MHz or a MBraun spectrometer operating at 400 MHz. The ^1H spectra for all molecules are reported relative to the peak for $SiMe_4$, with the residual ^1H solvent peak chemical shift as secondary standard. The ^{19}F and ^{31}P spectra for all molecules are reported relative to the peak for $CFCl_3$ and H_3PO_4, respectively. All voltametric data were obtained under inert atmosphere in the MBraun, drybox using the external ports. All samples were collected with 0.1 M $[nBu_4N][PF_6]$ as supporting electrolyte and referenced to Fc/Fc+ as the internal standard under experimental conditions. The solutions were analyzed with a 3 mm glassy carbon working electrode, Ag^0 wire quasi-reference electrode, and Pt wire counter electrode, with the analysis performed by either Ezra Coughlin or Jerod Keiser. UV-Vis spectra were recorded in a sealed 1 cm quartz cuvette at room temperature with a Cary 100 Scan UV-Visible spectrophotometer.

Single-crystals suitable for X-ray diffraction were isolated and coated with (poly)isobutylene oil in a drybox. Their transfer to a goniometer and subsequent data processing and analysis was either aided or performed by Ezra Coughlin or Dr. Matthias Zeller, though not data analysis.

Synthesis of $Yb(ap)_2(K)$:

To a 20 mL scintillation vial was added $YbCl_3$ (200 mg, 279.4 g/mol, 0.7158 mmol), ^{Dipp}iq (544 mg, 379.6 g/mol, 1.433 mmol, 2.00 equivalence), a magnetic stir bar and THF (18mL). This

solution was stirred at room temperature for 35 minutes before KC_8 (402 mg, 135.2g/mol, 2.973 mmol, 4.15 equivalence) was added portion-wise over 10 minutes, turning blood red. The solution stirred for 2 hours before being filtered through celite, rinsing with pentane. The volatiles were removed by high vacuum and the remaining dark red solid was washed with pentane (2 x 1.5 mL) at room temperature giving 250 mg of clean, bright red compound. The filtrate was then dried in vacuo and recrystallized as follows: The crude dark red and bright blue solid was dissolved in minimal pentane with an additional 2 mL pentane added before being cooled to -35 °C overnight. The solution was decanted, the bright red crystals washed with pentane (2x 2mL) yielding an additional 305 mg of the desired product, **Yb(ap)$_2$(K)**. (670 mg, 1259.8 g/mol, 0.4898 mmol, 68% yield).

Synthesis of Yb(isq)$_2$(PF-Tet):

To a 20 mL scintillation vial was added **Yb(ap)$_2$(K)** (25 mg, 0.019845 mmol, 1 eq), a magnetic stir bar, and 4 mL toluene. To the red solution was added 18-crown-6 ether (5.76 mg, 0.02183 mg, 1.1 eq) before it was stirred and cooled to -35°C for 1.5 hours. Pentafluorophenylazide (PFN_3) (8.30 mg, 0.03969 mmol, 2.0 eq) was added slowly, down the side of the cold vial, and then stirred at -35°C. The solution almost immediately turned black, lightening to brown within a minute before lightening to deep blue within 15 minutes of stirring at -35°C. The solution was stirred an additional 1.5 hours, warmed to room temperature, and the volatiles removed in vacuo yielding a dark blue powder, **Yb(isq)$_2$(PF-Tet)** (33 mg, 0.01942 mmol, 98% yield).

Synthesis of presumed Yb(ap)$_2$(DMAP)(THF):

To a 20 mL scintillation vial was added **Yb(ap)$_2$(K)** (103 mg, 0.0818 mmol, 1259.75 g/mol) in 15 mL of diethyl ether with a magnetic stir bar. To a black capped vial was added 18-crown-6 (34 mg, 0.0901 mmol, 1.1 equiv) and 2 mL of diethyl ether. This solution was added dropwise to the stirring, red ether solution of Ybap)$_2$(K) at room temperature. Some solid may precipitate then redissolve. After stirring for 30 minutes, DMAP (10 mg, 0.08197 mmol, 1 equiv) with 3 mL of diethyl ether was added dropwise over 10 minutes. The orange solution was stirred for an hour before reducing the volume to 3-4 mL. The solution was then filtered, removing a yellow solid

and then the volatiles removed by high vacuum, yielding **Yb(ap)$_2$(DMAP)(THF)** (95 mg, '1533.75 g/mol').

Synthesis of presumed Yb(DMAP)(imido):

To a 20 mL scintillation vial was added **Yb(ap)$_2$(DMAP)(THF)** (45 mg, 1533.75 g/mol, 0.0286 mmol) and 6 mL of toluene. The orange solution was frozen in liquid nitrogen (Coldwell), and layered with a toluene solution of PFN_3 -35°C (5.98 mg, 3.6 μL, 0.0286 mmol, 1 equiv, MW=209.09 g/mol, p~1.655 mg/mL), and frozen. The frozen solutions were then thawed at -78 °C for 1.5 hrs. The orange solution was then warmed to -35°C. Within 30 minutes the solution had turned green, with IR confirming azide consumption and new product after 50 minutes. The crude solid was triturated with pentane (3 x 1.5 mL), which can be discarded. The solid was washed with (3 x 1.5 mL) of diethyl ether and filtered through a pipet filter or fritted funnel, removing a steel blue precipitant. The green solution was then dried in vacuo leaving the **Yb(DMAP)(imido)** (44 mg, MW='1682.7 g/mol').

2.3 Rare Earth Metals and Redox Active Ligand

2.3.1 Introduction

Rare earth metals, particularly lanthanides, are often used and studied utilizing their core *f* electrons for their magnetic and luminescent properties for use in new technologies.[2] They are generally redox restricted, with the 3+ redox state being the most common. Other redox states are accessible depending on the metal, but frequently have high reduction potentials to obtain other oxidation states.[3] This limits their reactivity, but by using redox active ligands we can expand on these relatively redox inert metals. The electronic and magnetic properties of redox active ligand complexes of ytterbium, europium and other lanthanides with redox active ligands have been studied for their electronic and magnetic properties, particularly surrounding the redox isomerism between the core *f* electrons and ligand orbitals[4-5] and potential multiconfigurational oxidation states.[6-7] The synthetic utility and versatility of these complexes has not been well established.

The reactivity of complexes containing lanthanide ions with redox non-innocent ligands has been explored by our group previously,[8-9] but the synthesis of the a lanthanide imido has not been done successfully. With the reactivity of the iminosemiquinone ligand well established in our

group with both *f* block and transition metals, the synthesis of a monomeric, terminal lanthanide imido from an azide was investigated using the reaction of an ytterbium bis (^{Dipp}ap) complex.

2.3.2 Introduction: Transition Metal Tetrazenes

Transition metal tetrazenes are formed through the reaction of a metal imido with an equivalent of azide, and generally form a static metallacycle. Their reactivity is not always so straight forward however, as they can be in equilibrium with a metal-imido-azide complex,[10] can be UV reactive, generating a bis imido, [11] and can be redox active.[10, 12]

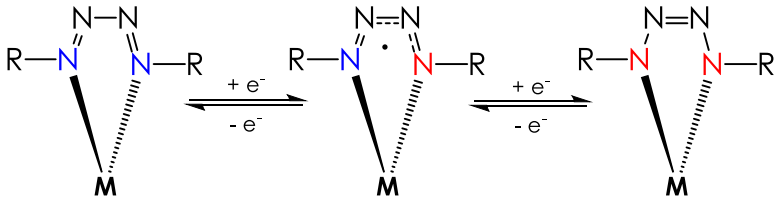

Figure 2-1: Potential electronic configurations for metal-tetrazene complexes.

2.4 Our Previous Work[8]

Initial synthesis of an ytterbium-redox active ligand system was achieved through the addition of two equivalents of ^{Dipp}iq ligand to $YbCl_3$, followed by the addition of four equivalents of KC_8 portion-wise in THF. The resulting complex was isolated as **Yb(ap)$_2$(K)**, along with its potassium sequestered analog, **Yb(ap)$_2$(K*18c6),** which can be easily generated in-situ or independently. Initial reactivity to generate an ytterbium imido with one equivalent of para-tolylazide (*p*TolN_3) resulted in the incomplete conversion of the **Yb(ap)$_2$(K)** starting material. Stoichiometric conversion of the ytterbium starting material necessitated two equivalents of azide at -35 °C to generate a clean reaction. Two crystalline products were characterized by X-ray diffraction and were grown from vapor diffusion of pentane into diethyl ether at -35 °C. The major structure was determined to be an ytterbium tetrazene, **Yb(*p*TolN$_4$-Tet)**, with isostructural crystals grown and analyzed using para trifluoromethyl azide. The minor product was solved as a ligand inserted product, Yb(*p*TolNap)$_2$. This minor product is the result of the azide insertion in to the ligand, presumably through a ytterbium imido intermediate, resulting in a 7-membered ring product.

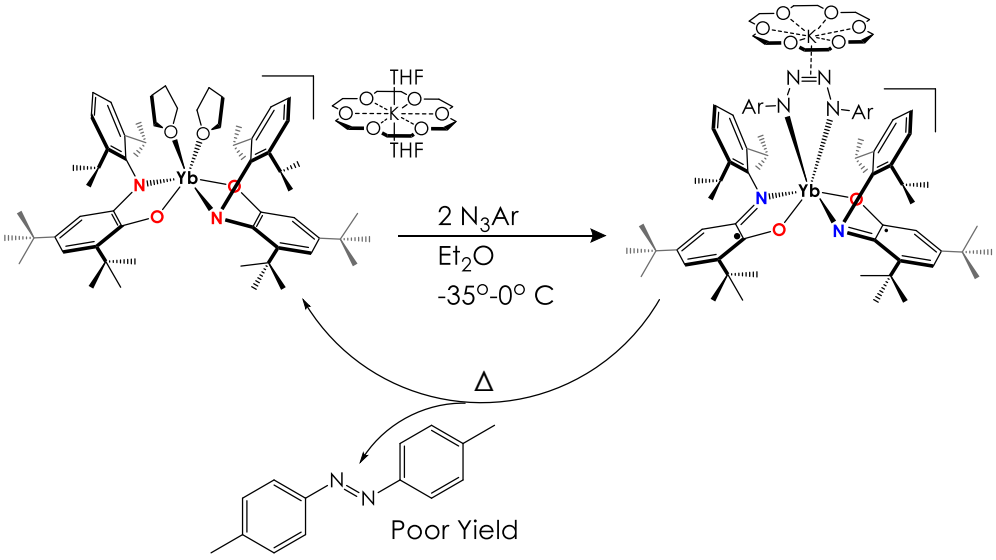

Figure 2-2: Synthesis of Yb tetrazene.

The bond distances of the ytterbium bis(amidophenolate) complex was compared to related structures, including the neodymium-^{Dipp}ap complexes previously synthesized by our group.[9] The ytterbium complex's ligand bond distances compares well to those of its neodymium analog. The ytterbium average C-O bond distance of 1.3455 Å is indicative of single bond character and is within error of the C-O bond distances of the Nd analog, with average C-O bond distance of 1.348 Å. The ytterbium ligand's average C-N bond distance of 1.4005 Å is indicative of single bond character and similar to the Nd complex's 1.389 Å average C-N bond distance. Each ytterbium ^{Dipp}ap ligand has C-O and C-N bond distances within error of their average, confirming the bis(amidophenolate) Yb(III) assignment, crystallographically suggesting a lack redox isomerism between the $Yb^{III}(^{Dipp}ap)_2$ and a Yb(II) with one ^{Dipp}isq and one ^{Dipp}ap ligand.

The ligand bond distances found in the tetrazrene complexes indicate the presence of two ^{Dipp}isq, with the average ^{Dipp}isq C-O bond distances for the perfluoro and *p*Tol tetrazenes of 1.2940 Å and 1.2895 Å, respectively. This is slightly shorter than the previously synthesized neodymium bis(^{Dipp}isq) C-O bond distances of 1.309 Å. This suggests a more double bond character and a more ligand bound radical in the Yb tetrazenes. The tetrazenes's C-N bond distances are in close agreement with the $NdI(^{Dipp}isq)_2$ bond distances, with the perfluoro and *p*Tol tetrazene average C-N bond distances of 1.349 Å and 1.346 Å and C-N bond distance of 1.344 Å for the neodymium complex.

The similarity between the tetrazenes' ^{Dipp}isq bond distances suggests C-O bond distance differences are metal based and not electronics based. This could be due to weaker spin coupling of the semiquinone ligands to the lone 4*f* electron compared to the more abundant 3 electrons the 4*f* orbitals of Nd(III).

Table 2-1: Selected bond distances for Yb-^{Dipp}ap and Yb-^{Dipp}isq complexes.

Compound	O-C	O-C2	**O-C avg**	N-C	N-C2	**N-C avg**
[Yb(ap)2][K(18c6)]	1.342(3)	1.349(3)	**1.3455**	1.403(5)	1.398(5)	**1.4005**
Yb(isq)$_2$(PFTet)	1.289(5)	1.299(5)	**1.2940**	1.349(6)	1.349(6)	**1.349**
Yb(isq)$_2$(*p*TolTet)	1.286(3)	1.296(3)	**1.2895**	1.348(3)	1.344(3)	**1.346**

In the azide inserted ligand minor product, both ^{Dipp}ap ligands react consistently, losing their planarity with small changes to the bond distances around the central ytterbium. The C-O bond distances of the ligands are 1.32 Å and 1.31 Å, which is approximately the average between the ^{Dipp}ap and ^{Dipp}isq ligand C-O bond distance. The C-C bond distances in the 7-membered ring are consistent with both the ^{Dipp}ap bond distances found in the starting material, **Yb(ap)$_2$(K*18c6)**, and aromatic C-C bonds generally. There are differences between each inserted ligand, however, with respect to the C-N bond distances, with one having a C-N bond distance of 1.36 Å and the other containing a C-N bond distance of 1.40 Å. The former falls between that of the ^{Dipp}ap and ^{Dipp}isq ligands, similar to the C-O bond distances, with the latter comparing well to the single bonded C-N of a ^{Dipp}ap. This suggests a complicated ligand environment, with potentially a mixed ligand system crystallagraphically unresolved around the ytterbium.

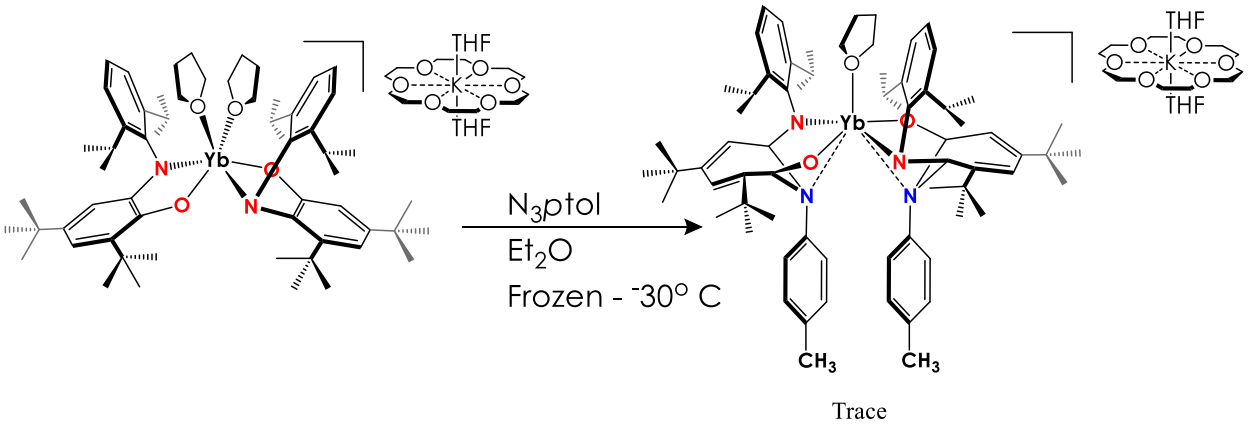

Figure 2-3: Synthesis of ^{Dipp}ap ring-inserted product.

Literature revealed this reaction was fairly unique, with only one similar reaction found, utilizing a copper oxide compound to insert ammonia into catechol, giving a 7 membered ring, cyclic N-acetyl acetamide in poor yield.[13] So, isolation of this product was attempted.

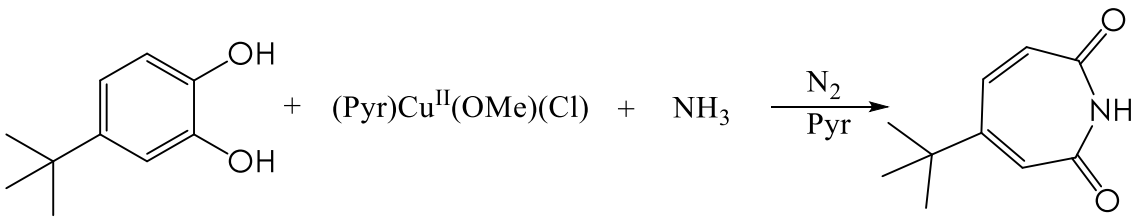

Figure 2-4: Catechol nitrogen ring insertion.

2.5 Data Analysis

Despite the colors that change after reacting with azide, the UV-Vis spectrum for all of the Yb compounds are fairly featureless, and can be seen in the Figure 2-4 below. This featuresless UV-Vis is indicative of a lack of charge transfer bands, which was seen in the square planar **3-ap crown** in chapter 1. This lack of this typical iminosemiquinone charge transfer band, even in the ytterbium iminosemiquinone products, suggests the ligands are isolated with no orbital delocaliztion, presumably due to the stark, non-planar geometry around the central metal. The lone, unpaired 4*f* electron is core in nature, supported experimentally by the extremely high redox potentials for lanthanides.[14]

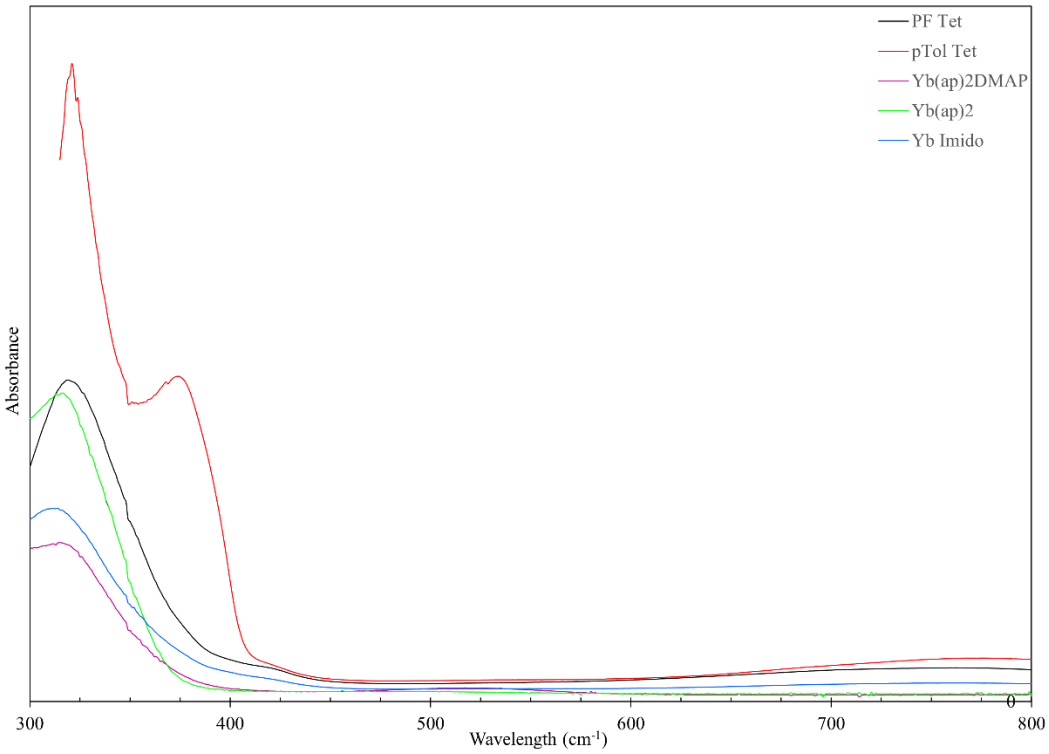

Figure 2-5: UV-Vis of the Yb ligand compounds.

The one except is the para methyl tetrazene, which has a peak at 374 nm as well as a much stronger absorbance around 325 nm compared to the other complexes. Absorbances of around 370 nm are most commonly associated with protein aromatic side groups, particularly tyrosine and its phenol at 375 nm, the biological analog the iminosemiquinone intended to help mimic,[15] indicating the possible presence of free ligand or imido inserted ligand impurity.

To evaluate the magnetic properties of the ytterbium complexes, the magnetic susceptibility, μ_{eff}, was taken at room temperature following standard NMR methodology, the Evan's method.[16] Briefly, to a C_6D_6 solution of a compound with known concentration, ferrocene is added. This solution is added to a standard NMR tube in which is an external reference consisting of a C_6D_6 solution of ferrocene placed a sealed capillary. The frequency shift (Hz) of ferrocene, $\Delta\nu$, caused by the paramagnetic Yb compound, can be used to calculate the mass susceptibility, χ_g ($\frac{cm^3}{g}$), using Equation 1[17] below:

$$\chi_{Molar} = \chi_g * M = \frac{3 * \Delta\upsilon}{4\pi * \upsilon * c} * M$$

where ν is the probe frequency (Hz) of the NMR, and c is the mass concentration ($\frac{g}{cm^3}$); this ignores solvent diamagnetism and the density correction since the concentration is under 10 mM.[17] Multiplying the mass susceptibility by the molecular mass ($\frac{g}{mol}$) of the compound in solution, M, gives the molar susceptibility, χ_{Molar} ($\frac{cm^3}{mol}$). The calculation of the effective magnetic moment, μ_{eff}, can be made from the molar susceptibility and accounting for the effect of paired electrons, via the diamagnetic correction, χ_D. This diamagnetic correction is unique to each system based on ligand and metal, and is here approximated with Equation 4[18] due to the redox non-innocent ligands themselves and the potential multiconfigurational oxidation state of these Yb(III) complexes of redox non-innocent ligands[6].

$$\mu_{eff} = 2.828\sqrt{(\chi_P T)}$$

$$\chi_P = \chi_{Molar} - \chi_D$$

$$\chi_D = -\frac{1}{2} MW * 10^{-6}$$

The predicted effective magnetic moment for the lone Yb(III) is μ_{eff} = 4.5 μ_B.[19] The theoretical magnetic moments for Yb(III) complexed with a spin-coupled ligand organic radical lies within the range of μ_{eff} = 3.4 - 5.6 μ_B, where a μ_{eff} = 3.4 μ_B is the theoretical spin of the Yb(III) lone, unpaired *f* electron antiferromagnetically spin coupled to the organic radical and μ_{eff} = 5.6 μ_B is the theoretical magnetic moment of the Yb(III) lone, unpaired *f* electron ferromagnetically spin coupled to the organic radical.[19] Table 1 shows the effective magnetic moments for the compounds synthesized, which range from μ_{eff} = 3.95 - 4.93 μ_B. This data in insufficient to determine the presence of a multiconfigurational ground state, i.e., intermediate valency. This is when the ligand and metal orbitals are close in energy and therefore partially occupied. This is highly temperature dependent, and best determined with utilizing the μ_{eff} at various temperatures. This data would also be necessary to determine redox isomerism, a temperature dependent charge transfer where the μ_{eff} abruptly changes at a particular temperature due to a larger gap in metal and ligand orbital energies.[4, 7, 20]

Table 2-2: Magnetic susceptibility and Evan's Method data

Compound	Δν (Hz)	χ_{Molar} ($10^3 \frac{cm^3}{mol}$)	μ_{eff} (μ_B)
$Yb(ap)_2$	54	6.01	3.95
$Yb(ap)_2$(DMAP)(THF)(K)	33	8.26	4.61
$Yb(isq)_2$(DMAP)(imido)(K)	42	9.37	4.89
$Yb(isq)_2$(PFTet)	57	9.17	4.84
$Yb(isq)_2$(p tolTet)	54	9.51	4.93

The ytterbium bis(^{Dipp}ap) complex has a lower magnetic susceptibility compared to the rest of the complexes synthesized, suggesting a stronger spin coupling. This is supported by the consistent bond distances within error to the ^{Dipp}ap ligand and therefore consistent oxidation statewithin the crystal structure. Once the Yb-^{Dipp}ap complex is either bound or reacted, the magnetic susceptibility becomes fairly consistent around 4.6-4.9 μ_B. Changes to the magnetic susceptibility seem dependent on the ligand bond angles, where a more planar O-Yb-O bond angle between the ligands, irrespective of oxidation state assignment of ^{Dipp}isq or ^{Dipp}ap, produces stronger ferromagnetic coupling, and the more acute O-Yb-O angle generating stronger antiferromagnetic coupling.

This implies that the ligand radicals themselves have no effect on the lone 4*f* electrons spin, and that the ligand-metal orbital overlap, dictated by geometry, is the major contributor to the Yb(III) coupling. This further supports the singular room temperature Yb(III) redox configuration of this system. The increased planarity increases the ligand-ligand spin coupling, causing a ferrocoupling with the Yb(III) *f* electron, whereas the acute angle reduces intraligand coupling, producing a stronger ferrocoupling between ligand a the Yb(III) *f* electron.

Table 2-3: Selected bond angles for Yb-^{Dipp}ap and Yb-^{Dipp}isq products.

	N_{ap}-Yb-N_{ap} angle	O_{ap}-Yb-O_{ap} angle
$Yb(ap)_2$ crown	170.91(9)	116.01(8)
$Yb(ap)_2$	166.0(2)	97.4(1)
Yb(PF-tet)$(isq)_2$	159.5(1)	92.4(1)
Yb(*p*Tol-tet)$(isq)_2$	157.29(7)	85.30(6)

2.6 Reactivity

2.6.1 Introduction to Rare Earth Imido

Rare earth imido complexes are of synthetic interest due to their highly polarized nature, facilitating novel chemistry when compared to that of most transition metal nitrogen double bond analog nitrenes or iminyl radicals; the electronic differences between these metal nitrogen double bonds is what facilitates their differentiating reactivity.[21-22] To date, most isolated rare earth imidos have been oligomeric or necessitated Lewis acid stabilization, frequently aluminum. They have also had limited synthetic routes, forming through rare earth anilido or amido deprotonation. These limit the utility and study of the synthetically valuable rare earth imido species.[23-26]

2.6.2 Reactivity of Yb(ap)$_2$K

With initial attempts to isolate the ytterbium monoimido being unsuccessful using *p*TolN$_3$, reactivity with pentafluorophenyl azide (PFN$_3$) and to a lower temperature range of reactivity was attempted, in order to better control the reaction through the more numerous cold baths below -35 °C. Reducing the temperature in the tetrazene synthesis produced a cleaner reaction, leading to the hypothesis that the inserted product was the thermal decomposition of the intermediate ytterbium imido. Isolation of the presumed kinetic, insertion product was initially achieved successfully with the Yb(N-ap)$_2$ product at room temperature instead of the standard -35°C. It was also noted that the insertion product was successfully achieved with prolonged time (4 weeks) at -35 °C. The room temperature reaction and the prolonged, low temperature reaction suggested different reaction kinetics, with the former suggesting the insertion as the least stable, kinetic product, while the slow and cold reaction suggests the insertion is the thermodynamic, more stable product. With conflicting hypothesis, the conditions were reproduced. Unfortunately, neither condition proved amenable to reproducibility. Reactions were carried out at -35 °C over a monitored period, at -78 °C and at room temperature within the standard 2 hours. All reactions yielded an impure tetrazene product and full consumption of starting material, with the -35 °C reaction going to completion within a week. Lower temperature control was attempted, thawing a frozen toluene solution of **Yb(ap)$_2$(K*18c6)** layered with, and subsequently frozen in $N_{2(l)}$, a 1 equivalent PFN$_3$ toluene solution. This layered, frozen toluene solution was then thawed at -94°C with a liquid nitrogen-acetone bath, with the initial red solution stable for 1.5 hours, indicative of

no reaction. Upon slight warming of solution, a color change to brown was observed and did not change upon re-cooling to -94°C for over an hour. Further slight warming led to the completion of the tetrazene product with starting material **Yb(ap)$_2$(K*18c6)**. The reaction was repeated with a controlled warming of a layered frozen solution of toluene from -89°C. Three layers of toluene was again frozen, as solutions containing **Yb(ap)$_2$(K*18c6)** and PFN_3 in the bottom and top layer, respectively. The red solution was thawed at -89°C and stirred for an hour before being warmed to -84 °C, stirring for a subsequent hour. Afterwards, the solution was warmed to -78°C and then -72 °C, each for an hour with no change in the red solution. Further warming to room temperature resulted in no visible change in reaction. Temperature control proved ineffective in isolating the desired ytterbium imido.

The stability of the Yb tetrazene compounds was investigated to determine the nature of the tetrazenes. The para-toluene ytterbium tetrazene, **Yb(isq)$_2$(*p*tol-tet)**, was found to have good thermal stability, surviving 20 hours at 75 °C. Decomposition was only after 48 hours at 90 °C, with only trace arylazo formed. It was stable to UV light for over 18 hours at room temperature. The ytterbium tetrazene did react very slowly with PPh_3, in the presence of DMAP to stabilize any potential intermediate, with one new peak at -0.7 ppm in ^{31}P NMR spectroscopy which is shifted from the starting material. This did not match literature for *p*TolN=PPh_3, and the PPh_3 remained largely unreactive so no further investigation was attempted.

With no way to isolate an ytterbium imido kinetically or through temperature control, thermodynamic stabilization was investigated. Steric bulk has shown to play a particularly important role in transition metal tetrazenes,[11, 27] preventing or facilitating reactivity using steric bulk. Tosyl azide has also been shown to facilitate blocking a coordination site with a sulfoxide oxygen, transitively stabilizing the imide.[28] It was also noted that with rare earth imidos, particularly scandium, stable imido complexes using DMAP to induce sterically driven hydride abstraction between the scandium methyl and anilido, yielding the scandium DMAP imido and methane.[23] Tetrazene formation requires two open coordination spheres, which are initially occupied with solvent in **Yb(ap)$_2$(K*18c6)**. Occupying one of those coordination spheres sterically could prevent the tetrazene formation can be seen in Figure 2-5. **Yb(ap)$_2$(K*18c6)** was generated *in-situ*, with a stoichiometric equivalent of DMAP analyzed consecutively. With a stoichiometric equivalent of DMAP, the red C_6D_6 solution of **Yb(ap)$_2$(K*18c6)** turned orange upon DMAP solvation, with ^{1}H NMR spectroscopic analysis showing peak broadening of the

DMAP protons, along with a small shifting of the starting material peaks, suggesting DMAP coordination with the paramagnetic Yb. Another equivalent of DMAP was then added, turning the orange solution yellow, and showing an increase in the broadened DMAP peaks. This crude ytterbium bis(DMAP) was reacted with one equivalent of PFN_3 to test the lability of the DMAP. No color change was observed and both IR and ^{19}F NMR spectroscopy confirmed the continued presence of the azide coexistenting in solution with the ytterbium bis(amidophenolate) complex longer than standard reaction conditions. With the hypothesis supported experimentally, the intermediate, ytterbium mono DMAP product was isolated and characterized for eventual reactivity with PFN_3.

To a solution of *in-situ* generated **Yb(ap)$_2$(K*18c6),** one equivalent of DMAP in toluene was added, which was subsequently frozen by $N_{2(l)}$ which was layered with a solution of PFN_3. The solution was frozen before combined with the frozen toluene solution of Yb which was thawed and mixed at -35 °C. The initial orange solution slowly turned dark green within 1.5 hours and was subsequently stirred overnight. After which, IR spectroscopy indicated the complete consumption of PFN_3, yielding a green solid upon solvent removal in vacuo. The crude, green, presumed ytterbium DMAP imido, **Yb(ap)$_2$(DMAP)(imido)**, was reacted at room temperature in both toluene and diethyl ether with a second equivalent of PFN_3, slowly changing to a dark blue solution over two hours, although it was unreactive in C_6D_6. Analysis by ^{19}F NMR spectroscopy indicated that the major product was the perfluoro tetrazene with the perfluoroaniline ($PFNH_2$) as a minor product. This supports the assignment of the DMAP imido intermediate. Attempts to synthesize a mixed tetrazene via addition of *p*TolN_3 to the green imido initially proved unsuccessful, presumably due to its reduced reactivity compared to PFN_3. This presumed imido was unreactive to PPh_3 in C_6D_6 at room temperature.

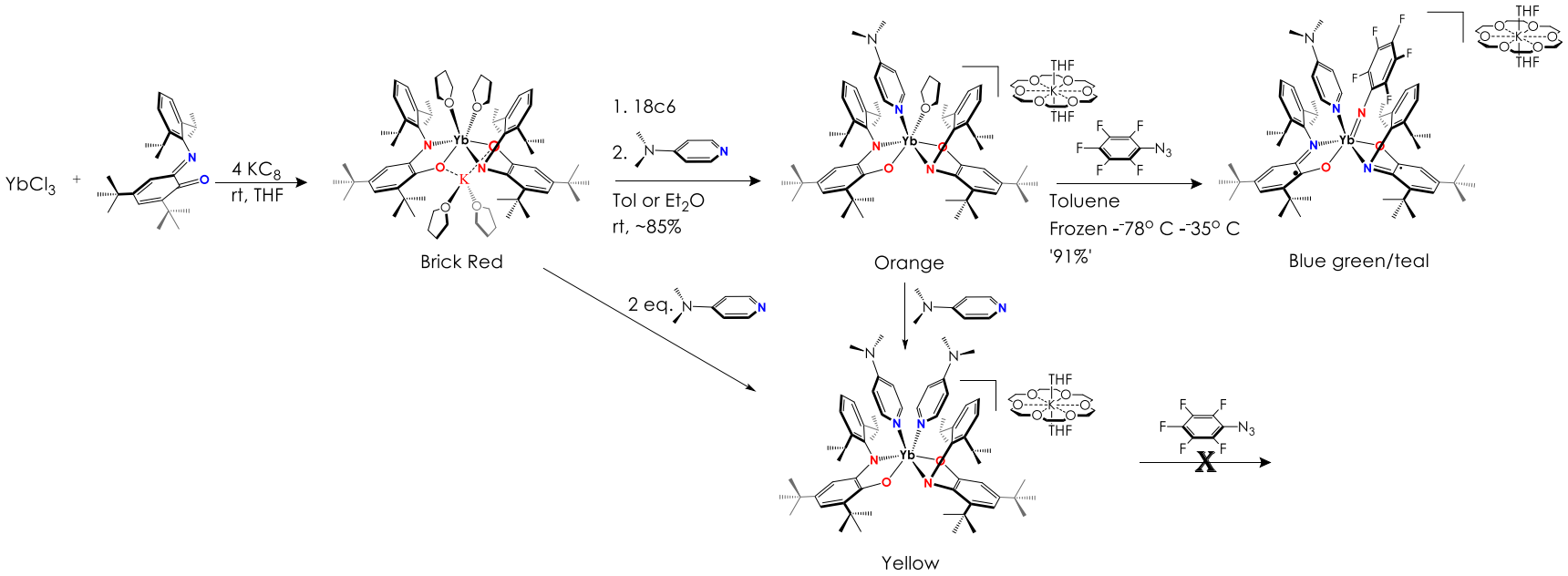

Figure 2-6: Synthetic route to Yb imido via DMAP steric hindrance.

When the green solid, presumed imido, is reacted with a second equivalent of PFN_3 in THF instead of toluene or diethyl ether the $PFNH_2$ was the sole product by ^{19}F NMR spectroscopy with no indication of tetrazene formation by ^{1}H NMR spectroscopy.

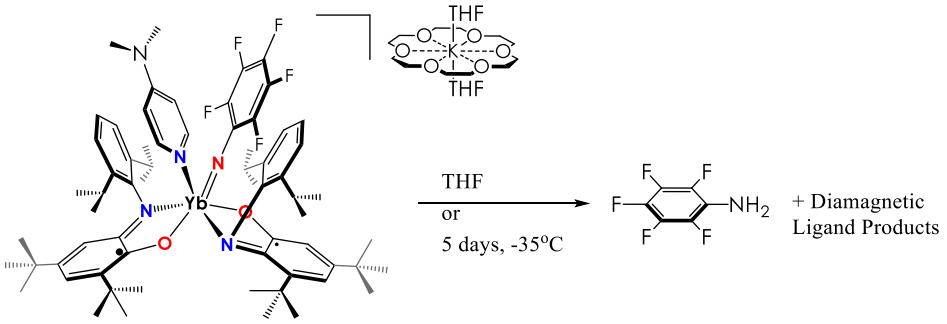

Figure 2-7: Decomposition pathways of Yb-imido complex.

Lowering the temperature to -35 °C yielded the same results, so the stability of the DMAP in the presumed imido was tested in THF overnight as a control. The presumed imido cleanly decomposes to the $PFNH_2$ by ^{19}F NMR spectroscopy. This solvent-based decomposition of the imido supports the necessity of the DMAP in stabilizing the compound: without the DMAP to occupy the coordination sphere, removed via ligand exchange with THF, the imido decomposes to $PFNH_2$ before reacting. The solid, presumed imido was thermally labile, even when stored at -35 °C, again decomposing to $PFNH_2$ doubtless through THF desolvation.

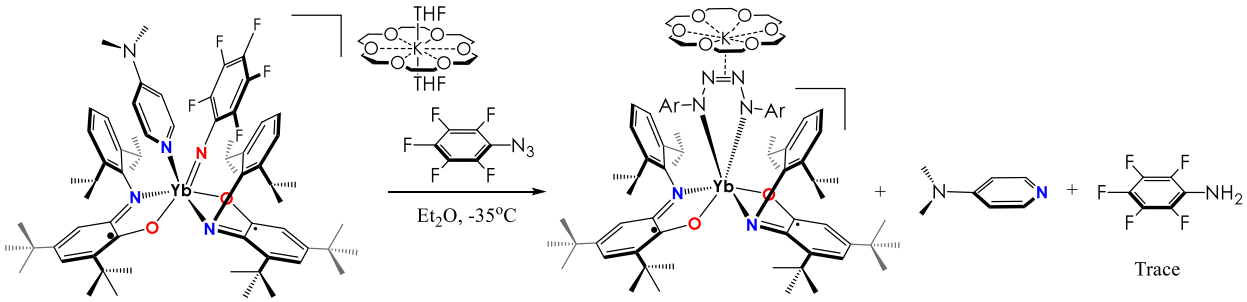

Figure 2-8: Reactivity of Yb-imido complex with azide.

Initial attempts to crystallize the presumed imido were unsuccessful due to the instability of the complex, even at -35 °C, based on the experimentally determined weak coordination of DMAP to ytterbium. With no efficient method to obtain all the desired characterization, a change of the

DMAP was made, making use of lanthanide's high oxophilicity.[29] Two choices were chosen for ease of synthesis, with pyridine N-oxide and triphenylphosphine oxide used to replace DMAP in initial coordination to prevent tetrazene formation. **Yb(ap)$_2$(K*18c6)** was reacted with one equivalent of N or phosphine oxide then cooled to -35 °C before azide addition. Upon reaction completion, the crude imidos showed acceptable crude stability as solids, so further studies were continued.

CHAPTER 3. ORGANIC SYNTHESIS

3.1 Potential Antibiotic Synthesis

A nosocomial, antibacterial resistance infection can cost an American anywhere from $30,998 – $74,306, with community on-set infections costing up to $104,422. In the United States (US), the total cost to treat just six types of multidrug-resistant microbes is around $4.6 billion annually.[64] Antibiotic resistant infections number 2.8 million each year within the US and kill more than 350,000 people.[65] Statins have been found to decrease mortality due to bacterial infection, with a presumed method of action based on the anti-inflammatory and immunomodulatory effects associated with inhibition of HMG-CoA reductase and cholesterol synthesis.[66-68] A desired inhibitor compound for this bacterial enzyme, Figure 3-1, was a derivative of the groups HMG-CoA reductase inhibitor class containing two parts, connected by an amide linker; the head was taken from Platensimycin A, a well-known antibiotic, and the tail was based on one previously optimized in lab.[69-71]

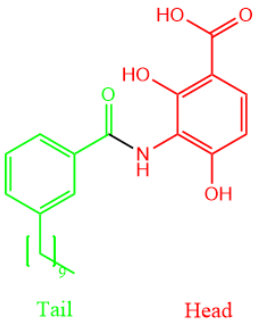

Figure 3-1: Desired HMG CoA reductase inhibitor.

3.2 Experimental

3.2.1 Non-Polar Tail

Esterification

To a flame-dried 50 mL round bottom flask fitted with a magnetic stirring bar was added 3-iodobenzoic acid (2.00 g, 8.07 mmol) and dry methanol (32 mL, [c] = 0.4 M), and concentrated sulfuric acid (3.6 mL, 66.2 mmol). The solution was heated to reflux and allowed to react

overnight. Upon completion, the reaction was adjusted to a basic pH by the addition of NaOH (aq, 1.0 M), and $NaHCO_3$ (aq, sat'd), after which it was extracted with DCM (4 x 25 mL). The combined organic layer was dried over $NaSO_4$, filtered, and the volatiles removed under reduced pressure to afford **3-2-1** (2.08 g, 7.94 mmol, 98% yield).

Sonagashira coupling

To a flame-dried, black-capped vial fitted with a magnetic stirring bar was added **3-2-1** (100 mg, 0.40 mmol), $Pd(PPh_3)_2Cl_2$ (28.3 mg, 0.040 mmol), CuI (15.4 mg, 0.080 mmol). Anhydrous Et_3N (1.00 mL, 7.17 mmol) was added, followed by 1-decyne (145 μL, 111 mg, 0.806 mol). An additional aliquot of 1-decyne (95 μL, 55 mg, 0.40 mmol) was added after 5.5 h. After 2 h, the solution was heated to 62° C for 2 h. Upon completion, the reaction mixture was diluted with $NaHCO_3$ (aq, sat'd), extracted with DCM (3 x 2 mL) and the combined organic layers washed with brine (2 x 2 mL), dried over NaSO4, and the volatiles removed under reduced pressure. The crude compound was purified by flash chromatography (1% ethyl acetate-hexanes, fractions 4-9) yielding the alkyne intermediate which was immediately carried on.

The alkyne intermediate was dissolved in ethanol (3.5 mL, [c] =0.23 M) and PtO_2 (24 mg, 0.105 mmol) was added. To the atmosphere was added H_2 via balloon and the solution was stirred at room temperature. Upon completion, the solution was diluted with EDTA (aq, sat'd), brine, and ethyl acetate. The organic layer was washed with a combined solution of EDTA and brine (2 x 4 mL) followed by a combined solution of $NaHCO_3$ (aq, sat'd) and brine (1 x 3 mL). The organic layer was dried, filtered, and purified by flash chromatography (6% ethyl acetate in hexanes) yielding **3-1-2** (111 mg, 0.402 mmol, 99.7% yield over 2 steps).

Ester hydrolysis

To a black-capped vial fitted with a magnetic stirring bar was added **3-1-2** (78 mg, 0.28 mmol) and aqueous NaOH (3 M, 1 mL). The solution was stirred at 60° C for 2 hours before adding THF (1 mL). The biphasic mixture was stirred an additional 2 hours before adding methanol (1 mL). The emulsion was stirred and continued heating overnight at 60° C. Upon completion, the emulsion was washed with ethyl acetate (1 x 3 mL), after which the organic layer was washed with NH_4Cl (aq, satd) and HCl (aq, 1 M). The volatiles were removed under reduced pressure yielding

3-1-3 as a solid (67 mg, 0.23 mmol, 90% yield). Acidification of the initial aqueous layer with aqueous HCl (12 M) and extraction with ethyl acetate (3 x 3 mL) yielded impurities.

3.2.2 Platensimycin head

Head esterification

To a flame-dried, 50 mL roundbottom flask fitted with a magnetic stirring bar was added 2,4-dihydroxybenzoic acid (1.00 g, 6.49 mmol) and dry methanol (16 mL, [c] = 0.4 M). Concentrated sulfuric acid (1.8 mL, 33 mmol) was added and the reaction heated to reflux overnight. The solution was cooled, diluted with brine and washed with ethyl acetate (3 x 15 mL). The combined organic layers were washed with $NaHCO_3$ (aq, sat'd), dried over $NaSO_4$ and filtered. The volatiles were removed from the filtrate under reduced pressure, yielding **3-1-4** (900 mg, 5.35 mmol, 83 % yield) as a solid.

Nitration

To a black-capped vial fitted with a magnetic stirring bar was added **3-1-4** (185 mg, 1.10 mmol), $NaNO_3$ (186 mg, 2.20 mmol), wet silica gel (50% w/w H_2O: silica gel, 222 mg,) and DCM (1.1 mL, [c] = 1 M). $NaHSO_4$ (264 mg, 2.2 mmol). The resulting suspension was stirred for 12 h, turning brown within 5 min. Upon completion, the suspension was filtered and the solid residue washed with DCM (2 x 2 mL). The volatiles were removed from the filtrate under reduced pressure and the product purified by flash chromatography (D=35 mm, 2 mL fractions, loaded with 200 mL 30% ethyl acetate in hexanes, 200 mL 30% ethyl acetate in hexanes, 250 mL 40% ethyl acetate in hexanes, 600 mL ethyl acetate in hexanes), affording the desired regioisomer **3-1-5** as a yellow solid (77 mg, 0.36 mmol, 32% yield) in fractions 22-40).

Nitro reduction

To a black-capped vial fitted with a magnetic stirring bar was added **3-1-5** (21 mg, 0.0981 mmol) and methanol (2.00 mL, [c] = 0.05 M). Glacial acetic acid (500 μL, 8.73 mmol) was added to the stirring solution before the addition of cleaned and activated Zn dust (35 mg, 0.53 mmol). The reaction was filtered after stirring for 1 h and the volatiles removed under reduced pressure, yielding **3-1-6** (12 mg, 0.0655 mmol, 67% yield)

3.2.3 Linking

Coupling

To a flame-dried black capped vial fitted with a magnetic stirring bar was added **3-1-3** (15 mg, 0.057 mmol). The system was purged with dry Ar for 5 sec and subsequently gently pressurized with dry Ar for 5 sec; this purge/pressurize cycle was repeated two more times to remove latent air. Dry DCM (100 μL, [c] = 0.57 M] was added before subsequent additions of oxalyl chloride (3.6 μL, 5.3 mg, 0.042 mmol) and a single drop of anhydrous DMF. Immediate bubbling occurred and the solution was stirred over 2 h.

To a second black-capped vial was added **3-1-6** (15.4 mg, 0.0840 mmol), Et_3N (20 μL, 15 mg, 0.147 mmol) and dry THF (210 μL, [c] =0.2 M). The THF solution was cooled to 0° C was transferred down the sides of the vial containing the 3-Tail solution over two aliquots, one of 100 μL and another of 185 μL. The solution was warmed to room temperature before heating to 45° C overnight. Upon completion, the solution was diluted with ethyl acetate and acidified brine. The aqueous layer was washed with ethyl aceteate (1 x 1 mL) and the combined organics washed with $NaHCO_3$ (aq, sat'd, 1 x 1 mL) before drying over $MgSO_4$ and filtering. The volatiles were removed under reduced pressure and the crude product purified by flash chromatography (25% ethyl acetate in hexanes) yielding **3-7** (9 mg, 0.02 mmol, 53% yield).

Ester hydrolysis

To a black-capped vial fitted with a magnetic stirring bar was added **3-1-7** (7 mg, 0.02 mmol) and aqueous NaOH (3 M, 24.6 μL, 0.0438 mmol) and distilled water (74.4 μL, [c] = 0.164 M). The solution was stirred at 60° C for 8 h and stirred overnight at 40 °C. Upon completion, the solution was neutralized with aqueous HCl (3 M, 50 μL), diluted with ethyl acetate and brine, and the aqueous layer washed with ethyl acetate (2 x 1 mL). The combined organics were dried over $MgSO_4$, filtered, and the volatiles removed under reduced pressure, yielding 6 mg of crude product. The crude product was analyzed by UPLC (2 peaks, m/z = 413 and m/z = 418, 50% ACN:H_2O) and purified by HPLC to afford pure **3-1-8** (3.0 mg, 0.0070 mmol, 43%).

3.2.4 Synthetic Route

The synthetic route for the tail started with *meta*-iodobenzic acid. Fischer esterification in dry methanol yielded the methyl ester in good yield. The ester was found to be necessary for efficient Sonagashira coupling with 1-decyne; the coupling using the acid was limited to 15% yield. The protected alkyne product was reduced using PtO_2 under a hydrogen atmosphere, before deprotection yielded the desired carboxylic acid.

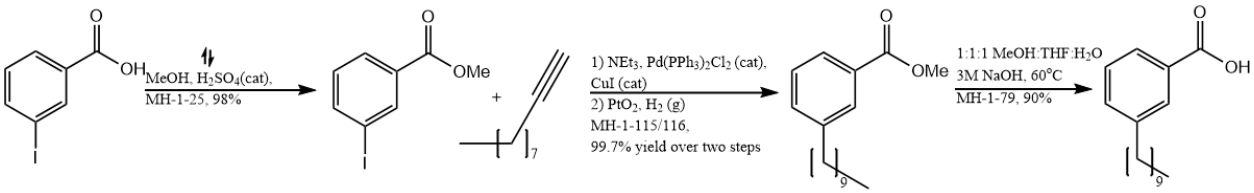

Figure 3-2: Synthetic strategy for inhibitor tail.

For the platensimycin head, 2,4 dihydroxybenzoic acid was esterified before being nitrated. Initial nitration procedures utilized nitric acid in acetic acid and acetic anhydride, but an alternate procedure utilizing wet silica, sodium nitrate, and sodium hydrogen sulfate was safer, better yielding, and more environmentally friendly. The desired 3-nitro substituted product, 3-**1-5**, was reduced using zinc dust in acetic acid in good yields.

Figure 3-3: Synthetic strategy for the inhibitor head.

Three strategies for amide coupling the head to the tail were attempted, with oxalyl chloride being the most efficient method. EDCI coupling was not compatible with an unprotected phenol, and EDCI coupling using TBS protection was poor yielding at 27%; TFFH yielded multiple products.

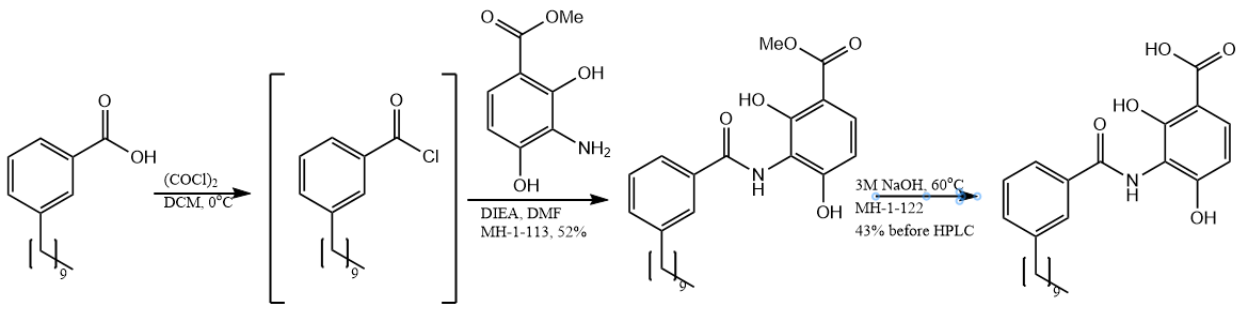

Figure 3-4: Final coupling and deprotection.

The hydrolysis of the penultimate methyl ester was challenging, with multiple conditions shown in Table 3-1. All tested basic hydrolysis methods yielded an impurity 5 m/z higher than the desired compound and only removable by HPLC.

Table 3-1: Hydrolysis methods attempted for desired product deprotection.

Base (equiv)	T (°C); solvent	Time (hours)	Yield (% before HPLC)
LiOH (28)	45; THF	2	NR
LiOH (28)	45; MeOH	2	NR
NaOH (5)	60; H_2O	4	24
NaOH (5)	60; H_2O	Overnight (o/n)	28
NaOH (5)	60; 1:1:1 THF: MeOH: H_2O	o/n	20
NaOH (4.5)	42; H_2O	16	36
NaOH (4.5)	60, then 44; H_2O	8 then o/n	43

3.3 Cyclopropene Synthesis

Certain plants use ethylene gas as a growth hormone, making it the small molecule responsible for fruit ripening, flower aging and wilting, and leaf senescence in these species. The ethylene receptor, ETR, proteins, consistently inhibit aging until bound by ethylene, stopping growth suppression.[72] Inhibitors to this mechanism were first discovered by Professor Sisler, who eventually invented ethylene antagonist 1-methylcyclopropene (1-MCP), an active ingredient still commercially available today.[73-74] This ethylene antagonist, however, is a gas with limited water solubility, that dimerizes at room temperature, requiring specialized handling and storage for use. The synthesis of water-soluble ethylene antagonist alternatives has had limited success in literature, giving broad spectrum possibilities.[73-76]

3.3.1 Experimental

Barbier Allylation

(2-1) To a black-capped vial was added diethyl ether and water (1:1, 2 mL total, [c] = 0.31 M), Sn powder (97.1 mg, 0.818 mmol), and 1,2-dibromopropene (164 mg 0.818 mmol). At room temperature, several drops of fuming HBr (48% aqueous) were added via disposable pipet.To the biphasic mixture was added formaldehyde (51.5 μL, 37% aq solution, 0.6296 mmol), which was subsequently stirred vigorously overnight. Upon completion, the mixture was diluted with diethyl ether and water, washed with diethyl ether (3 x 1 mL) and the combined organic phase dried over $MgSO_4$. The ether solution was passed over activated charcoal and the volatiles removed under reduced pressure, leaving **3-2-1** as a light yellow oil (85.5 mg, 0.566 mmol, 92% yield).

TIPS protection

(2-2) To a flame-dried black-cap vial fitted with magnetic stirring bar was added imidazole (33.8 mg, 0.497 mmol), dimethylformamide (100 μL, [c] = 2 M), and **3-2-1** (30 mg, 0.20 mmol). At room temperature, TIPS-Cl (52 μL, 46.8 mg, 0.243 mmol) was added and the reaction stirred overnight. Upon completion, the reaction mixture was diluted with diethyl ether and NH_4Cl (sat'd, aq). After separation, the aqueous layer was washed with diethyl ether (3 x 1 mL), the combined organic layer washed with brine (2 x 1 mL) and then dried over $MgSO_4$. The volatiles were removed under reduced pressure and the crude product purified by flash chromatography[77] (100% hexanes, D=15 mm, fractions 4-9), yielding pure product **3-2-2** (43 mg, 0.16 mmol, 82% yield).

Bn protection

(2-3) To a flame-dried black capped vial fitted with a magnetic stirring bar was added **3-2-1** (30 mg, 0.20 mmol), benzyl bromide (26 μL, 37 mg, 0.22 mmol) which had been passed through a pipet column of basic alumina, and dry dimethyl formamide (230 μL, [c] = 0.86 M). The reaction was cooled in an ice bath before NaH (5.5 mg, 0.23 mmol) was added and the reaction stirred overnight. Upon completion, the solution was washed with NH_4Cl (1 mL, aq, sat'd) and diethyl ether (1 mL). The aqueous layer was washed with diethyl ether (3 x 1 mL), the combined organic layers washed with brine (2 x 1 mL) and dried over $MgSO_4$. The volatiles were removed before

the crude product was purified by flash chromatography (5% Ethyl acetate in hexanes, D=15 mm, fractions 5-9) yielding the pure compound **3-Bn** (35.7 mg, 0.125 mmol, 62%).

Cyclopropanation

(2-8) To a black capped vial was added **3-2-2** (41 mg, 0.16 mmol), bromoform (27 μL, 78 mg, 0.31 mmol) and the phase transfer catalyst tributylbenzylammonium chloride (approx. 5 mg) in dichloromethane (100 μL, [c] = 1.6 M). The solution was cooled in an ice bath before adding NaOH (37 mg, 0.93 mmol) and stirring over the weekend (60 h). Upon completion, the volatiles were removed under reduced pressure and the crude mixture purified by flash chromatography (100% hexanes for 30 fractions to remove excess bromoform; D=15 mm, 5% ethyl acetate in hexanes, pure within 10 fractions) yielding **3-2-3** (39 mg, 0.089 mmol, 58% yield) as a brown oil.

Ethoxyethyl ether protection

(2-11) To a flame-dried 10 mL roundbottom flask fitted with a magnetic stirring bar was added $CaSO_4$ and dry THF (4 mL, [c] = 0.1 M), pTSA•H_2O (3.5 mg, 0.020 mmol), and **3-2-1** (60 mg, 0.40 mmol). The solution was cooled in an ice bath before the dropwise addition of ethyl vinyl ether (114 μL, 86 mg, 1.2 mmol) and stirring overnight. The yellow solution was cooled to 0 °C before quenching with $NaHCO_3$ (aq, sat'd). The reaction mixture was extracted with diethyl ether (3 x 4 mL) and the combined organic layers dried over $MgSO_4$. The volatiles were removed under reduced pressure producing **3-2-4** (74 mg, 0.33 mmol, 83% yield).

3.3.2 Reactivity

Based on the previous work by Zhang, dimethyl malonate was used as the initial handle for cyclopropene derivatization.[78] Strategic problems were found early, though.

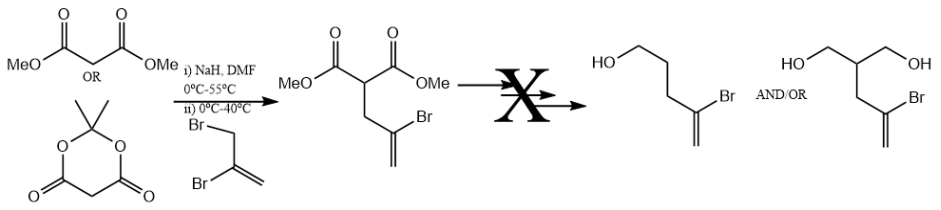

Figure 3-5: Initial synthetic strategy for ethylene antagonist handle.

Alkylation of dimethyl malonate with 2,3-dibromopropene worked efficiently, but the decarboxylation proved intractable. Multiple Krapcho decarboxylation conditions (Table 2) proved ineffective, and ester hydrolysis, table 3, under basic or acidic conditions caused either decomposition or took over 24 hours. The decarboxylation of the dicarboxylic acid was also ineffective, and Meldrum's acid shared the same limitations as dimethyl malonate.

Table 3-2: Krapcho decarboxylation conditions.

Book-pp	Solvent (equiv)	T (^oC), time (hour)	Nucleophile (equiv)	Yield
1-134	DMSO, H_2O (6)	140, o/n	NaCl-(2.2)	16%
1-135	Boric acid (1)	190, 4	Boric acid (1)	Incomplete, Evaporation
1-141	Dmso, H_2O-5	80, 24	NaCl (5)	Decomposition
1-147	DMSO, DMF, neat, DMAniline	87, o/n	-	NR
1-153A	DMF, $CsCO_3$(0.6)	78, o/n	Thiophenol,	Decomposition
1-153B	DMF, $CsCO_3$(0.6)	78, o/n	Boric acid	Decomposition
1-153C	DMF, $CsCO_3$(0.6)	78, o/n	H_2O_2	Decomposition

A new strategy was utilized, where 2,3-dribromopropene is converted to an allyl nitrile via nucleophilic addition of sodium cyanide (NaCN), which can be hydrolyzed and reduced to the same amenable handle. S_N2 displacement of bromide with NaCN yielded multiple products with crude yields <50% under multiple conditions, but it was found that the Barbier allylation, using tin dust or $SnCl_2$, cleanly yielded the desired alcohol from formaldehyde and 2,3-dibromopropene in one step with good yields.

Table 3-3: Substituted dimethyl malonate conditions.

Base (equiv)	Solvent	T (^{o}C), t (hr)	Yield
NaOH (2.5)	1:1:1 THF:MeOH:H_2O	60, 2	Decomp
NaOH (2.0)	1:1:1 THF:MeOH:H_2O	Rt, 48	60%
LiOH (2.0)	1:1:1 THF:MeOH:H_2O	Rt, 24+	Incomplete
NaOH (1.0)	1:1:1 THF:MeOH:H_2O	40, 1	84
NaOH (1.0)	1:1:1 THF:MeOH:H_2O	40, 24+	Incomplete
NaOH (6), $CHBr_3$ (2)	DCM, PTC (2%)	Rt, o/n	Crude prod

Protecting groups for the alcohol were tested before cyclopropanation, with TIPS being superior to Bn in yield during protecting and the subsequent carbene cyclopropanation. Cyclopropanation was found to take 40-60 hours under optimized conditions. The product 1,1,2-tribromocyclopropane, has limited solution stability at rt and is not amenable to column chromatography. MeLi converted the 1,1,2-tribromocyclopropane into the desired cyclopropene, albeit the reaction was incomplete. The crude, neat protected cyclopropene was stable at 0^{o}C over 24 hours; the long term tribromocyclopropane and the crude cyclopropene stability are currently being evaluated neat at 0 ^{o}C.

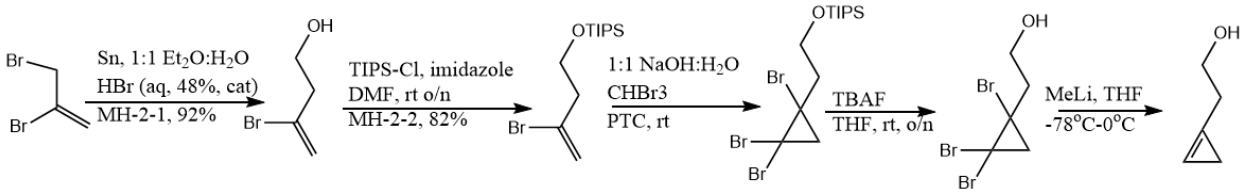

Figure 3-6: Current synthetic strategy for cyclopropene handle.

An initial HMG inhibitor was synthesized, with an emphasis on lab technique, synthetic problem solving, and time management as major learning objectives. Competency within these objectives was demonstrated via inhibitor and peptide linker syntheses. A synthetic strategy, Figure 3-7 below, has been tested and is currently being optimized.

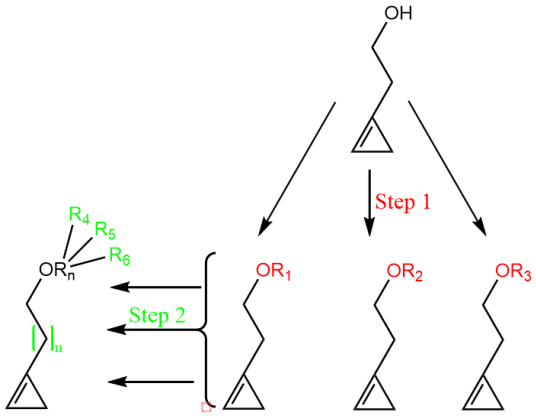

Figure 3-7: General future plans.

REFERENCES

1. Thomas, F., Ten Years of a Biomimetic Approach to the Copper(II) Radical Site of Galactose Oxidase. *European Journal of Inorganic Chemistry* **2007,** *2007* (17), 2379-2404.

2. Speier, G.; Whalen, A. M.; Csihony, J.; Pierpont, C. G., Iminosemiquinone Complexes of Copper, Structural, Magnetic, and Electrochemical Characterization of Complexes of the Phenoxazinolate Semiquinone Radical. *Inorganic Chemistry* **1995,** *34* (6), 1355-1360.

3. Rajabimoghadam, K.; Darwish, Y.; Bashir, U.; Pitman, D.; Eichelberger, S.; Siegler, M. A.; Swart, M.; Garcia-Bosch, I., Catalytic Aerobic Oxidation of Alcohols by Copper Complexes Bearing Redox-Active Ligands with Tunable H-Bonding Groups. *J Am Chem Soc* **2018,** *140* (48), 16625-16634.

4. Largeron, M., Aerobic catalytic systems inspired by copper amine oxidases: recent developments and synthetic applications. *Org Biomol Chem* **2017,** *15* (22), 4722-4730.

5. Lu, W.; Xi, C., CuCl-catalyzed aerobic oxidative reaction of primary aromatic amines. *Tetrahedron Letters* **2008,** *49* (25), 4011-4015.

6. Chaudhuri, P.; Hess, M.; Müller, J.; Hildenbrand, K.; Bill, E.; Weyhermüller, T.; Wieghardt, K., Aerobic Oxidation of Primary Alcohols (Including Methanol) by Copper(II)− and Zinc(II)−Phenoxyl Radical Catalysts. *Journal of the American Chemical Society* **1999,** *121* (41), 9599-9610.

7. Speier, G.; Csihony, J.; Whalen, A. M.; Pierpont, C. G., Studies on Aerobic Reactions of Ammonia/3,5-Di-tert-butylcatechol Schiff-Base Condensation Products with Copper, Copper(I), and Copper(II). Strong Copper(II)−Radical Ferromagnetic Exchange and Observations on a Unique N−N Coupling Reaction. *Inorganic Chemistry* **1996,** *35* (12), 3519-3524.

8. Ren, Y.; Cheaib, K.; Jacquet, J.; Vezin, H.; Fensterbank, L.; Orio, M.; Blanchard, S.; Desage-El Murr, M., Copper-Catalyzed Aziridination with Redox-Active Ligands: Molecular Spin Catalysis. *Chemistry* **2018,** *24* (20), 5086-5090.

9. Wilfred L.F. Armarego, C. C., Purification of Organic Chemicals. In *Purification of Laboratory Chemicals*, Seventh Edition ed.; Wilfred L.F. Armarego, C. C., Ed. Elsevier: 2013; pp 103-554.

10. Jacquet, J.; Blanchard, S.; Derat, E.; Desage-El Murr, M.; Fensterbank, L., Redox-ligand sustains controlled generation of CF3 radicals by well-defined copper complex. *Chem Sci* **2016,** *7* (3), 2030-2036.

11. Jacquet, J.; Salanouve, E.; Orio, M.; Vezin, H.; Blanchard, S.; Derat, E.; Desage-El Murr, M.; Fensterbank, L., Iminosemiquinone radical ligands enable access to a well-defined redox-active Cu(II)-CF(3) complex. *Chem Commun (Camb)* **2014,** *50* (72), 10394-7.

12. Smith, A. L.; Hardcastle, K. I.; Soper, J. D., Redox-Active Ligand-Mediated Oxidative Addition and Reductive Elimination at Square Planar Cobalt(III): Multielectron Reactions for Cross-Coupling. *Journal of the American Chemical Society* **2010,** *132* (41), 14358-14360.

13. Coughlin, E. J. Facilitating Multi-Electron Chemsitry in the F-Block Using Iminoquinone Ligands. PhD. Dissertation, Purdue University, West Lafayette, 2019.

14. Mukherjee, C.; Weyhermüller, T.; Bothe, E.; Chaudhuri, P., Oxidation of an o-Iminobenzosemiquinone Radical Ligand by Molecular Bromine: Structural, Spectroscopic, and Reactivity Studies of a Copper(II) o-Iminobenzoquinone Complex. *Inorg. Chem.* **2008,** *47* (7), 2740-2746.

15. Mondal, M. K.; Biswas, A. K.; Ganguly, B.; Mukherjee, C., Unprecedented iminobenzosemiquinone and iminobenzoquinone coordinated mononuclear Cu(ii) complex formation under air. *Dalton Trans.* **2015,** *44* (20), 9375-9381.

16. Balaghi, S. E.; Safaei, E.; Chiang, L.; Wong, E. W. Y.; Savard, D.; Clarke, R. M.; Storr, T., Synthesis, characterization and catalytic activity of copper(ii) complexes containing a redox-active benzoxazole iminosemiquinone ligand. *Dalton Trans.* **2013,** *42* (19), 6829-6839.

17. Paul, G. C.; Das, K.; Maity, S.; Begum, S.; Srivastava, H. K.; Mukherjee, C., Geometry-Driven Iminosemiquinone Radical to Cu(II) Electron Transfer and Stabilization of an Elusive Five-Coordinate Cu(I) Complex: Synthesis, Characterization, and Reactivity with KO2. *Inorg Chem* **2019,** *58* (3), 1782-1793.

18. Mondal, M. K.; Mukherjee, C., An unprecedented one-step synthesis of octahedral Cu(ii)-bis(iminoquinone) complexes and their reactivity with NaBH4. *Dalton Trans* **2016,** *45* (34), 13532-40.

19. Ghaffari, B.; Vanchura, B. A.; Chotana, G. A.; Staples, R. J.; Holmes, D.; Maleczka, R. E.; Smith, M. R., Reversible Borylene Formation from Ring Opening of Pinacolborane and Other Intermediates Generated from Five-Coordinate Tris-Boryl Complexes: Implications for Catalytic C–H Borylation. *Organometallics* **2015,** *34* (19), 4732-4740.

20. Coughlin Ezra, J.; Zeller, M.; Bart Suzanne, C., Neodymium(III) Complexes Capable of Multi-Electron Redox Chemistry. *Angew. Chem.* **2017,** *129* (40), 12310-12313.

21. Chaudhuri, P.; Verani, C. N.; Bill, E.; Bothe, E.; Weyhermüller, T.; Wieghardt, K., Electronic Structure of Bis(o-iminobenzosemiquinonato)metal Complexes (Cu, Ni, Pd). The Art of Establishing Physical Oxidation States in Transition-Metal Complexes Containing Radical Ligands. *Journal of the American Chemical Society* **2001,** *123* (10), 2213-2223.

22. Ye, S.; Sarkar, B.; Lissner, F.; Schleid, T.; Van Slageren, J.; Fiedler, J.; Kaim, W., Three-Spin System with a Twist: A Bis(semiquinonato)copper Complex with a Nonplanar Configuration at the Copper(II) Center. *Angewandte Chemie International Edition* **2005,** *44* (14), 2103-2106.

23. LANGE, C. G. P. a. C. W., The Chemistry of Transition Metal ComplexesContaining Catechol and Semiquinone Ligands. **1994**.

24. Piskunov, A. V.; Pashanova, K. I.; Bogomyakov, A. S.; Smolyaninov, I. V.; Berberova, N. T.; Fukin, G. K., Copper(II) complexes bearing o-iminosemiquinonate ligands with augmented aromatic substituents. *Polyhedron* **2016,** *119*, 286-292.

25. Lyaskovskyy, V.; De Bruin, B., Redox Non-Innocent Ligands: Versatile New Tools to Control Catalytic Reactions. *ACS Catalysis* **2012,** *2* (2), 270-279.

26. Broere, D. L. J.; Plessius, R.; Van Der Vlugt, J. I., New avenues for ligand-mediated processes – expanding metal reactivity by the use of redox-active catechol, o-aminophenol and o-phenylenediamine ligands. *Chemical Society Reviews* **2015,** *44* (19), 6886-6915.

27. Kaim, W., The Shrinking World of Innocent Ligands: Conventionaland Non-Conventional Redox-Active Ligands. *European Journal of Inorganic Chemistry* **2012,** *2012* (3), 343-348.

28. Rakshit, R.; Mukherjee, C., Secondary Interactions versus Intramolecular π-π Interactions in CuII-Diradical Complexes. *European Journal of Inorganic Chemistry* **2016,** *2016* (17), 2731-2737.

29. Carsch, K. M.; Dimucci, I. M.; Iovan, D. A.; Li, A.; Zheng, S.-L.; Titus, C. J.; Lee, S. J.; Irwin, K. D.; Nordlund, D.; Lancaster, K. M.; Betley, T. A., Synthesis of a copper-supported triplet nitrene complex pertinent to copper-catalyzed amination. *Science* **2019,** *365* (6458), 1138-1143.

30. Mindiola, D. J., Oxidatively Induced Abstraction Reactions. A Synthetic Approach to Low-Coordinate and Reactive Early Transition Metal Complexes Containing Metal−Ligand Multiple Bonds. *Accounts of Chemical Research* **2006,** *39* (11), 813-821.

31. Hoffmann, R.; Alvarez, S.; Mealli, C.; Falceto, A.; Cahill, T. J.; Zeng, T.; Manca, G., From Widely Accepted Concepts in Coordination Chemistry to Inverted Ligand Fields. *Chemical Reviews* **2016,** *116* (14), 8173-8192.

32. Walroth, R. C.; Lukens, J. T.; Macmillan, S. N.; Finkelstein, K. D.; Lancaster, K. M., Spectroscopic Evidence for a 3d10 Ground State Electronic Configuration and Ligand Field Inversion in [Cu(CF3)4]1–. *Journal of the American Chemical Society* **2016,** *138* (6), 1922-1931.

33. Conner, K. M.; Perugini, A. L.; Malabute, M.; Brown, S. N., Group 10 Bis(iminosemiquinone) Complexes: Measurement of Singlet–Triplet Gaps and Analysis of the Effects of Metal and Geometry on Electronic Structure. *Inorganic Chemistry* **2018,** *57* (6), 3272-3286.

34. Jacquet, J.; Cheaib, K.; Ren, Y.; Vezin, H.; Orio, M.; Blanchard, S.; Fensterbank, L.; Desage-El Murr, M., Circumventing Intrinsic Metal Reactivity: Radical Generation with Redox-Active Ligands. *Chemistry* **2017,** *23* (60), 15030-15034.

35. Balaghi, S. E.; Safaei, E.; Chiang, L.; Wong, E. W.; Savard, D.; Clarke, R. M.; Storr, T., Synthesis, characterization and catalytic activity of copper(II) complexes containing a redox-active benzoxazole iminosemiquinone ligand. *Dalton Trans* **2013,** *42* (19), 6829-39.

36. Piskunov, A. V.; Meshcheryakova, I. N.; Smolyaninov, I. V.; Fukin, G. K.; Cherkasov, V. K.; Abakumov, G. A., Stable organomercury compounds containing an o-iminosemiquinone radical ligand. *Russian Chemical Bulletin* **2013,** *62* (1), 147-156.

37. Carsch, K. M.; Lukens, J. T.; DiMucci, I. M.; Iovan, D. A.; Zheng, S. L.; Lancaster, K. M.; Betley, T. A., Electronic Structures and Reactivity Profiles of Aryl Nitrenoid-Bridged Dicopper Complexes. *J Am Chem Soc* **2020,** *142* (5), 2264-2276.

38. Rajput, A.; Sharma, A. K.; Barman, S. K.; Saha, A.; Mukherjee, R., Valence tautomerism and delocalization in transition metal complexes of o-amidophenolates and other redox-active ligands. Some recent results. *Coordination Chemistry Reviews* **2020,** *414*, 213240.

39. Chang, H.-C.; Lo, F.-C.; Liu, W.-C.; Lin, T.-H.; Liaw, W.-F.; Kuo, T.-S.; Lee, W.-Z., Ambient Stable Trigonal Bipyramidal Copper(III) Complexes Equipped with an Exchangeable Axial Ligand. *Inorganic Chemistry* **2015,** *54* (11), 5527-5533.

40. Murugesu, M.; Schelter, E. J., Not Just Lewis Acids: Preface for the Forum on New Trends and Applications for Lanthanides. *Inorganic Chemistry* **2016,** *55* (20), 9951-9953.

41. Macdonald, M. R.; Bates, J. E.; Ziller, J. W.; Furche, F.; Evans, W. J., Completing the Series of +2 Ions for the Lanthanide Elements: Synthesis of Molecular Complexes of Pr2+, Gd2+, Tb2+, and Lu2+. *Journal of the American Chemical Society* **2013,** *135* (26), 9857-9868.

42. Fedushkin, I. L.; Yambulatov, D. S.; Skatova, A. A.; Baranov, E. V.; Demeshko, S.; Bogomyakov, A. S.; Ovcharenko, V. I.; Zueva, E. M., Ytterbium and Europium Complexes of Redox-Active Ligands: Searching for Redox Isomerism. *Inorganic Chemistry* **2017,** *56* (16), 9825-9833.

43. Fedushkin, I. L.; Maslova, O. V.; Morozov, A. G.; Dechert, S.; Demeshko, S.; Meyer, F., Genuine Redox Isomerism in a Rare-Earth-Metal Complex. *Angewandte Chemie International Edition* **2012,** *51* (42), 10584-10587.

44. Halbach, R. L.; Nocton, G.; Amaro-Estrada, J. I.; Maron, L.; Booth, C. H.; Andersen, R. A., Understanding the Multiconfigurational Ground and Excited States in Lanthanide Tetrakis Bipyridine Complexes from Experimental and CASSCF Computational Studies. *Inorganic Chemistry* **2019,** *58* (18), 12083-12098.

45. Booth, C. H.; Walter, M. D.; Kazhdan, D.; Hu, Y.-J.; Lukens, W. W.; Bauer, E. D.; Maron, L.; Eisenstein, O.; Andersen, R. A., Decamethylytterbocene Complexes of Bipyridines and Diazabutadienes: Multiconfigurational Ground States and Open-Shell Singlet Formation. *Journal of the American Chemical Society* **2009,** *131* (18), 6480-6491.

46. Coughlin, E. J.; Zeller, M.; Bart, S. C., Neodymium(III) Complexes Capable of Multi-Electron Redox Chemistry. *Angewandte Chemie International Edition* **2017,** *56* (40), 12142-12145.

47. Vaddypally, S.; McKendry, I. G.; Tomlinson, W.; Hooper, J. P.; Zdilla, M. J., Electronic Structure of Manganese Complexes of the Redox-Non-innocent Tetrazene Ligand and Evidence for the Metal-Azide/Imido Cycloaddition Intermediate. *Chemistry - A European Journal* **2016,** *22* (30), 10548-10557.

48. Aldrich, K. E.; Odom, A. L., A photochemical route to a square planar, ruthenium(iv)-bis(imide). *Chemical Communications* **2019,** *55* (30), 4403-4406.

49. Hakey, B. M.; Darmon, J. M.; Akhmedov, N. G.; Petersen, J. L.; Milsmann, C., Reactivity of Pyridine Dipyrrolide Iron(II) Complexes with Organic Azides: C–H Amination and Iron Tetrazene Formation. *Inorganic Chemistry* **2019,** *58* (16), 11028-11042.

50. Demmin, T. R.; Swerdloff, M. D.; Rogic, M. M., Copper(II)-induced oxidations of aromatic substrates: catalytic conversion of catechols to o-benzoquinones. Copper phenoxides as intermediates in the oxidation of phenol, and a single-step conversion of phenol, ammonia, and oxygen into muconic acid mononi. *Journal of the American Chemical Society* **1981,** *103* (19), 5795-5804.

51. *CRC Handbook of Chemistry and Physics*. 87th ed.; CRC Press: Boca Raton, FL, 2006.

52. Evans, D. F., 400. The determination of the paramagnetic susceptibility of substances in solution by nuclear magnetic resonance. *Journal of the Chemical Society (Resumed)* **1959**, 2003.

53. Bera, P.; Brandão, P.; Mondal, G.; Jana, H.; Jana, A.; Santra, A.; Bera, P., Synthesis of a new pyridinyl thiazole ligand with hydrazone moiety and its cobalt(III) complex: X-ray crystallography, in vitro evaluation of antibacterial activity. *Polyhedron* **2017,** *134*, 230-237.

54. Bain, G. A.; Berry, J. F., Diamagnetic Corrections and Pascal's Constants. *Journal of Chemical Education* **2008,** *85* (4), 532.

55. Schultz, M.; Boncella, J. M.; Berg, D. J.; Tilley, T. D.; Andersen, R. A., Coordination of 2,2‘-Bipyridyl and 1,10-Phenanthroline to Substituted Ytterbocenes: An Experimental Investigation of Spin Coupling in Lanthanide Complexes. *Organometallics* **2002,** *21* (3), 460-472.

56. Lukens, W. W.; Magnani, N.; Booth, C. H., Application of the Hubbard Model to Cp*2Yb(bipy), a Model System for Strong Exchange Coupling in Lanthanide Systems. *Inorganic Chemistry* **2012,** *51* (19), 10105-10110.

57. Lu, E.; Chu, J.; Chen, Y., Scandium Terminal Imido Chemistry. *Accounts of Chemical Research* **2018,** *51* (2), 557-566.

58. Schädle, D.; Meermann-Zimmermann, M.; Schädle, C.; Maichle-Mössmer, C.; Anwander, R., Rare-Earth Metal Complexes with Terminal Imido Ligands. *European Journal of Inorganic Chemistry* **2015,** *2015* (8), 1334-1339.

59. Schadle, D.; Anwander, R., Rare-earth metal and actinide organoimide chemistry. *Chem Soc Rev* **2019,** *48* (24), 5752-5805.

60. Solola, L. A.; Zabula, A. V.; Dorfner, W. L.; Manor, B. C.; Carroll, P. J.; Schelter, E. J., Cerium(IV) Imido Complexes: Structural, Computational, and Reactivity Studies. *J Am Chem Soc* **2017,** *139* (6), 2435-2442.

61. Yousif, M.; Wannipurage, D.; Huizenga, C. D.; Washnock-Schmid, E.; Peraino, N. J.; Ozarowski, A.; Stoian, S. A.; Lord, R. L.; Groysman, S., Catalytic Nitrene Homocoupling by an Iron(II) Bis(alkoxide) Complex: Bulking Up the Alkoxide Enables a Wider Range of Substrates and Provides Insight into the Reaction Mechanism. *Inorganic Chemistry* **2018,** *57* (15), 9425-9438.

62. Ng, W.-M.; Guo, X.; Cheung, W.-M.; So, Y.-M.; Chong, M.-C.; Sung, H. H. Y.; Williams, I. D.; Lin, Z.; Leung, W.-H., 4-Coordinated, 14-electron ruthenium(ii) chalcogenolate complexes: synthesis, electronic structure and reactions with PhICl2 and organic azides. *Dalton Transactions* **2019,** *48* (35), 13315-13325.

63. Kepp, K. P., A Quantitative Scale of Oxophilicity and Thiophilicity. *Inorganic Chemistry* **2016,** *55* (18), 9461-9470.

64. Nelson, R. E.; Hatfield, K. M.; Wolford, H.; Samore, M. H.; Scott, R. D.; Reddy, S. C.; Olubajo, B.; Paul, P.; Jernigan, J. A.; Baggs, J., National Estimates of Healthcare Costs Associated With Multidrug-Resistant Bacterial Infections Among Hospitalized Patients in the United States. *Clinical Infectious Diseases* **2021,** *72* (Supplement_1), S17-S26.

65. Antibiotic resistance threats in the United States, 2019. **2019**.

66. Björkhem-Bergman, L.; Bergman, P.; Andersson, J.; Lindh, J. D., Statin Treatment and Mortality in Bacterial Infections – A Systematic Review and Meta-Analysis. *PLoS ONE* **2010,** *5* (5), e10702.

67. Hsu, J.; Andes, D. R.; Knasinski, V.; Pirsch, J.; Safdar, N., Statins are associated with improved outcomes of bloodstream infection in solid-organ transplant recipients. *European Journal of Clinical Microbiology & Infectious Diseases* **2009,** *28* (11), 1343-1351.

68. Jerwood, S.; Cohen, J., Unexpected antimicrobial effect of statins. *Journal of Antimicrobial Chemotherapy* **2007,** *61* (2), 362-364.

69. Stauffacher; Cynthia (Lafayette, I., Lipton; Mark Alfred (Lafayette, IN), Seleem; Mohamed Naguieb (West Lafayette, IN), Schmidt; Tim Jonathan (Lafayette, IN), Steussy, Jr.; Calvin Nicklaus (Indianapolis, IN), Rodwell; Victor W (West Lafayette, IN) Class II HMG-CoA reductase inhibitors and methods of use. 9,604,925, 2017.

70. Singh, S. B.; Jayasuriya, H.; Ondeyka, J. G.; Herath, K. B.; Zhang, C.; Zink, D. L.; Tsou, N. N.; Ball, R. G.; Basilio, A.; Genilloud, O.; Diez, M. T.; Vicente, F.; Pelaez, F.; Young, K.; Wang, J., Isolation, Structure, and Absolute Stereochemistry of Platensimycin, A Broad Spectrum Antibiotic Discovered Using an Antisense Differential Sensitivity Strategy. *Journal of the American Chemical Society* **2006,** *128* (36), 11916-11920.

71. Singh, S. B.; Jayasuriya, H.; Ondeyka, J. G.; Herath, K. B.; Zhang, C.; Zink, D. L.; Tsou, N. N.; Ball, R. G.; Basilio, A.; Genilloud, O.; Diez, M. T.; Vicente, F.; Pelaez, F.; Young, K.; Wang, J., Isolation, Structure, and Absolute Stereochemistry of Platensimycin, A Broad Spectrum Antibiotic Discovered Using an Antisense Differential Sensitivity Strategy [J. Am. Chem. Soc.2006,128, 11916−11920]. *Journal of the American Chemical Society* **2006,** *128* (48), 15547-15547.

72. Lacey, R. F.; Binder, B. M., How plants sense ethylene gas — The ethylene receptors. *Journal of Inorganic Biochemistry* **2014,** *133*, 58-62.

73. Edward C. Sisler, R., NC Methods of Blocking Ethylene Resposne in Plants. 6,194,350 B1, 2001.

74. Edward C. Sisler, R. S. M. B., Apex, both of N.C. Method of counteracting an ethylene response in plants. 5,518,988, May 21, 1996, 1996.

75. Goren, R.; Huberman, M.; Riov, J.; Goldschmidt, E. E.; Sisler, E. C.; Apelbaum, A., Effect of 3-cyclopropyl-1-enlyl-propanoic acid sodium salt, a novel water soluble antagonist of ethylene action, on plant responses to ethylene. *Plant Growth Regulation* **2011,** *65* (2), 327-334.

76. Pirrung, M. C.; Bleecker, A. B.; Inoue, Y.; Rodríguez, F. I.; Sugawara, N.; Wada, T.; Zou, Y.; Binder, B. M., Ethylene Receptor Antagonists: Strained Alkenes Are Necessary but Not Sufficient. *Chemistry & Biology* **2008,** *15* (4), 313-321.

77. Still, W. C.; Kahn, M.; Mitra, A., Rapid chromatographic technique for preparative separations with moderate resolution. *The Journal of Organic Chemistry* **1978,** *43* (14), 2923-2925.

78. Zhang, B. Synthesis of Ethylene Antagonists and an Anticancer DUPA Conjugate. Masters, Purdue University, West Lafayette, IN, 2018.

79. 5-(Trifluoromethyl)dibenzothiopheniumtrifluoromethanesulfonate

80. Pangborn, A. B.; Giardello, M. A.; Grubbs, R. H.; Rosen, R. K.; Timmers, F. J., Safe and Convenient Procedure for Solvent Purification. *Organometallics* **1996,** *15*, 1518-1520.

81. Abakumov, G. A.; Cherkasov, V. K.; Piskunov, A. V.; Meshcheryakova, I. N.; Maleeva, A. V.; Poddel'skii, A. I.; Fukin, G. K., Zinc molecular complexes with sterically hindered o-quinone and o-iminoquinone. *Dokl. Chem.* **2009,** *427* (1), 168-171.

82. Chakraborty, S.; Chattopadhyay, J.; Guo, W.; Billups, W. E., *Angew. Chem. Int. Ed.* **2007,** *46* (24), 4486-4488.

83. 2013/2014., B. *Apex3 v2016.9-0, Saint V8.34A,SAINT V8.37A*, Madison, WI, USA 2016.

84. Sheldrick, G. M., Crystal structure refinement with SHELXL. *Acta Crystallogr., Sect. C: Struct. Chem.* **2015,** *71* (1), 3-8.

85. Huebschle, C. B.; Sheldrick, G. M.; Dittrich, B., ShelXle: a Qt graphical user interface for SHELXL. *J. Appl. Crystallogr.* **2011,** *44* (6), 1281-1284.

86. Ranis, L. G.; Werellapatha, K.; Pietrini, N. J.; Bunker, B. A.; Brown, S. N., Metal and Ligand Effects on Bonding in Group 6 Complexes of Redox-Active Amidodiphenoxides. *Inorg. Chem.* **2014,** *53* (19), 10203-10216.

VITA

EDUCATION

PhD Purdue University, Synthetic Chemistry Expected Aug 2021

BS The Ohio State University, Chemistry May 4, 2014

RESEARCH EXPERIENCE

Redox Active Ligands to Facilitate Novel Reactivity from Redox Restricted Metals, Purdue University, Lafayette, IN Current

Advisor: Suzanne Bart

- Synthesizes copper and ytterbium organometallic complexes within a glovebox
- Develops project reactivity targets for compound elucidation
- Overcomes project difficulties utilizing literature inspired creativity and innovation
- Employs innovative approaches to synthesize a novel rare earth (lanthanide) imido and tetrazene complexes
- Synthesizes an independent nitrene/imido (as currently characterized) with copper complex counterion
- Characterization by ^{1}H and multinuclear NMR, X-Ray Diffraction, FTIR, & UV-Vis spectroscopies

Advisor: Mark Lipton 2017 to 2018

- Developed a synthetic strategy incorporating a structure-activity relationship (SAR) table
- Optimized synthetic routes and performed air sensitive reactions using Schlenk line techniques
- Synthesized a cyclopropene intermediate as a novel ethylene antagonist
- Synthesized a HMG CoA Reductase inhibitor as a potential antibiotic for *S. Aureus* and MRSA
- Characterization by UPLC, HPLC, along with ^{1}H NMR and FTIR spectroscopies

Non-Thesis Research

Advisor: Alexander Wei, Purdue University 2015 to 2017

- Synthesized hydroxylamines for field effect catalysis using Schlenk line techniques
- Characterization by ^{1}H NMR spectroscopy and GC/MS

Advisor: Christopher Callam, The Ohio State University 2010 to 2014

- Synthesized oligosaccharides for fluoroaffinity purification

WORK EXPERIENCE

E&J Gallo Winery, Modesto, CA

Graduate Student Research Internship Jun 2020 to December 2020

- Designs experiments to correlate wine sensory mouthfeel with wine chemistry using an Isothermal Titration Calorimeter (ITC)
- Develops a SOP, quality control processes, and maintenance plans for the ITC

- Acquires and analyzes complex ITC data to elucidate the thermodynamic profiles of the interactions between wine tannins and saliva proteins
- Supports wine macromolecules characterization utilizing gel permeation chromatography (GPC) and ion chromatography (IC)
- Leads a team in processing smoke tainted grape samples into lab samples

Purdue University, West Lafayette, IN

- Graduate Teaching Assistant, Organic Chemistry 255, 256, and 257; Aug 2015 to August 2021

The Ohio State University, Columbus, OH

- Undergraduate Teaching Assistant, General Chemistry 110 Aug 2014 to May 2015
- Organic Compound Spectroscopic Library
  Summer 2011

SELECTED PUBLICATIONS

- Hewitt, M.C., Coughlin, E.J, Lin, N., Zeller, M. and Bart, S.C., "Ion stabilized iminyl radical via copper bis(amidophenolate) complex" Manuscript in Progress
- Hewitt, M.C., Coughlin, E.J, Zeller, M. and Bart, S.C., "Terminal ytterbium(III) imido and tetrazene complexes" Manuscript in Progress

PRESENTATIONS AND INVITED LECTURES

- **Poster Presentation**, "Redox active ligands for redox restricted metals," PINDU, 11-11-2019.
- **Poster Presentation**, "Highly reduced amidophenolate copper (II) complex," Ohio Inorganic Weekend, 11-1-2019.
- **Poster Presentation**, "Polyfluorooligosaccharides for easy carbohydrate purification," Denman Undergraduate Research Forum, 5-2014.

HONORS AND AWARDS

- **Eagle Scout** 2009

COMMUNITY SERVICE

National Chemistry Week

- Volunteer, Lafayette School District, 2015, 2017 to 2018

Science Olympiad

- Volunteer, The Ohio State University, 2011-2014

ACTIVITIES

Phi Lambda Upsilon-Honorary Chemical Society

- Member Current

Graduate Student Advisory Board (GSAB)

- Member 2011 to 2014
- Scholarship Chair 2011 to 2012

Alpha Tau Zeta Chapter of FarmHouse International Fraternity

- Member 2011 to 2014
- Scholarship Chair 2011 to 2012

PUBLICATIONS

Incomplete Copper Manuscript

Electronic Structure and Reactivity of Copper Iminoquinone Complexes

*Matthew Hewitt, Ezra J. Coughlin, Nathan Lin, Matthias Zeller, Shiliang Tian, and Suzanne C. Bart**

H.C. Brown Laboratory, Department of Chemistry, Purdue University, West Lafayette, Indiana 47907, United States

Introduction

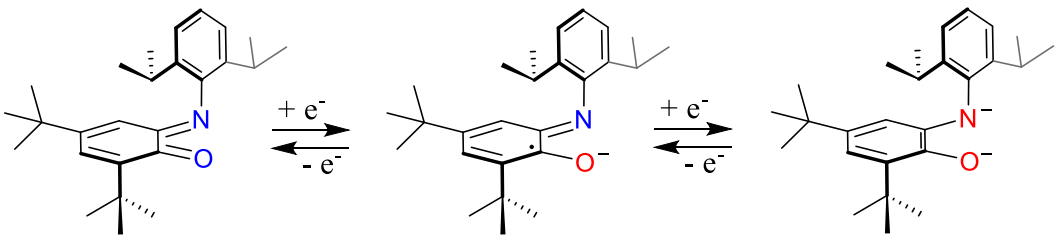

Figure 1: Reduction of the iminoquinone ligand, demonstrating its versatile redox chemistry.

Metalloenzymes have been a large source of novel organometallic complexes since the mid-1990s.[1] Organic radicals were shown to be instrumental to enzymatic electron transfer in the copper based metalloenzyme, Galactose Oxidase (GAO). GAO became the standard reference for such reactivity, which uses a tyrosine phenoxyl radical for oxidation. This enzyme, along with

related quinone-like cofactor containing enzymes such as pterin-dependent hydroxylases[2], have been the basis for using the iminosemiquinone ligand with copper to perform redox facilitated organic transformations. The initial focus was replicating the biomolecular activity of aerobic oxidation,[3-7] but the system's reactivity has recently been expanded.[8, 10] Using the iminosemiquinone ligand system became of interest to facilitate expanding the chemistry of copper and to isolate rare or novel catalytically important intermediates.

Copper nitrene chemistry has been important for N incorporation in organic molecules as a proposed intermediate to alkene aziridination and C-H amination. The electronic structure of the Cu-N multiple bond is important to determining the reactivity and nitrene transfer chemistry, allowing for improved characterization and targeted catalyst design for reaction specificity.[29] Metal ligand multiple bonds are quite rare for late, first row transition metals due to the poor orbital and spatial overlap of these harder metals. The copper iminosemiquinone system has already been shown to be a good catalyst for nitrene transfer.[8] Furthermore, the low lying redox active ligand orbitals could facilitate an increased stability of a copper nitrene with more control over the desired reactivity through ligand substitution; this would facilitate an easy and expedited study of the effects of electronics through a combination of ligand substitution and redox chemistry. The bond distances of the iminosemiquinone ligand could also be a substitute for potentially expensive and time consuming XAS of a reactive complex, facilitating easy ligand and metal oxidation state analysis.[1-2, 10, 16-18, 33-36] The redox non-innocent nature of both the nitrogen ligand and copper complex scaffold have been important in the most recent works of copper/nitrogen multiple bonds, whether a copper nitrene, imide, or iminyl.[29, 37]

The reactivity of various copper(II) iminosemiquinone species were initially investigated as galactose oxidase metalloenzyme mimics, focusing on aerobic oxidation of alcohols and amines.[3-7] Once established, alternative reactions testing reversibility and redox chemistry of the system were investigated including $CuCl_2$[18, 35] various oxidants, and KO_2.[17] Copper(II) iminoquinone was shown to oxidize hydrides to dihydrogen (H_2)[18] and copper(II) iminosemiquinones radical reactivity have also been shown using the trifluoromethyl carbocation donor (CF_3^+) Umemoto's reagent[79] both stoichiometrically and to catalytically trifluoromethylate various radical acceptors.[10-11] Most intriguingly, copper(II) iminosemiquinones have been shown to catalytically aziridinate styrene and its derivatives, as well as other alkenes, thanks to the 'spin fluxionality' of the species, where the redox active ligands and copper(II) shifting spin coupling allow it to access

typically high energy, spin forbidden mechanistic pathways.[8] This ability to modulate its spin to expand the reactivity of copper(II) reactivity lead to our investigation of the system further in an effort to stabilize a copper nitrene.

Experimental Section

General Considerations. All air- and moisture-sensitive manipulations were performed using standard Schlenk techniques or in an MBraun inert atmosphere drybox with an atmosphere of purified nitrogen. The MBraun drybox was equipped with two −35 °C freezers for cooling samples and crystallizations. Solvents for sensitive manipulations were dried and deoxygenated using literature procedures with a Seca solvent purification system.[80] Benzene-d_6 and pyridine-d_5 were purchased from Cambridge Isotope Laboratories, dried over CaH_2 and vacuum transferred into molecular sieves. 4,6-di-*tert*-butyl-2-[(2,6-diisopropylphenyl)imino]quinone (^{Dipp}iq)[81] and potassium graphite (KC_8)[82], were prepared according to literature procedures. CuI, $[(CuOTf)_2tol]_2$ 18-crown-6 (18-C-6) were purchased from Sigma Aldrich and dried under vacuum at room temperature on a Schlenk line overnight prior to use.

^{1}H NMR spectra were recorded on a Varian Inova 300 spectrometer operating at 299.992 MHz. All chemical shifts are reported relative to the peak for $SiMe_4$, using ^{1}H (residual) chemical shifts of the solvent as a secondary standard. The spectra for all paramagnetic molecules were obtained by using an acquisition time of 0.5 s, thus the peak widths reported have an error of ±2 Hz. For all diamagnetic molecules, the ^{1}H NMR data are reported with the chemical shift, followed by the multiplicity, coupling constant in Hz, the integration value, and, where possible, the peak assignment. For all paramagnetic molecules, the ^{1}H NMR data are reported with the chemical shift, followed by the peak width at half height in Hz, the integration value, and, where possible, the peak assignment; the ^{19}F NMR data are reported with chemical shift, integration value, and where possible, the peak assignment. ^{11}B NMR spectra were recorded on a Varian Inova 300 spectrometer operating at a frequency of 96.24 MHz. ^{11}B chemical shifts are reported relative to the peak for BF_3Et_2O (0.0 ppm). ^{19}F NMR spectra were recorded on a Varian Inova 300 spectrometer.^{19}F are reported relative to $CFCl_3$ (0.0 ppm).

All voltammetric data were obtained under inert atmosphere conditions using external electrical ports of the MBraun inert drybox. All data were obtained using a Gamry Instruments Interface 1000 model potentiostat using the Gamry Instruments Laboratory software. All data were collected on samples in THF with 0.1 M $[Bu_4N][PF_6]$ supporting electrolyte concentration, and

using an internal resistance compensation of approximately 2000 ohms. Solutions were analyzed in 10 mL beakers, with a 3 mm glassy carbon working electrode, a Pt wire counter electrode, and an Ag wire quasi-reference electrode. Potential corrections were performed at the end of the experiment using the Fc/Fc^+ couple as an internal standard.

X-Band EPR spectra were recorded on a Bruker EMX EPR spectrometer and simulated using the EasySpin toolbox in MATLAB. Electronic absorption measurements were recorded at 294 K in THF in a sealed, 1 cm quartz cuvettes with a Cary 6000i UV-vis-NIR spectrophotometer. Elemental analyses were performed by Midwest Microlab (Indianapolis, IN). Solid state (KBr) infrared spectra were recorded using a Thermo Nicolet 6700 spectrophotometer.

General Crystallographic Details. Crystals of **2-isq** suitable for X-ray diffraction, were coated with poly(isobutylene) oil in a glovebox and quickly transferred to the goniometer head of a Bruker Quest diffractometer with a fixed chi angle, a sealed tube fine focus X-ray tube, single crystal curved graphite incident beam monochromator and a Photon100 CMOS area detector. Examination and data collection were performed with Mo Kα radiation (λ = 0.71073 Å). Crystals of **1-iq, 3-ap** and **3-ap crown** suitable for X-ray diffraction, were coated with poly(isobutylene) oil in a glovebox and quickly transferred to the goniometer head of a Bruker Quest diffractometer with kappa geometry, an I-μ-S microsource X-ray tube, laterally graded multilayer (Goebel) mirror single crystal for monochromatization, a Photon2 CMOS area detector and an Oxford Cryosystems low temperature device. Examination and data collection were performed with Cu Kα radiation (λ = 1.54184 Å). Data were collected, reflections were indexed and processed, and the files scaled and corrected for absorption using APEX3.[83] All data were collected with Oxford Cryosystems low temperature devices operating at 100 or 150 K.

Data were collected, reflections were indexed and processed, and the files scaled and corrected for absorption using APEX3. The space groups were assigned and the structures were solved by direct methods using XPREP within the SHELXTL suite of programs and refined by full matrix least squares against F^2 with all reflections using Shelxl2014[84] using the graphical interface Shelxle.[85] If not specified otherwise, H atoms attached to carbon and nitrogen atoms were positioned geometrically and constrained to ride on their parent atoms, with carbon hydrogen bond distances of 0.95 Å for and aromatic C-H, 1.00, 0.99 and 0.98 Å for aliphatic C-H, CH_2 and CH_3 moieties, respectively. Methyl H atoms were allowed to rotate, but not to tip, to best fit the

experimental electron density. U_{iso}(H) values were set to a multiple of U_{eq}(C) with 1.5 for CH_3, and 1.2 for CH_2 and C-H units, respectively.

Synthesis of (^{Dipp}iq)$_2$Cu^{I}(OTf) (1-iq).

A 20-mL scintillation vial was charged with [(CuOTf)$_2$tol]$_2$ (0.075 g, 0.145 mmol) and 10 mL diethyl ether. A separate 20-mL scintillation vial was charged with ^{Dipp}iq (0.220 g, 0.580 mmol), dissolved in 8 mL diethyl ether and added dropwise to the stirring [CuOTf)Tol]$_2$ slurry. A reddish-brown solution was observed. After 24 hours, the solution was filtered over Celite and volatiles were removed *in vacuo.* The resulting reddish-black solid was washed with cold pentane (3 × 10 mL) to afford a dark red powder (0.209 g, 0.215 mmol, 74% yield) assigned as (**1-iq**). X-ray quality crystals were obtained from a concentrated toluene solution stored at -35 °C. Elemental analysis of $C_{53}H_{74}N_2O_5F_3S_1Cu_1$: Calculated, C, 65.51; H, 7.68; N, 2.88. Found, C, 64.88; H, 7.83; N, 2.73. ^{1}H NMR (C_6D_6, 25 °C): δ = 1.09 (s, 18H, C(C*H*$_3$)$_3$), 1.24 (s, 18H, C(C*H*$_3$)$_3$), 1.34 (s, 12H, CH(C*H*$_3$)$_2$), 1.49 (s, 12H, CH(C*H*$_3$)$_2$), 3.97 (s, 4H, C*H*(CH$_3$)$_2$), 4.29 (s, 2H, C*H*), 6.06 (t, 7, 2H, C*H*), 7.31 (d, 6 4H, C*H*). ^{19}F NMR (C_6D_6, 25 °C): δ = -78.47 (s, 3F, -OTf).

Synthesis of (^{Dipp}isq)$_2$Cu^{II} (2-isq).

A 20-mL scintillation vial was charged with CuI (0.140 g, 0.735 mmol) and 10 mL THF. A separate 20-mL scintillation vial was charged with ^{Dipp}iq (0.558 g, 1.470 mmol), dissolved in 8 mL THF and added dropwise to the stirring CuI slurry. After stirring for 15 minutes, KC_8 (0.099 g, 0.735 mmol) was weighed by difference and added, resulting in a rapid color change from brown to dark green. After 2 hours, the solution was filtered over Celite and volatiles were removed *in vacuo*. The remaining mixture was washed with cold *n*-pentane (1 × 10 mL) to afford a green powder (0.526 g, 0.639 mmol, 87% yield) assigned as (**2-isq**). Single, X-ray quality crystals were obtained from a concentrated toluene solution at -35 °C. Elemental analysis of $C_{52}H_{74}N_2O_2Cu$: Calculated, C, 75.92; H, 9.07; N, 3.41. Found, C, 75.42; H, 9.28; N, 3.52. ^{1}H NMR (C_6D_6, 25 °C): δ = -108 (1023, 2H, C*H*), -30.0 (34, 2H, C*H*), -6.1 (32, 2H, C*H*), 1.9 (37, 18H, C(C*H*$_3$)$_3$), 3.6 (37, 12H, CH(C*H*$_3$)$_2$), 4.0 (22, 12H, CH(C*H*$_3$)$_2$), 6.5 (22, 18H, C(C*H*$_3$)$_3$), 13.1 (152, 4H, C*H*(CH$_3$)$_2$), 28.3 (43, 4H, C*H*).

Synthesis of [(^{Dipp}ap)$_2$CU^{II}][K(THF)$_2$]$_2$ (3ap) from CuCl.

To a 20 mL scintillation vial was added CuCl (99 mg, 1.00468 mmol) and ^{Dipp}iq (763 mg, 2.01 mmol, 2.0 equivalence) and 10 mL THF. The brown slurry was stirred for 30 minutes before

adding KC_8 (410 mg, 3.03 mmol, 3.0 equivalence) portion-wise over 15 minutes. The slurry was stirred for 1 hour before being filtered over Celite and the volatiles removed by high vacuum. The solid was washed with *n*-pentane (5 x 3.0 mL) yielding a purple powder (988 mg, 0.945 mmol, 94% yield). (MH-1-10) Elemental analysis of $C_{60}H_{90}N_2O_4K_2Cu_1$: Calculated, C, 68.95; H, 8.68; N, 2.68. Found, C, 68.44; H, 8.54; N, 2.57. ^{1}H NMR (C_5D_6N, 25 °C): δ = -108 (n, 2H, C*H*), -30.0 (n, 2H, C*H*), -6.1 (n, 2H, C*H*), 1.9 (n, 18H, C(CH_3)$_3$), 3.6 (n, 12H, CH(CH_3)$_2$), 4.0 (n, 12H, CH(CH_3)$_2$), 6.5 (n, 18H, C(CH_3)$_3$), 13.1 (n, 4H, C*H*(CH_3)$_2$), 28.3 (n, 4H, C*H*).

Synthesis of [(^{Dipp}ap)$_2$Cu^{II}][K(THF)$_2$]$_2$ (3-ap) from 2-isq

A 20-mL scintillation vial was charged with **2-isq** (0.100 g, 0.122 mmol) and 10 mL THF. While stirring, KC_8 (0.033 g, 0.243 mmol) was weighed by difference and added, resulting in a rapid color change from dark green to purple. After 1 hour, the solution was filtered over Celite and volatiles were removed *in vacuo*. The crude mixture was washed with cold *n*-pentane (2 × 5 mL) to afford a purple powder (0.099 g, 0.095 mmol, 78% yield) assigned as **3-ap**. Single, X-ray quality crystals were obtained from a concentrated diethyl ether solution at -35 °C.

Synthesis of [(^{Dipp}ap)$_2$Cu^{II}][K(18-crown-6)(THF)$_2$]$_2$ (3-ap crown) from 3-ap.

A 20-mL scintillation vial was charged with **3-ap** (0.330 g, 0.316 mmol) and 15 mL THF forming a red solution. While stirring, 18-crown-6 (0.167 g, 0.632 mmol) was weighed by difference and added. Immediately, a tan precipitate formed and was suspended in the THF solution. After stirring the slurry for 3 hours, volatiles were removed *in vacuo*. The crude mixture was washed with cold diethyl ether (2 × 10 mL) to afford a tan powder (0.472 g, 0.275 mmol, 87% yield) assigned as **3-ap crown**. X-ray quality crystals were obtained from a concentrated THF solution stored at -35 °C. Elemental analysis of $C_{92}H_{154}N_2O_{18}K_2Cu_1$: Calculated, C, 64.32; H, 9.04; N, 1.63. Found, C, 64.05; H, 8.89; N, 1.50.

Synthesis of [(^{Dipp}ap)$_2$Cu^{II}][K(18-crown-6)(Pyr)$_2$]$_2$ from 2-isq.

A 20-mL scintillation vial was charged with **2-isq** (0.100 g, 0.122 mmol), a stir bar, and 15 mL THF forming a green solution. While stirring, 18-crown-6 (0.075 g, 0.284 mmol) was weighed by difference and added in 5 portions over 2 minutes with frequent agitation. After 5 minutes of stirring the green solution, KC_8 (0.033 g, mmol) was added in 5 portions over 5 minutes. The solution became dark brown and a tan precipitate formed and was suspended in the THF solution. After stirring the slurry for 2 hours, the suspension was filtered over a bed of celite in a 15 mL medium frit to separate graphite and 3-ap crown from the THF solution. The filter cake was

washed with cold diethyl ether (3 × 10 mL) and cold pentane (3 × 5 mL) to remove residual impurities and the dirty filter flask was replaced with a clean filter flask. Pyridine was then used to dissolve the tan solids in the frit, revealing a dark orange solution. The solution was triturated with an equal volume of diethyl ether and a beige solid precipitated from the solution. Volatiles were removed *in vacuo* to afford a beige powder assigned as **3-ap crown** (0.120 g, 0.069 mmol, 57% yield).

Results and Discussion

Synthesis and Characterization of Copper Complexes

Studies were commenced by targeting a copper iminoquinone complex featuring two neutral ligands. Treating cuprous triflate was with two equivalents of ligand caused a darkening of the solution to red. After workup, a reddish-black solid was obtained in good yield (74%). ^{1}H NMR spectroscopic analysis revealed 8 diamagnetic resonances corresponding to the iminoquinone ligand, consistent with a Cu(I) formulation. ^{19}F NMR spectroscopy confirmed the presence of a triflate ion with a resonance at -78 ppm.

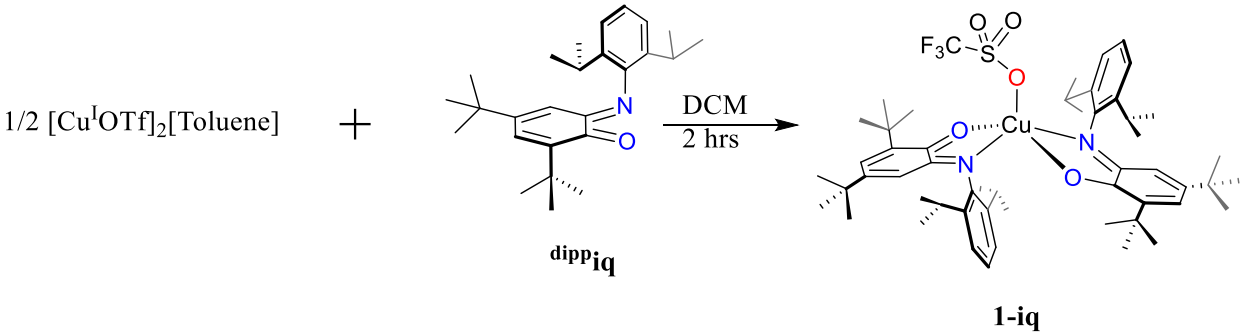

Figure 2: Reaction generating **1-iq**.

The molecular structure of **1-iq** was probed using X-ray crystallography of single crystals obtained from a concentrated toluene solution. Analysis shows a five-coordinate copper complex (Figure 2) in a pseudo-trigonal bipyramidal geometry (τ_5=0.61) with two diisopropyl iminoquinone (^{Dipp}iq) ligands and one triflate anion completing the coordination sphere. The interaction of the triflate anion with the copper atom is weak, as demonstrated by the relatively long bond distance of 2.1977(13) Å. Around the copper center, the Cu-O bonds of 2.1688(12) and 2.1832(12) Å are indicative of dative bonds, consistent with the iminoquinone form of the ligand. Likewise, the Cu-N distances (1.9345(14) Å, 1.9352(14) Å) point towards dative interactions.

These structural data confirm that the ligands in **1-iq** are indeed iminoquinones, making **1-iq** a rare example of a Cu(I) iminoquinone species, as Copper(II) species are more prevalent.[7, 14-16]

Figure 8: Molecular structures of **1-iq** (left) and **2-isq** (right) shown at 30% probability ellipsoids. Co-crystallized solvent molecules and hydrogen atoms have been removed for clarity.

In terms of intraligand distances, which are useful indicators of ligand oxidation states, those observed for **1-iq** are consistent with other copper iminoquinone species. The C-O distances of 1.238(2) and 1.236(2) and C-N distances of 1.307(2) and 1.305(2) match well with those observed for the free ligand (C-O = 1.221(2) and C-N = 1.287(2) Å), as well as for Copper(II) iminoquinone derivatives in the literature, including $[Cu^{II}(LBQ)_2Br_2]$ (C-O = 1.223(3); C-N = 1.298(3))[14] and [CuLS(IBQ/ISQ)Cl] (C-O 1.229(3); C-N 1.303(4)).[15] For **1-iq**, the Metrical Oxidation State (MOS)[86] values for each ligand are -0.06 and -0.07. This number corresponds well with assignment as two, neutral ligands.

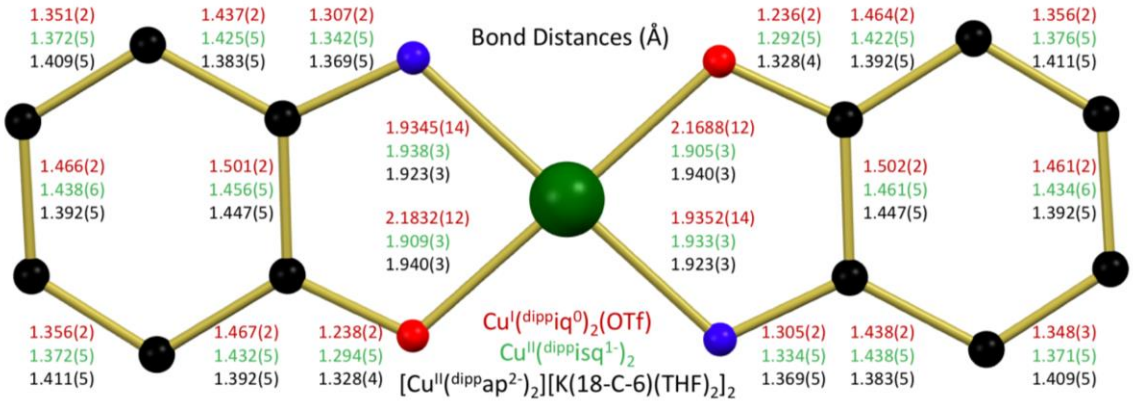

Figure 9: Bond distance comparison for **1-iq**, **2-isq** and **3-ap crown**.

From here, chemical reduction of the complex was attempted to form the bis diisopropyl iminosemiquinone (bis(^{Dipp}isq)) species, isqCu^{II}isq (**2-isq**). Unfortunately, **1-iq** was not a suitable precursor for this chemistry; instead, a copper bis(^{Dipp}isq) complex was generated by reduction of copper iodide with one equivalent of KC_8 in the presence of two equivalents of the iminoquinone ligand. Upon addition of KC_8, the solution changed from brown/red to green, corresponding to the change in oxidation state of the ligand rather than the copper source.[20] The ^{1}H NMR spectrum features broad, paramagnetic resonances ranging from -30 to +30 ppm.

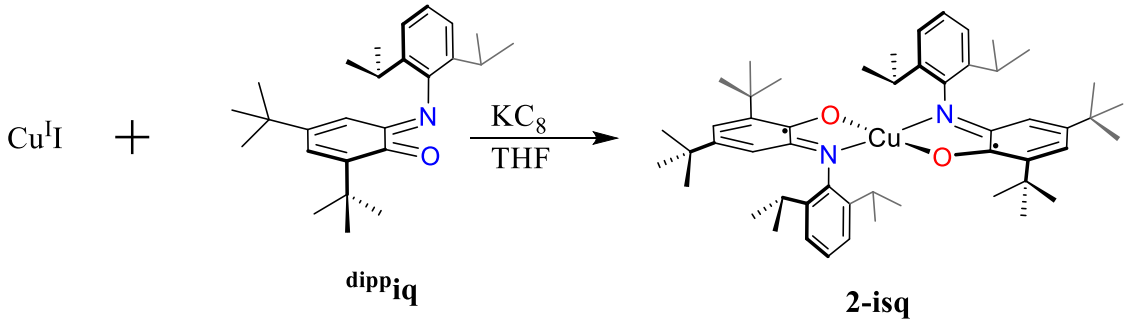

Figure 10: Synthesis of **2-isq**.

X-ray diffraction analysis of crystals grown from a concentrated toluene solution revealed a square planar coordination complex (τ_4'=0.04) with two ^{Dipp}isq ligands bound to the copper center with a *trans* arrangement of nitrogen atoms as **2-isq**. This isomer is likely preferred due to the sterically favorable positions of the large diisopropylphenyl substituents. The Cu-O bond distances are shorter than in **1-iq** at 1.909(3) and 1.905(3) Å, signifying anionic linkages due to ligand reduction to the ^{Dipp}isq ligand. Conversely, the copper-nitrogen bond distances of 1.938(3) and 1.933(3) Å are on par with those of **1-iq**, suggesting they maintain their dative bonding as would be expected for the ^{Dipp}isq resonance form of the ligand.

In **2-isq**, single reduction at each ligand lengthens the C-O bonds to 1.294(5) and 1.292(5) Å and C-N bonds to 1.334(5) and 1.342(5) Å, indicating bond character in between a single and double bond. A comparison of **2-isq** ligand and metal centered bond distances with previously synthesized copper(II) bis(iminosemiquinone) complexes can be found in Table 1. Ligand bond distances for C-O and C-N match well to related complexes with differing steric demands, generally falling within the error of the crystallographically determined bond distances. The bond distances around the copper center, Cu-O and Cu-N, also match up well, suggesting moderate steric differences have little impact on the iminosemiquinone complexation to copper.

Table 34: Copper(II) bis(iminosemiquinone) complexes and selected bond distances.

Complex	**2-isq**	$Cu^{II}(^{Ph}isq^{1-})_2$[21]	$Cu^{II}(^{biPh}isq^{1-})_2$[17]
Cu-O1	1.905(3),1.909(3)	1.912	1.9083(11),1.9046(11)
Cu-N1	1.938(3),1.933(3)	1.936(2)	1.9267(13),1.9307(13)
O1-C1	1.292(5),1.294(5)	1.290(4)	1.2961(19),1.2953(19)
N1-C6	1.345(5),1.334(5)	1.335(4)	1.334(2),1.336(2)

The MOS of **2-isq** was calculated to be -0.77 and -0.81. These values are close to -1 and could be slightly too high because the model is based on all iminoquinone complexes, and not just the Dipp-substituted ones.

To study the redox chemistry of **2-isq**, electrochemistry was employed. Cyclic voltammograms of THF solutions of **2-isq** were acquired at ambient temperature. Analysis of cathodic scans revealed one reversible oxidation at -0.51 V; however, further scanning yielded poor reversibility and rapid decay of the signal. This signifies decomposition of **2-isq**, likely stemming from ^{Dipp}iq ligand dissociation, which is common for neutral ligands. Anodic scans showed two, quasi-reversible reductions at -1.59 and -2.40 V (Figure 6), corresponding to the sequential reduction of the system, here assigned as the one electron reduction of each ligand by one electron, forming the bis diisopropyl amidophenolate (^{Dipp}ap) species. Only one previous example[18] has shown evidence for metal centered reduction of a bis(iminosemiquinone) species, based on the appearance of two new oxidations in subsequent scans. The CV generated in THF did not contain these newly generated peaks, supporting the ligand reduction hypothesis. A comparison of literature reduction potentials can be found in Table 2.

Table 2: Solvent changes to CV, compared to literature.

Compound	**2-isq**	**2-isq**	$Cu(^{Ph}biisq)_2$[6]	$Cu(^{Ph}isq)_2$[21]
Ered2 (V)	-2.40	-1.82	-1.42	-1.32
Ered1 (V)	-1.59	-1.25	-0.66	-1.02
Solvent	THF	DCM	DCM	DCM
Electrolyte	0.1 M $TBAPF_6$	0.1 M $TBAPF_6$	0.1 M $TBAPF_6$	0.1 M $TBAPF_6$
Reference	Fc	Fc	Fc	Fc

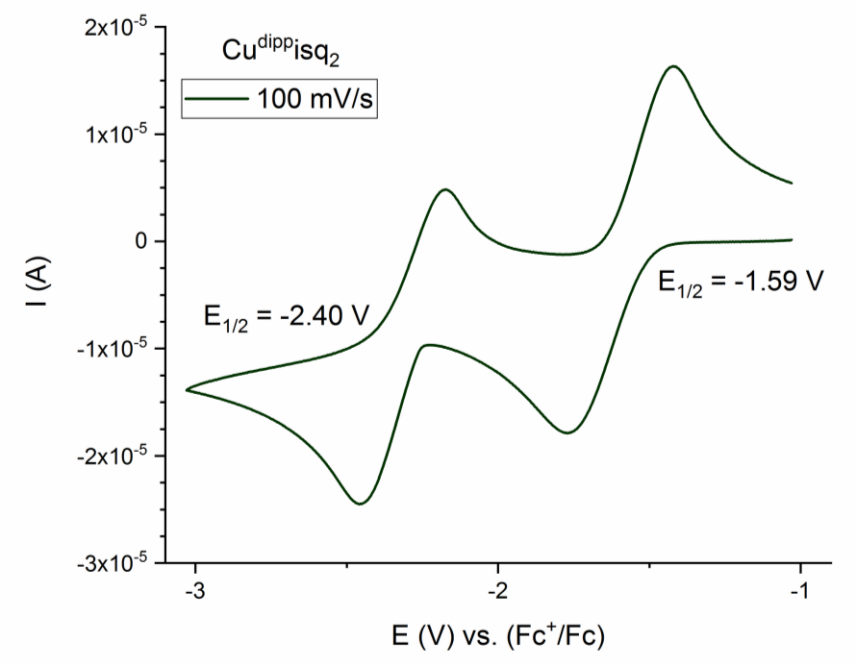

Figure 11: Cyclic voltammetry of **2-isq** in a 0.1 M $[(nBu)_4N][PF_6]$ THF solution. Reversible waves noted at -2.40 and -1.59 V.

Table 35: Reduction potentials of selected Copper(II) iminosemiquinone complexes.

Compound	**2-isq**	$Cu^{I}(^{Ph}iq)CF_3$[11]	$Cu(^{Ph}biisq)_2$[6]	$Cu(^{Ph}isq)_2$[21]	$Cu(^{biPh}isq)_2$[17]	$Cu(^{SPh}isq)_2$[22]
Ered2 (V)	-2.40	-1.35 vs Fc	-1.42	-1.32	-1.480	-1.49
Ered1 (V)	-1.59	-1.04 vs Fc	-0.66	-1.02	-1.117	-1.07
Solvent	THF	DCM	DCM	DCM	DCM	DCM
Electrolyte	0.1 M $TBAPF_6$	0.1M $TBABF_4$	0.1 M $TBAPF_6$	0.10 M $TBAPF_6$	0.10 M $TBAClO_4$	0.1 M $TBAPF_6$
Reference	Fc	SCE	Fc	Fc	Fc	Fc

Red1 product: $[isqCu^{II}ap]^-$; Red2 product: $[apCu^{II}ap]^{2-}$

Comparing the reduction potentials to those in the literature (Table 3) show most DCM solutions giving a first reduction potential around ~ -1 V and a second reduction potential at ~ -1.4 V. Linking the two ligands into a single, tetradentate ligand reduced the first reduction potential by ~ 400 mV, presumably due to the increased delocalization of the ligand stabilizing the monoradical, iminosemiquinone-amidophenolate complex. The CV in THF, however, shows a significant increase in the reduction potentials, by ~500 mV and ~1 V for the first and second reductions, respectively. This dramatic solvent-based increase in reduction potential is presumed to be due to

coordinating THF. This is supported by the quasi-reversible nature of the reduction potentials in THF which are reversible when in DCM, suggesting a solvent dependent, ligand rearrangement.

Further evidence for solvent ligation to $Cu^{II}(isq)_2$ complexes is shown in the EPR spectrum of $Cu(^{Ph}isq)_2$, which was taken in both THF and DCM at room temperature. In THF, ligand hyperfine splitting was simulated to be from 2 ^{14}N (I=1), predominately along the $g_\perp$ axes. This hyperfine splitting is absent in DCM, with copper hyperfine splitting dominating the EPR spectrum in this solvent.[21] This spectrum shows a solvent-based change in the electron coupling, where the ligand radicals antiferromagnetically couple to each other, leaving a mostly isolated copper based radical. In THF, antiferromagnetic coupling is prevalent between a ligand radical and the metal radical, as seen by the added nitrogen hyperfine splitting and increased anisotropy presumed to be from spin density associated with an antiferromagnetically coupled electron in the $d_{x^2-y^2}$ orbital, as would be expected of Cu(I). This solvent based spin mixing in THF is presumed to be due to the ligation changing the geometry of the $Cu^{II}(isq)_2$ complex, as changes in geometry are known to disrupt the orthogonality of the ligand-metal magnetic orbitals.[23] Geometric changes altering spin coupling of copper complexes has been previously noted in literature,[17, 25-27] with planar complexes producing increased ligand to ligand coupling, leaving a Cu centered radical.[28] This delocalization of the radicals across the aromatic system has been shown to lower the energy of otherwise spin-forbidden reactions.[8, 25]

We see this change in geometry and increased reduction potential in other copper(II) iminosemiquinone systems as well. When a coordinating sulfur was added to the aniline ring of the ligand, the subsequent S-Cu coordination perturbed the complexes planar geometry and shifted the ligand to ligand antiferromagnetic coupling to metal to ligand antiferromagnetic coupling.[22] This complex also had an increased second reduction potential by approximately 100 mV, making it comparable to that of a biphenyl substituted iminosemiquinone copper complex.[24] This complex also has a minorly distorted geometry (τ_4= 0.06) with a 9 degree dihedral angle between the planes of the two ligands, but has no additional coordination to the copper center. This suggests that these increases in reduction potential are strictly due to the distortion of the geometry, and not an electronic effect due to the coordination itself. This loss of planarity potentially breaks the magnetic coupling between the ligands, producing a more spin-isolated ligand based radical over the metal based radical in a square planar geometry. And this change in spin and geometry could

be the cause for the increased reduction potential, as well as potential increases to copper back bonding into the π* aromatic system, whose destabilization could increase reduction potential.

The more significant reduction potential change occurs when **2-isq** is in THF and is presumed to be due to a geometry change due to THF coordination. This leads to more pronounced degradation of interligand orbital overlap, giving rise to stronger metal-ligand coupling.

With the reducibility of **2-isq** confirmed by CV, reduction of **2-isq** was facilitated using two equivalents of KC_8, which caused a striking color change from green to purple. Upon workup, a purple solid was attained in a good yield of 78%.

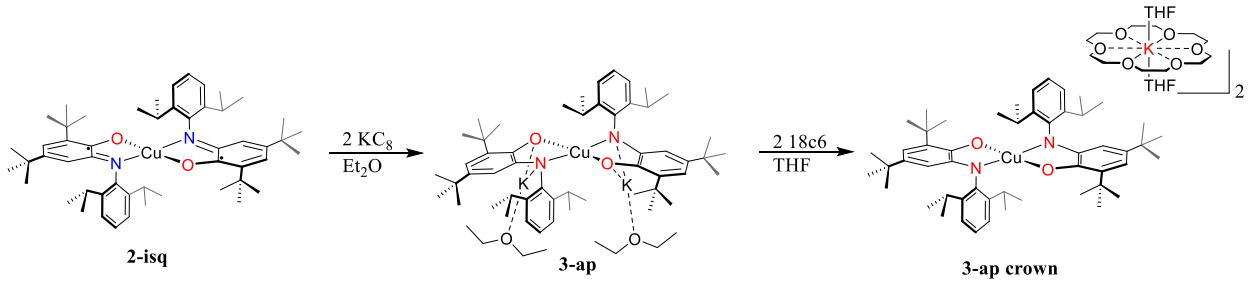

Figure 12: Synthesis of **3-ap** and **3-ap crown**.

This product, assigned as a bis(^{Dipp}ap) copper(II) complex (**3-ap**), crystallized readily from diethyl ether. Analysis by X-ray crystallography showed the copper center sits on a 2-fold rotation axis, creating crystallographically symmetric ligands. The diethyl ether-bound potassium ions coordinated to the oxygen atoms of the ligands appearing to bend them into a pseudo-tetrahedral geometry (τ_4=0.67, τ_4'=0.65) (Figure SX). Due to the influence of the potassium counter cations on the molecular structure, the corresponding molecule where the potassium ions are encapsulated by 18-crown-6 was synthesized (**3-ap-crown**) and analyzed as well.

Sequestration of the potassium ions provides a meaningful comparison of bond distances with neutral **1-iq** and **2-isq**. Compound **3-ap crown** crystallizes from a concentrated THF solution producing crystals in the triclinic space group P-1 as a 1:1 rotational twin. Refinement of the data revealed two potassium ions sequestered by crown ether and tetrahydrofuran molecules completing their coordination sphere. The copper center is ligated by two ^{Dipp}ap ligands in a square planar geometry (τ_4'=0.00), similar to **2-isq**. The copper atom is located on an inversion center, producing crystallographically symmetric ligands, with nitrogen atoms *trans* to each other. The Cu-O (1.940(3) Å) and Cu-N (1.923(3) Å) bond distances are shorter as compared to **2-isq**, consistent with anionic bonds. Furthermore, reduction of the ligand in **3-ap crown** lengthens the

C-O bonds to 1.328 Å and C-N bonds to 1.369(5) Å as expected for the amidophenolate resonance structures. This is the first known copper bis amidophenolate molecule to be isolated and fully characterized.[38] While other complexes have been characterized with amidophenolate ligands on copper(II), either structural data was not obtained,[22] or it is averaged over a singular tri or tetra-dentate ligand with different oxidation states.[6-7]

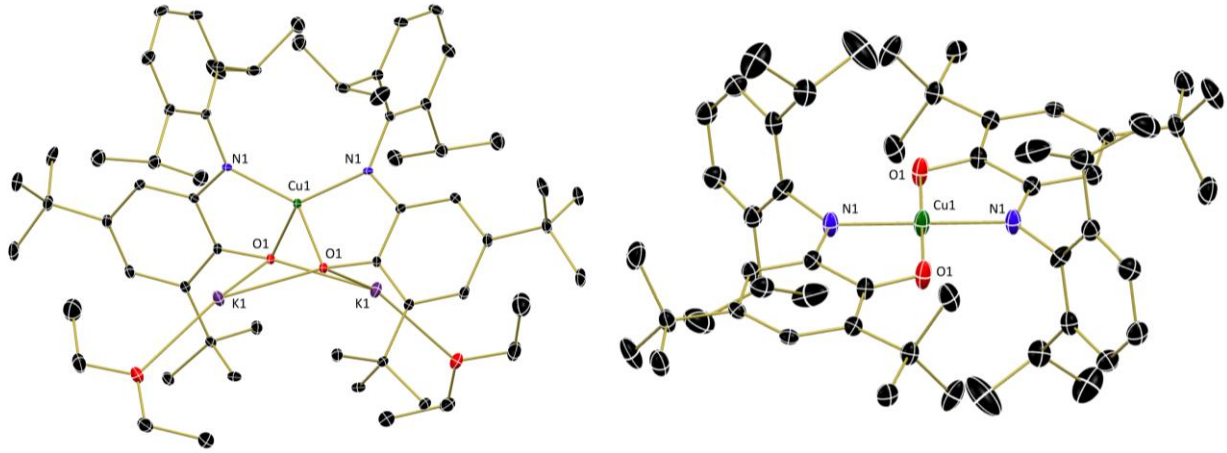

Figure 13: Molecular structures of **3-ap** (left) and **3-ap crown** (right) shown at 30% probability ellipsoids. Co-crystallized solvent molecules, hydrogen atoms, and the potassium counter cation have been removed for clarity.

The one electron reduced, mixed ^{Dipp}isq-^{Dipp}ap copper complex was synthesized to facilitate bond distance comparisons. Its synthesis can be achieved in THF through either reduction of **2-isq** with KC_8 or through comproportionation of **2-isq** with **3-ap** or **3-ap crown**. Oxidation of **3-ap** with I_2 proved amenable to the synthesis of the mixed ligand, copper(II) ^{Dipp}isq/^{Dipp}ap complex, $[isqCu^{II}ap]^{-}[K]^{+}$ (**4-isq ap**). Selected ligand bond distances for the reduced copper complexes found in Table 4.

Table 6: Selected bond distances from Cu-^{Dipp}ap and Cu-^{Dipp}isq complexes

	2-isq (avg)	**5-NTs**	**Avg(isq/ap)**	**4-isq ap crown**	**3-ap crown**
Cu-O1	1.907	1.929	1.9235	1.939	1.940(3)
Cu-N1	1.9355	1.901	1.9293	1.910	1.923(3)
O1-C1	1.293	1.315(4)	1.311	1.323(3)	1.328(4)
N1-C6	1.3395	1.358(4)	1.3543	1.356(3)	1.369(5)

The mixed ligand, ^{Dipp}isq/^{Dipp}ap complexes, Cu-O, O-C, and N-C bond distances, irrespective of the counter ion, fall between **2-isq** and **3-ap crown**, verifying the oxidation state of the ligands as between that of the bis(^{Dipp}isq) and bis(^{Dipp}ap) – an iminosemiquinone and amidophenolate ligand delocalized across each other. This gives the copper complex an overall negative charge, balanced by the cation potassium and, by charge balance, an overall mono-cationic bis potassium N-tosyl ion.

When fully reduced to the bis(^{Dipp}ap), the nitrogen becomes anionic. This change explains the elongation of the Cu-N bond distance seen only in this fully reduced form. When fully reduced, the charge around the small, dicationic copper becomes 4^-, facilitating the charge repulsion of the two nitrogen atoms. Since the less reduced ligand system as nitrogen atoms closer to the metal center, steric hinderance is not a factor in the N-C bond elongation in **3-ap crown**.

Interestingly, the counter ion to the copper mixed ligand, ^{Dipp}isq/^{Dipp}ap system seems to influence bond distances both around the copper center and of the ligands. When paired with the closed shell potassium ion, the mixed ligand species bond distances are closer to those of **3-ap crown**. In **4-isq ap crown**, the lone ligand radical is stabilized as if paired, as the distances around the oxygen are completely monoanionic in nature. Its Cu-O bond distance is within error to that of **3-ap crown**, with the O-C bond distances overlapping within each other's error. The concomitant change with Cu-O and O-C bond distances suggests an effect related to the ligand oxidation state, and not of due to interactions with the copper.

This is not the case in **5-NTs**, when the cation consists of the bis potassium, N-tosyl moiety. The copper complex still retains bond distances between that of **2-isq** and **3-ap crown**, giving the copper complex ion an overall negative charge. The Cu-O, O-C, and N-C bond distances do not have the amidophenolate character seen with close shell potassium counter cation. Instead, these bond distances are almost exactly the average between **2-isq** and **3-ap crown**, as would be expected of a fully delocalized ^{Dipp}isq/^{Dipp}ap ligand system or two crystallographically equivalent ligands comprised of a ^{Dipp}isq and ^{Dipp}ap ligand.

Unfortunately, the extreme symmetry and disorder of **5-NTs** required manually solving for the bond distances around the bis potassium N-tosyl cation, making all the bonds in that complex ion. By charge balance, the overall positive charge, with two potassium ions bound to the nitrogen suggests the nitrogen an overall 1^- charge.

For **3-ap crown**, the MOS calculation produces a value of -1.61 for each ligand. While this could suggest that one ligand is -1 and one is -2 (averaging to -1.5), due to the low MOS values of -0.77 and -0.81 seen for **2-isq**, the **3-ap crown** MOS value being approximately double the 2-isq MOS value is consistent with the expected doubling of the ligands charge from -1 to -2.

The distinctive colors of **1-iq**, **2-isq**, and **3-ap** make these species well suited for study by electronic absorption spectroscopy. The spectra of **1-iq**, **2-isq**, and **3-ap crown** were all recorded in toluene solutions at ambient temperature from 350-900 nm (Figure XX). The spectrum of **1-iq** shows two strong absorptions. The peak at 452 (4100 M^{-1} cm^{-1}) nm was previously assigned as a π- π * transition of the Cu(I) coordinated iminoquinone intraligand charge transfer (ILCT).[17-18] and 734 nm (6600 M^{-1} cm^{-1}), the latter of which is responsible for the observed dark green color as a copper(II) d-d transition.[18]

Green **2-isq** has a more complicated spectrum, displaying 3 absorbances in the visible region at 796 (7,933 M^{-1} cm^{-1}), 452 (5,969 M^{-1} cm^{-1}), and 415 (6,049 M^{-1} cm^{-1}) nm. The absorption at 796 nm that shows the highest molar absorptivity is again responsible for the color observed for **2-isq** and has been previously assigned as a combination of metal to ligand (MLCT) and ligand to ligand (LLCT) charge transfer.[17] The absorptions between 400-500 nm were assigned as ligand to metal charge transfers (MLCT).

The ligand charge transfer absorbances of iminosemiquinone complexes have also been supported by the UV induced reduction of DCM to 1,2 dichloroethane with by a Zn tetradentate diiminosemiquinone species (Zn(L3), generating the Zn diiminobenzoquinone dicationic complex. Zn(L3) has a CT at UV wavelength = 506 cm^{-1} (4.4 x10^3 M^{-1} cm^{-1}) and 405 (3.0 x10^3 M^{-1} cm^{-1}). $Zn(L4)^+$ has abs at 411 nm (3.8x10^3 M^{-1} cm^{-1}) and 385 nm (4.2x10^3 M^{-1} cm^{-1}). The copper equivalent complex, $Cu(L3)^0$ is also photoreductive, but not cleanly, producing both the 1 electron oxidized and 2 electron oxidized species as products.[6]

In solution, **3-ap** displays the spectrum with the lowest molar absorptivity overall, with 3 absorbances at 891 nm (4,634 M^{-1} cm^{-1}), 569 nm (1,574 M^{-1} cm^{-1}), a shoulder at ~400 nm. The 569 nm absorptions are likely responsible for producing the bright purple color observed for **3-ap**.

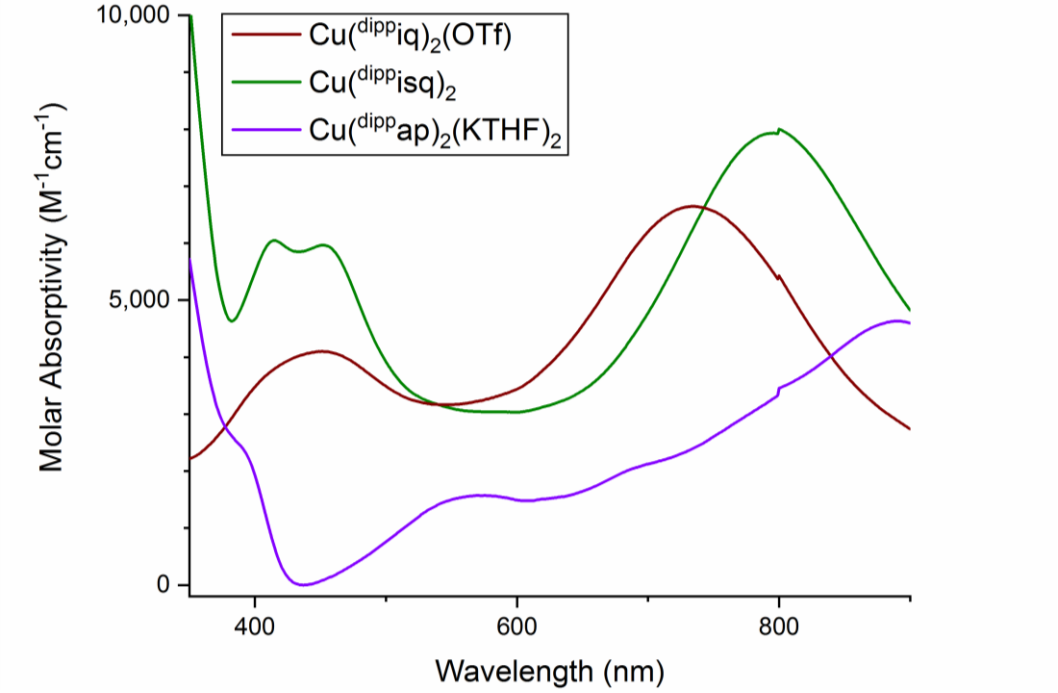

Figure 8: Electronic absorption spectra of **1-iq** (red-brown), **2-isq** (green) and **3-ap** (purple) recorded in toluene at 25 °C.

The color associated with **3-ap** is interesting. Being a d^9 system with two closed shell ligands, there are no charge transfer transitions that would be expected to occur. Previous work has shown the has shown redox activation and charge transfer of copper(II) complexes mediated by ligating ions,[17-18, 39] suggesting the unique geometry of this complex, where its inner-sphere coordinating ions facilitate these charge transfer bands observed in the UV-Vis spectra. This is supported by an observed solvatochromism of **3-ap.** Non-polar solvents such as pentane, toluene, and benzene made purple solutions of **3-ap**, similar to the color of the powder. However, dissolving **3-ap** in THF caused a bleaching of the purple solution to a faint red color. With the ion facilitated charge transfer as the hypothesis for the color, analysis of **3-ap crown** was also performed.

Compound **3-ap crown** is a tan powder that is insoluble in non-polar solvents, but faintly red-colored in polar ones. This suggests that the potassium ions in **3-ap** are encapsulated with THF molecules in this solvent. This is further supported by the UV-Vis spectrum of **3-ap** and **3-ap crown** in THF, which show nearly identical features with only one strong absorption at ~375 nm. In contrast, the spectrum of **2-isq** collected in THF retains its strong absorption features, indicating no interaction with THF solvent. Notably, the spectrum of **3-ap** in toluene is very different from that recorded in THF, featuring more absorptions that are higher in intensity.

The only other previously studied copper(II) bis amidophenolate species was synthesized and characterized via spectroelectrochemistry. This in-situ generated species, whose cations would have been derived from the noncoordinating [Bu_4N][PF_6] electrolyte, was also found to have no intense absorptions above 450 nm.[22] This suggests the inner-sphere, the potassium ions of **3-ap** facilitate charge transfer bands seen in the UV and visible spectrum, giving rise to its purple coloration. When these ions are forced outer-sphere, either through solvent or crown ether chelation, the square planar geometry returns to the copper complex and the charge transfer bands are dramatically reduced in intensity, bleaching the color of the compounds.

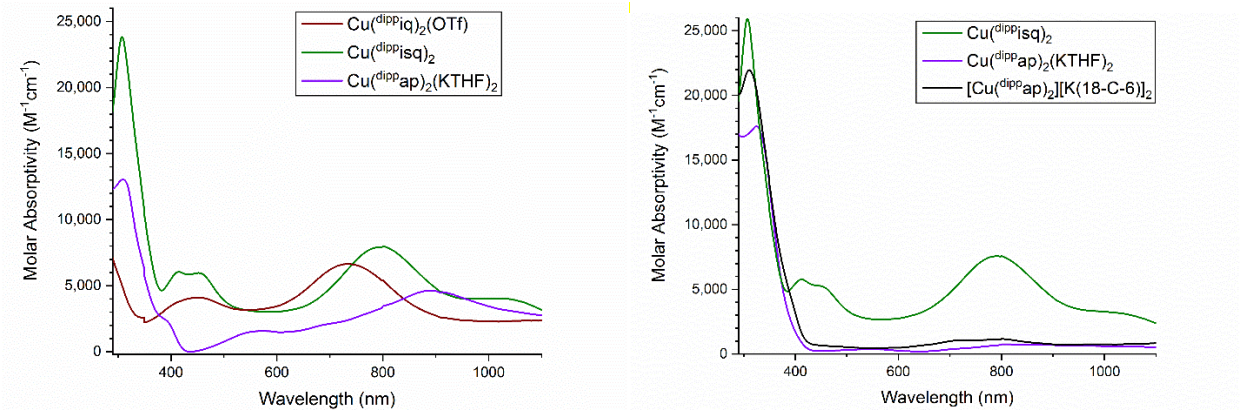

Figure 9: Electronic absorption spectra collected in the UV-Vis/NIR regions of **1-iq** (red-brown), **2-isq** (green) and **3-ap** (purple) recorded in toluene at 25 °C (left). Electronic absorption spectra collected in the UV-Vis/NIR region of **2-isq**, **3-ap** and **3-ap crown** recorded in THF at 25 °C (right).

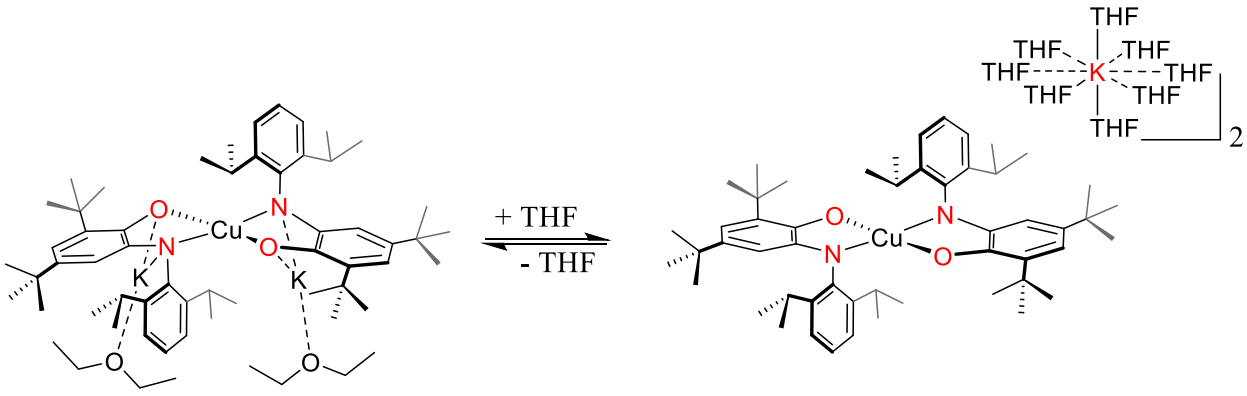

Figure 14: Proposed equilibrium responsible for the purple and colorless forms of **3-ap**.

These spectra of the synthesized copper(II) compounds gives us a window into their reactivity. The planarity of the Cu complexes facilitates ligand to ligand electron spin coupling and charge

transfer transitions. When a radical is present on the ligands, distortion of this geometry, by ligand design, solvent, or reagent, breaks the interligand orbital overlap. This disrupts the interligand charge transfer and spin coupling, which facilitates increased reduction potential and reactivity by changing the spin isolated radical from metal based to ligand based. With closed shell ligands, charge transfer of the metal-based radical is facilitated by the inner-sphere ion and the non-planar geometry they induce. When these ions are forced outer-sphere, either by solvent or other chelating agent, the planarity, and therefore interligand orbital overlap, is reestablished, isolating the radical to the metal surrounded by heavily reduced, highly charged ligands. [6, 8, 17, 21-22, 39]

The electronic structure of the copper complexes was probed using EPR spectroscopy, given these species both contain an unpaired *d*-electron from the Cu^{2+}, d^9 species. Furthermore, **2-isq** also contains two iminosemiquinone radicals that should be evident using this technique. Toluene solutions of **2-isq** and **3-ap** were analyzed at both 105 and 293 K.

Reactivity

To assess the reactivity this new copper family, strong oxidants were added to determine where oxidation occurs, the ligand or the metal. Compound **3-ap** proved unreactive with one equivalent of the strong oxidant para-toluene azide (benzene or toluene), even with UV irradiation. This can most likely be explained by the structure of **3-ap**, where the inner-sphere, bound potassium ions both sterically block access to the copper center. Smaller, more reactive MeI was added to **3-ap** in C_6D_6, generating **4-isq ap crown** and ethane gas, characterized by ^{1}H NMR spectroscopy; subsequent degassing by three freeze-pump-thaw cycles removed the ethane resonance from the spectrum. Two equivalents of MeI resulted in the generation of ethane with residual MeI remaining in solution.

It was found that oxidation by an organoazide was successful in a more polar solvent, such as diethyl ether, resulting in the one electron oxidation of **3-ap**. This is supported by single crystals analyzed by X-ray crystallography, which show a mixed oxidation state ligand system, **4-isq ap crown,** which has bond metrics between those of **2-isq** and **3-ap** (detailed analysis above). When two equivalents of azide were added to **3-ap** in diethyl ether, decomposition of the copper complex was noted, as well as a blue product that was present in small quantities. By contrast, if two equivalents of an alternative, hypervalent iodine nitrene precursor, imino-λ^3-iodane (PhI=NTs), is used as the nitrene precursor, **2-isq** is generated, confirmed by both ^{1}H NMR spectroscopy and X-ray crystallography. An unidentified compound and a golden-yellow precipitate were also formed.

With these results failing to produce an isolable copper nitrene or nitrenoid species, encapsulation of the potassium ions was then performed using 18-crown-6, to help stabilize them during reactivity, as well as move them to the outer sphere. The necessity of encapsulating the potassium ions for improved reactivity was emphasized by the non-innocent reaction of adding 18-crown-6 to **3-ap**; encapsulating the potassium ions produces a significant amount of free potassium ^{Dipp}isq ligand as a blue salt (**K-isq**) when performed in diethyl ether and requires THF to generate **3-ap crown** without these significant impurities, with the yield of the desired product around 80%.

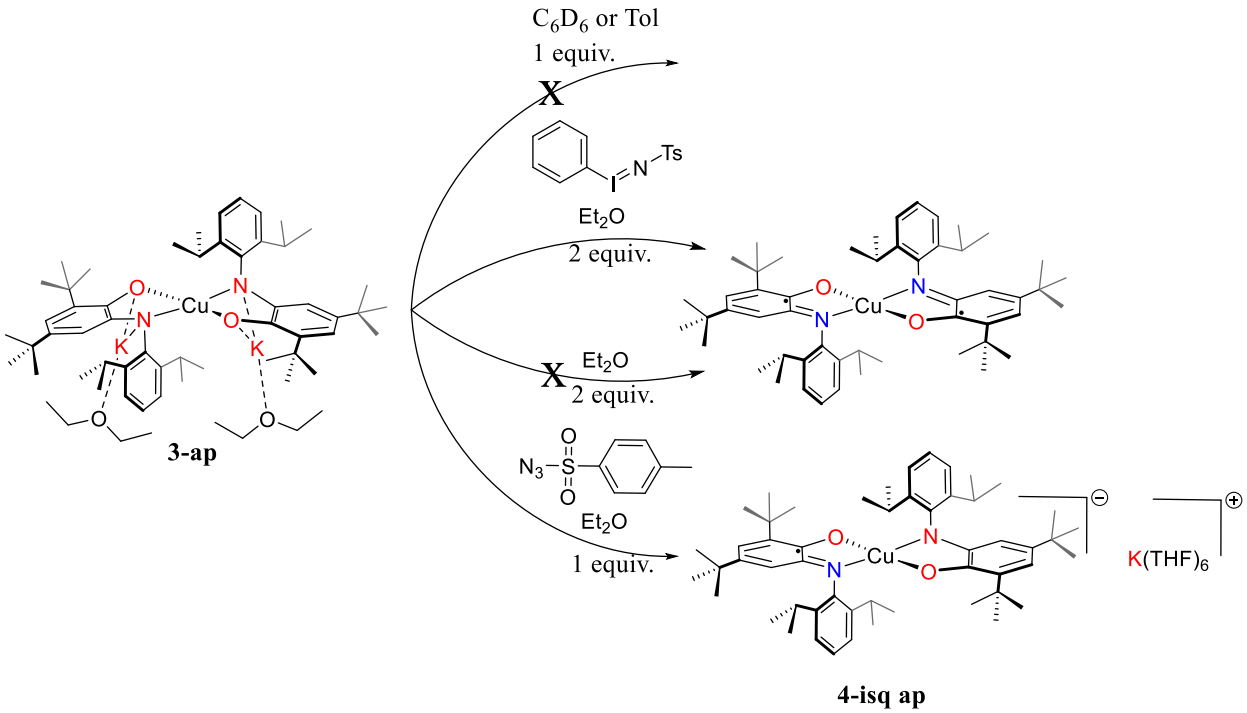

Figure 15: Reactions of **3-ap** with nitrene precursors.

Continuing the attempts to isolate a copper nitrene, 1 equivalent of PhI=NTs was reacted with **3-ap crown**, the product of which was analyzed using X ray diffraction (Figure 12). Crystals generated by layering pentane onto a saturated solution of benzene at room temperature yielded the structure **5-NTs**. The crystal was heavily disordered, so another crystal was grown through the vapor diffusion of pentane into a saturated solution of diethyl ether at -35 °C; crystals grown in this solvent system were also heavily disordered in the same manner. As described previously, **5-NTs** consists of a monoanionic copper complex, whose ligand oxidation state is confirmed by ligand bond distances, and a cation complex consisting of both encapsulated potassium ions from

3-ap crown bound to a N-tosyl moiety. A matching ^{1}H NMR spectrum was generated using the alternative nitrene precursor, tosyl azide, (N_3Ts).

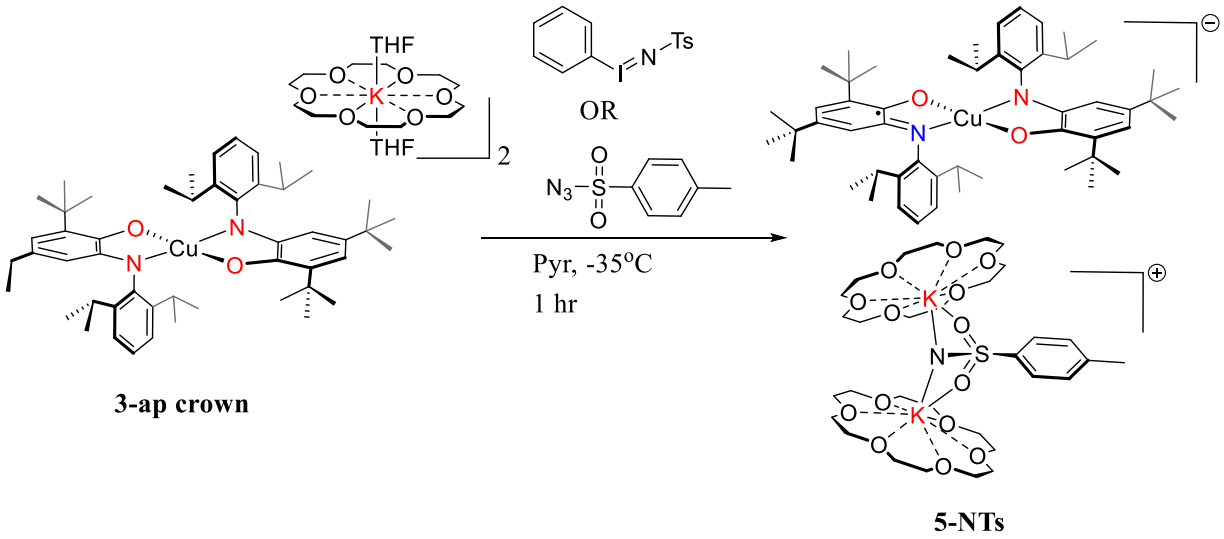

Figure 16: Reaction to generate **5-NTs**

With initial yields around 25%, X-ray diffraction was also performed on the impurities of the reaction between **3-ap crown** and PhI=NTs, yielding two products. The first is the monodeprotonated tosyl sulfonamide salt, $[K(18c6)]^{-}[HNTs]^{+}$. The second product crystalized was **4-isq ap crown** complex, the one electron oxidation of **3-ap crown**.

Conclusion

The synthesis and characterization of a series of copper complexes bearing the redox-active iminoquinone/amidophenolate family of ligands has been synthesized and fully characterized, demonstrating the ability of this ligand to exist in three different oxidation states on copper. The electronic structure, bonding preferences, and reactivity were studied using multinuclear NMR, EPR, UV-Vis, and X-ray crystallography. Notably, the iminoquinone derivative, **1-iq**, is a rare example of this ligand on a copper(I) center. Similarly, **3-ap**, the bis(^{Dipp}ap) copper(II) complex, is an unusual example that has been structurally characterized, slowing comparison for the whole reduction series. This highly reduced complex is stabilized by potassium coordination to the ligands, which forces a pseudo-tetrahedral environment. Sequestering the potassium ions (as in **3-ap crown**) from the copper coordination sphere regenerates the square planar geometries, and dramatically bleaches the color of the complex from purple to tan.

AUTHOR INFORMATION

Corresponding Author

*Email: sbart@purdue.edu

ORCID

Ezra J. Coughlin 0000-0002-9938-6649

Matthias Zeller 0000-0002-3305-852X

Suzanne C. Bart 0000-0002-8918-9051

Notes

The authors declare no competing financial interest.

ACKNOWLEDGMENT

The X-ray crystallographic data in this work was obtained on instruments funded by the National Science Foundation through the Major Research Instrumentation Program under Grant No. CHE 1625543.

REFERENCES

1. Thomas, F., Ten Years of a Biomimetic Approach to the Copper(II) Radical Site of Galactose Oxidase. *European Journal of Inorganic Chemistry* **2007,** *2007* (17), 2379-2404.
2. Speier, G.; Whalen, A. M.; Csihony, J.; Pierpont, C. G., Iminosemiquinone Complexes of Copper, Structural, Magnetic, and Electrochemical Characterization of Complexes of the Phenoxazinolate Semiquinone Radical. *Inorganic Chemistry* **1995,** *34* (6), 1355-1360.
3. Rajabimoghadam, K.; Darwish, Y.; Bashir, U.; Pitman, D.; Eichelberger, S.; Siegler, M. A.; Swart, M.; Garcia-Bosch, I., Catalytic Aerobic Oxidation of Alcohols by Copper Complexes Bearing Redox-Active Ligands with Tunable H-Bonding Groups. *J Am Chem Soc* **2018,** *140* (48), 16625-16634.
4. Largeron, M., Aerobic catalytic systems inspired by copper amine oxidases: recent developments and synthetic applications. *Org Biomol Chem* **2017,** *15* (22), 4722-4730.
5. Lu, W.; Xi, C., CuCl-catalyzed aerobic oxidative reaction of primary aromatic amines. *Tetrahedron Letters* **2008,** *49* (25), 4011-4015.
6. Chaudhuri, P.; Hess, M.; Müller, J.; Hildenbrand, K.; Bill, E.; Weyhermüller, T.; Wieghardt, K., Aerobic Oxidation of Primary Alcohols (Including Methanol) by Copper(II)− and Zinc(II)−Phenoxyl Radical Catalysts. *Journal of the American Chemical Society* **1999,** *121* (41), 9599-9610.
7. Speier, G.; Csihony, J.; Whalen, A. M.; Pierpont, C. G., Studies on Aerobic Reactions of Ammonia/3,5-Di-tert-butylcatechol Schiff-Base Condensation Products with Copper, Copper(I), and Copper(II). Strong Copper(II)−Radical Ferromagnetic Exchange and Observations on a Unique N−N Coupling Reaction. *Inorganic Chemistry* **1996,** *35* (12), 3519-3524.

8. Jacquet, J.; Blanchard, S.; Derat, E.; Desage-El Murr, M.; Fensterbank, L., Redox-ligand sustains controlled generation of CF3 radicals by well-defined copper complex. *Chem Sci* **2016,** *7* (3), 2030-2036.
9. Ren, Y.; Cheaib, K.; Jacquet, J.; Vezin, H.; Fensterbank, L.; Orio, M.; Blanchard, S.; Desage-El Murr, M., Copper-Catalyzed Aziridination with Redox-Active Ligands: Molecular Spin Catalysis. *Chemistry* **2018,** *24* (20), 5086-5090.
10. Carsch, K. M.; Dimucci, I. M.; Iovan, D. A.; Li, A.; Zheng, S.-L.; Titus, C. J.; Lee, S. J.; Irwin, K. D.; Nordlund, D.; Lancaster, K. M.; Betley, T. A., Synthesis of a copper-supported triplet nitrene complex pertinent to copper-catalyzed amination. *Science* **2019,** *365* (6458), 1138-1143.
11. Paul, G. C.; Das, K.; Maity, S.; Begum, S.; Srivastava, H. K.; Mukherjee, C., Geometry-Driven Iminosemiquinone Radical to Cu(II) Electron Transfer and Stabilization of an Elusive Five-Coordinate Cu(I) Complex: Synthesis, Characterization, and Reactivity with KO2. *Inorg Chem* **2019,** *58* (3), 1782-1793.
12. Conner, K. M.; Perugini, A. L.; Malabute, M.; Brown, S. N., Group 10 Bis(iminosemiquinone) Complexes: Measurement of Singlet–Triplet Gaps and Analysis of the Effects of Metal and Geometry on Electronic Structure. *Inorganic Chemistry* **2018,** *57* (6), 3272-3286.
13. Jacquet, J.; Cheaib, K.; Ren, Y.; Vezin, H.; Orio, M.; Blanchard, S.; Fensterbank, L.; Desage-El Murr, M., Circumventing Intrinsic Metal Reactivity: Radical Generation with Redox-Active Ligands. *Chemistry* **2017,** *23* (60), 15030-15034.
14. Mondal, M. K.; Mukherjee, C., An unprecedented one-step synthesis of octahedral Cu(ii)-bis(iminoquinone) complexes and their reactivity with NaBH4. *Dalton Trans* **2016,** *45* (34), 13532-40.
15. Balaghi, S. E.; Safaei, E.; Chiang, L.; Wong, E. W.; Savard, D.; Clarke, R. M.; Storr, T., Synthesis, characterization and catalytic activity of copper(II) complexes containing a redox-active benzoxazole iminosemiquinone ligand. *Dalton Trans* **2013,** *42* (19), 6829-39.
16. Piskunov, A. V.; Meshcheryakova, I. N.; Smolyaninov, I. V.; Fukin, G. K.; Cherkasov, V. K.; Abakumov, G. A., Stable organomercury compounds containing an o-iminosemiquinone radical ligand. *Russian Chemical Bulletin* **2013,** *62* (1), 147-156.
17. Balaghi, S. E.; Safaei, E.; Chiang, L.; Wong, E. W. Y.; Savard, D.; Clarke, R. M.; Storr, T., Synthesis, characterization and catalytic activity of copper(ii) complexes containing a redox-active benzoxazole iminosemiquinone ligand. *Dalton Transactions* **2013,** *42* (19), 6829-6839.
18. Carsch, K. M.; Lukens, J. T.; DiMucci, I. M.; Iovan, D. A.; Zheng, S. L.; Lancaster, K. M.; Betley, T. A., Electronic Structures and Reactivity Profiles of Aryl Nitrenoid-Bridged Dicopper Complexes. *J Am Chem Soc* **2020,** *142* (5), 2264-2276.
19. 5-(Trifluoromethyl)dibenzothiopheniumtrifluoromethanesulfonate
20. Jacquet, J.; Salanouve, E.; Orio, M.; Vezin, H.; Blanchard, S.; Derat, E.; Desage-El Murr, M.; Fensterbank, L., Iminosemiquinone radical ligands enable access to a well-defined redox-active Cu(II)-CF(3) complex. *Chem Commun (Camb)* **2014,** *50* (72), 10394-7.
21. Pangborn, A. B.; Giardello, M. A.; Grubbs, R. H.; Rosen, R. K.; Timmers, F. J., Safe and Convenient Procedure for Solvent Purification. *Organometallics* **1996,** *15*, 1518-1520.
22. Abakumov, G. A.; Cherkasov, V. K.; Piskunov, A. V.; Meshcheryakova, I. N.; Maleeva, A. V.; Poddel'skii, A. I.; Fukin, G. K., Zinc molecular complexes with sterically hindered o-quinone and o-iminoquinone. *Dokl. Chem.* **2009,** *427* (1), 168-171.
23. Chakraborty, S.; Chattopadhyay, J.; Guo, W.; Billups, W. E., *Angew. Chem. Int. Ed.* **2007,** *46* (24), 4486-4488.

24. 2013/2014., B. *Apex3 v2016.9-0, Saint V8.34A,SAINT V8.37A*, Madison, WI, USA 2016.
25. Sheldrick, G. M., Crystal structure refinement with SHELXL. *Acta Crystallogr., Sect. C: Struct. Chem.* **2015,** *71* (1), 3-8.
26. Huebschle, C. B.; Sheldrick, G. M.; Dittrich, B., ShelXle: a Qt graphical user interface for SHELXL. *J. Appl. Crystallogr.* **2011,** *44* (6), 1281-1284.
27. Mukherjee, C.; Weyhermüller, T.; Bothe, E.; Chaudhuri, P., Oxidation of an o-Iminobenzosemiquinone Radical Ligand by Molecular Bromine: Structural, Spectroscopic, and Reactivity Studies of a Copper(II) o-Iminobenzoquinone Complex. *Inorg. Chem.* **2008,** *47* (7), 2740-2746.
28. Mondal, M. K.; Biswas, A. K.; Ganguly, B.; Mukherjee, C., Unprecedented iminobenzosemiquinone and iminobenzoquinone coordinated mononuclear Cu(ii) complex formation under air. *Dalton Trans.* **2015,** *44* (20), 9375-9381.
29. Ranis, L. G.; Werellapatha, K.; Pietrini, N. J.; Bunker, B. A.; Brown, S. N., Metal and Ligand Effects on Bonding in Group 6 Complexes of Redox-Active Amidodiphenoxides. *Inorg. Chem.* **2014,** *53* (19), 10203-10216.
30. Coughlin Ezra, J.; Zeller, M.; Bart Suzanne, C., Neodymium(III) Complexes Capable of Multi-Electron Redox Chemistry. *Angew. Chem.* **2017,** *129* (40), 12310-12313.
31. Chaudhuri, P.; Verani, C. N.; Bill, E.; Bothe, E.; Weyhermüller, T.; Wieghardt, K., Electronic Structure of Bis(o-iminobenzosemiquinonato)metal Complexes (Cu, Ni, Pd). The Art of Establishing Physical Oxidation States in Transition-Metal Complexes Containing Radical Ligands. *Journal of the American Chemical Society* **2001,** *123* (10), 2213-2223.
32. Ye, S.; Sarkar, B.; Lissner, F.; Schleid, T.; Van Slageren, J.; Fiedler, J.; Kaim, W., Three-Spin System with a Twist: A Bis(semiquinonato)copper Complex with a Nonplanar Configuration at the Copper(II) Center. *Angewandte Chemie International Edition* **2005,** *44* (14), 2103-2106.
33. LANGE, C. G. P. a. C. W., The Chemistry of Transition Metal Complexes Containing Catechol and Semiquinone Ligands. **1994**.
34. Lyaskovskyy, V.; De Bruin, B., Redox Non-Innocent Ligands: Versatile New Tools to Control Catalytic Reactions. *ACS Catalysis* **2012,** *2* (2), 270-279.
35. Broere, D. L. J.; Plessius, R.; Van Der Vlugt, J. I., New avenues for ligand-mediated processes – expanding metal reactivity by the use of redox-active catechol, o-aminophenol and o-phenylenediamine ligands. *Chemical Society Reviews* **2015,** *44* (19), 6886-6915.
36. Kaim, W., The Shrinking World of Innocent Ligands: Conventionaland Non-Conventional Redox-Active Ligands. *European Journal of Inorganic Chemistry* **2012,** *2012* (3), 343-348.
37. Rakshit, R.; Mukherjee, C., Secondary Interactions versus Intramolecular π-π Interactions in CuII-Diradical Complexes. *European Journal of Inorganic Chemistry* **2016,** *2016* (17), 2731-2737.
38. Piskunov, A. V.; Pashanova, K. I.; Bogomyakov, A. S.; Smolyaninov, I. V.; Berberova, N. T.; Fukin, G. K., Copper(II) complexes bearing o-iminosemiquinonate ligands with augmented aromatic substituents. *Polyhedron* **2016,** *119*, 286-292.
39. Rajput, A.; Sharma, A. K.; Barman, S. K.; Saha, A.; Mukherjee, R., Valence tautomerism and delocalization in transition metal complexes of o-amidophenolates and other redox-active ligands. Some recent results. *Coordination Chemistry Reviews* **2020,** *414*, 213240.
40. Chang, H.-C.; Lo, F.-C.; Liu, W.-C.; Lin, T.-H.; Liaw, W.-F.; Kuo, T.-S.; Lee, W.-Z., Ambient Stable Trigonal Bipyramidal Copper(III) Complexes Equipped with an Exchangeable Axial Ligand. *Inorganic Chemistry* **2015,** *54* (11), 5527-5533.

Incomplete Ytterbium Manuscript

Isolation of an ytterbium imido

*Matthew Hewitt, Ezra J. Coughlin, Matthias Zeller, and Suzanne C. Bart**

H.C. Brown Laboratory, Department of Chemistry, Purdue University, West Lafayette, Indiana 47907, United States

Procedure

Synthesis of $Yb(ap)_2$: To a 20 mL scintillation vial was added $YbCl_3$ (200 mg, 279.4 g/mol, 0.7158 mmol), iq ligand (544 mg, 379.6 g/mol, 1.433 mmol, 2.00 equivalence), a magnetic stir bar and THF (18mL). This solution was stirred at room temperature for 35 minutes before KC8 (402 mg, 135.2g/mol, 2.973 mmol, 4.15 equivalence) was added portion-wise over 10 minutes, turning blood red. The solution stirred for 2 hours before being filtered through celite, rinsing with pentane. The volatiles were removed by high vacuum and the remaining dark red solid was washed with pentane (2x 1.5 mL) at room temperature giving 250 mg clean, bright red compound. The filtrate was then vacuumed down and recrystallized as follows: The crude dark red and bright blue solid was dissolved in minimal pentane with an additional 2 mL pentane added before being cooled to -35 °C overnight. The solution was decanted, the bright red crystals washed with pentane (2x 2mL) yielding an additional 305 mg of the desired product, **$Yb(ap)_2$**. (670 mg, 1259.8 g/mol, 0.4898 mmol, 68% yield).

Synthesis of $Yb(ap)_2$(DMAP): To a 20 mL scintillation vial was added **Yb(ap)2(K)** (103 mg, 0.0818 mmol, MW=1259.75 g/mol) in 15 mL diethyl ether with a magnetic stir bar. To a black capped vial was added 18-crown-6 (34 mg, 0.0901 mmol, 1.1 equiv) and 2 mL diethyl ether. This solution was added dropwise to the stirring, red ether solution of Yb at room temperature. Some solid may precipitate then redissolve. After stirring for 30 minutes DMAP (10 mg, 0.08197 mmol, 1 equiv) with 3 mL diethyl ether was added dropwise over 10 minutes. The organe solution was

stirred for an hour before reducing the volume to 3-4 mL. The solution was then filtered, removing a yellow solid and then the volatiles removed by high vacuum, yielding **Yb(ap)$_2$(DMAP)** (95 mg, MW='1533.75 g/mol')

Synthesis of Yb(isq)$_2$(DMAP)(imido): To a 20 mL scintillation vial was added **Yb(ap)$_2$(DMAP)** (45 mg, MW=1533.75 g/mol, 0.0286 mmol) and 6 mL toluene. The orange solution was frozen in liquid nitrogen (Coldwell), and layered with a toluene solution of $N_3C_6F_5$ -35°C (5.98 mg, 3.6 uL, 0.0286 mmol, 1 equiv, MW=209.09 g/mol, p~1.655 mg/mL), and frozen. The frozen solutions were then thawed at -78 °C for 1.5 hrs. The orange solution was then warmed to -35°C. Within 30 minutes the solution had turned green, with IR confirming azide consumption and new product after 50 minutes. The crude solid was triturated with pentane (3 x 1.5 mL), which can be discarded. The solid was washed with (3 x 1.5 mL) diethyl ether and filtered through a pipet filter (v slow) or fritted funnel, removing a steel blue ppt. The green solution was then vacuumed leaving the **Yb(DMAP)(imido)** (44 mg, MW='1682.7 g/mol').

Synthesis of Yb(PF-tet): To a 20 mL scintillation vial was added **Yb(ap)$_2$** (25 mg, 0.019845 mmol, 1 eq), a magnetic stir bar, and 4 mL toluene. To the red solution was added 18-crown-6 ether (5.76 mg, 0.02183 mg, 1.1 eq) before it was stirred and cooled to -35°C for 1.5 hours. Pentafluorophenylazide (8.30 mg, 0.03969 mmol, 2.0 eq) was added slowly, down the side of the cold vial, and then stirred at -35°C. The solution almost immediately turned black, lightening to brown within a minute before lightening to deep blue within 15 minutes of stirring at -35°C. The solution was stirred an additional 1.5 hours, warmed to room temperature, and the volatiles removed by high vacuum yielding a dark blue powder (33 mg, 0.01942 mmol, 98% yield).

RESULTS AND DISCUSSION

Synthesis of Yb(III) bis amidophenolate and its azide reactivity.

The chemistry of rare earth metals, including lanthanides, have grown in recent years into technology, medicine and beyond thanks to their unique luminescent and magnetic properties.[40] Their redox chemistry is generally constant as 3+ ions, though certain lanthanides have reductively accessible 2+ oxidation states.[41] The electronic and magnetic properties of redox active ligand

complexes of ytterbium, along with europium and others that have this accessible redox chemistry, have been investigated for their redox isomerism[42-43] and potential multiconfigurational oxidation states.[44-45] The reactivity of these species has not been well investigated.

The reactivity of lanthanide complexes with redox non-innocent ligands has been explored by our group previously,[13, 46] With the reactivity of these ligands well established, the synthesis of a monomeric, terminal lanthanide imido from an azide was investigated using the reaction of a ytterbium bis N-diisopropylphenyl 3,5-tertbutyl-amidophenolate (^{Dipp}ap) complex (Yb(ap)$_2$ crown), whose counter cation potassium has been sequestered by 18-crown-6 (18c6).

Initial attempts to synthesis an ytterbium imido yielded a mixture of compounds. Two equivalents of para-toluene azide (pTolN$_3$) were necessary for complete consumption of the Yb(ap)$_2$ starting material at -35°C. Washing with pentane yielded a blue powder product and a small amount of side product, both of which were crystallized from a vapor diffusion of pentane into diethyl ether at -35°C. Crystals were isolated and analyzed via X-ray diffraction spectroscopy, yielding two structures. The major structure was determined to be an ytterbium bis(iminosemiquinone) (^{Dipp}isq) tetrazene, (Yb(isq)$_2$(pTol-Tet)), as seen in Figure 1.

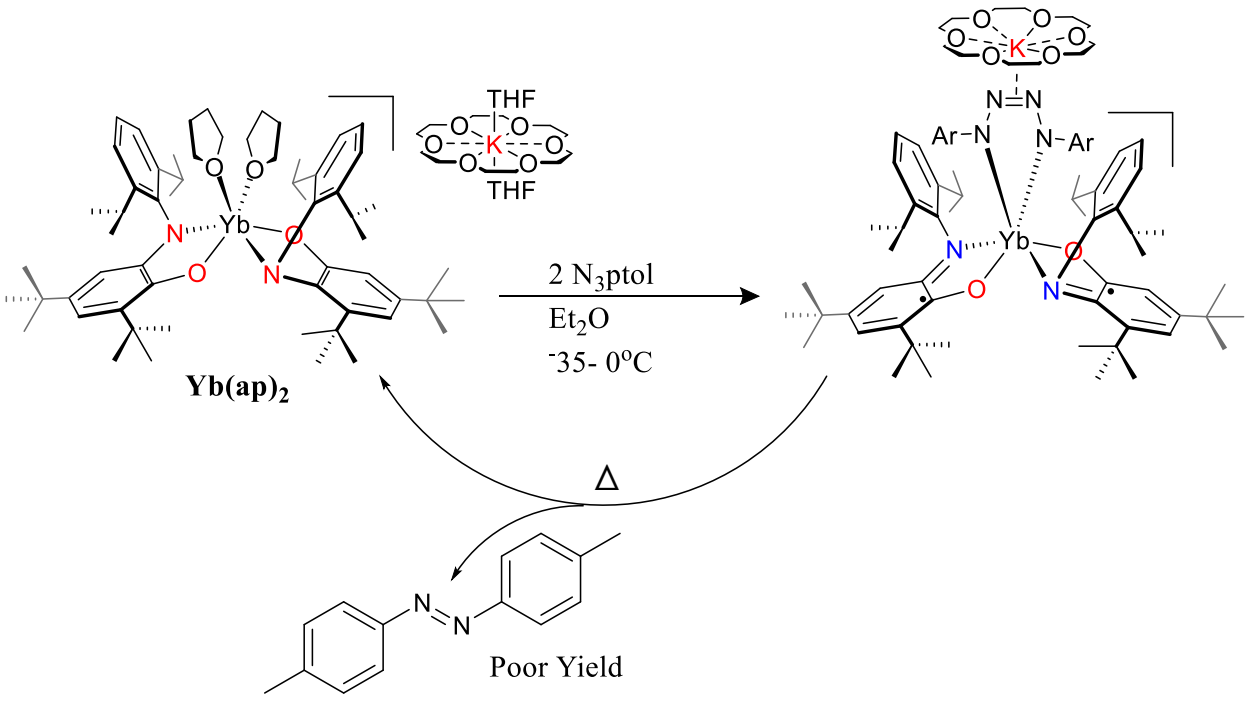

Figure 17: General synthesis of a Yb tetrazene.

A minor product was also crystallized and analyzed by X-ray diffraction and can be seen in Figure 2. In this product, the aryl azide has inserted into the initial ^{Dipp}ap ligand between the

phenol and aniline, resulting in a 7-membered ring product (Yb(N-ap)$_2$). Cooling the reaction of Yb(ap)$_2$ crown with pTolN$_3$ further inhibited reactivity, so more reactive azides were tested.

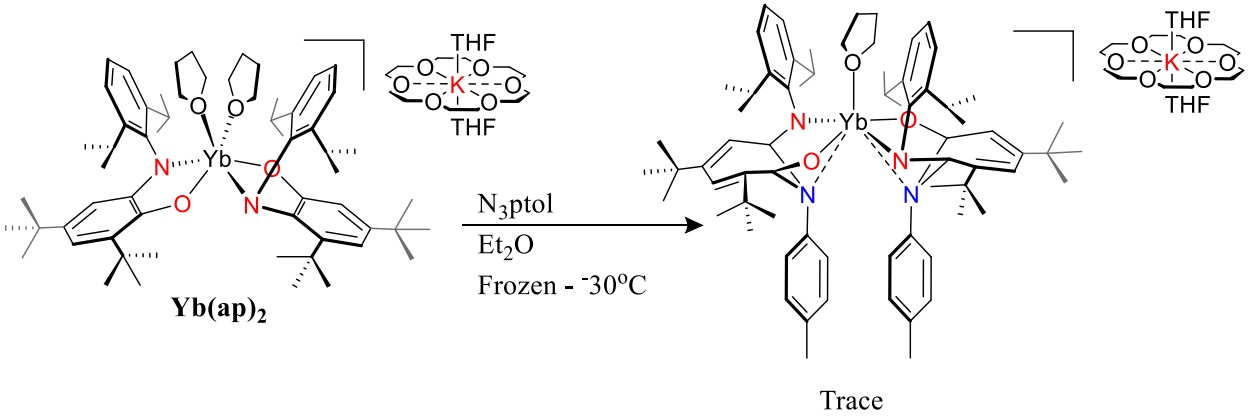

Figure 18: Synthesis of ^{Dipp}ap ring-inserted product

With initial attempts to isolate the monoimido were unsuccessful with pTolN$_3$, attempts were then shifted to the more reactive pentafluorophenyl azide (PFN$_3$) to lower the temperature range of reactivity, facilitating more control through the more numerous cold baths below -35°C. The pentafluorotetrazene ytterbium (Yb(isq)$_2$(PF-Tet)) was synthesized cleanly, as with previous azides, reacting the Yb(ap)$_2$ crown and 2 equivalents of PFN$_3$ at -35°C. Attempts to isolate an ytterbium monoimido through temperature control were unsuccessful, and attempts to selectively isolate Yb(N-ap)$_2$ were initially successful but proved inconsistent, with tetrazene formation predominating most frequently. A change in strategy was needed.

Steric hinderance has shown to play a particularly important role in transition metal tetrazenes,[48, 61] preventing or facilitating reactivity using steric bulk. Tosyl azide has also been shown to facilitate blocking a coordination site with a sulfoxide oxygen, transitively stabilizing the imide.[62] Scandium imidos were initially synthesized from scandium alkyl anilido reactions, generated through the coordination with 4-dimethylaminopyridine (DMAP) and subsequent anilido deprotonation to create the first rare earth monomeric imido[57]. These data formed the basis of a novel strategy to generate an ytterbium monoimido, through steric hinderance. Displacing a THF with DMAP at one of the coordination sites of the Yb(ap)$_2$ crown would sterically block the tetrazene and stabilize the ytterbium imido that had not been amenable to isolation by temperature, stoichiometry, or kinetic controls.

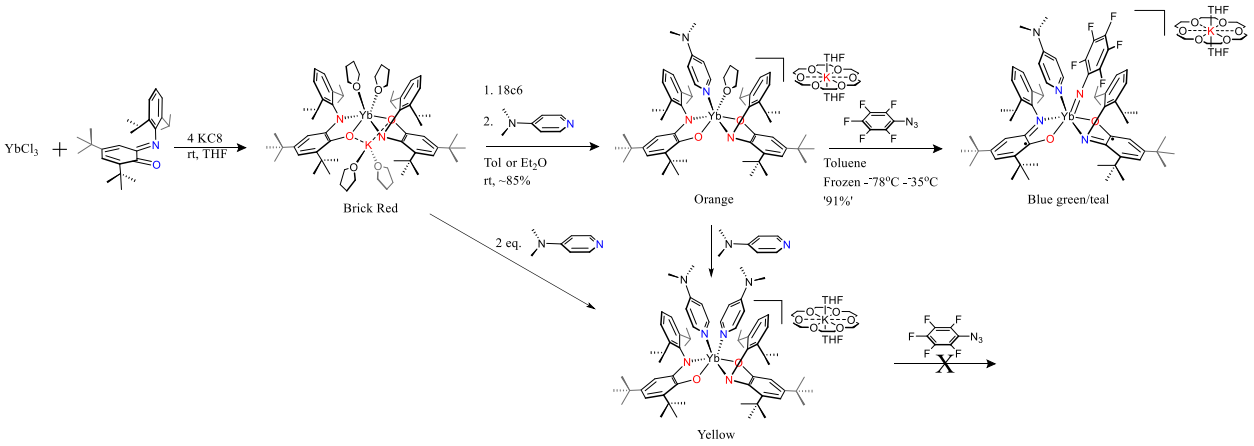

Figure 3: Synthetic route to Yb imido via DMAP steric hindrance.

One equivalent of DMAP was added to $Yb(ap)_2$ crown, followed by the subsequent addition of PFN_3. The reactivities of this intermediate, as well as the Yb bis(DMAP) complex ($Yb(ap)_2(DMAP)_2$), was investigated in addition to their spectroscopic analysis.

With an encapsulated, outer-sphere potassium ion, $Yb(ap)_2$ crown and the products that formed by its reaction with azides and DMAP were investigated through a comparison of crystallographically determined bond distances. In particular, ytterbium ligand bond distances compare well to the neodymium-^{Dipp}ap complexes previously synthesized by our group.[46] The $Yb(ap)_2$ crown ^{Dipp}ap average O-C bond distance of 1.3455 Å is within error to Nd complex's O-C bond distance of 1.348(3) Å. The Yb ^{Dipp}ap N-C average bond distance of 1.4005 Å is quite similar to the Nd complex's 1.389(3) Å. Importantly, both ligands of $Yb(ap)_2$ crown have consistent O-C and N-C bond distances, confirming the assignment of a Yb(III) with two closed ligand ^{Dipp}ap instead of a mixed ligand Yb(II), with one diisopropylphenyl iminosemiquinone (^{Dipp}isq) and one ^{Dipp}ap ligand.

For the ligands present in the ytterbium tetrazenes, the average O-C bond distances are slightly shorter than the 1.309(16) Å of the Nd(^{Dipp}isq)$_2$I complex, at 1.2940 Å for the $Yb(isq)_2$(PF-tet) and 1.2895 Å for Yb(isq)2(pTol-tet). This gives more double bond carbonyl character with a more ligand bound radical. The ^{Dipp}isq N-C bond distances in the tetrazene complexes are 1.349 Å for $Yb(isq)_2$(PF-tet) and 1.346 Å for $Yb(isq)_2$(pTol-tet) which are in close agreement to the Nd ^{Dipp}isq bond distance of 1.344(15) Å. The similarity between the tetrazenes' ^{Dipp}isq bond distances suggests O-C bond distance differences are metal based and not electronics based. This could be due to weaker spin coupling of the iminosemiquinone ligands to the lone 4f electron compared to the more abundant 3 electrons the 4f orbitals of Nd(III).

Table 1: Selected ligand bond distances for Yb-^{Dipp}ap and Yb-^{Dipp}isq complexes.

Compound	O-C	O-C2	**O-C avg**	N-C	N-C2	**N-C avg**
$Yb(ap)_2(K*18c6)$	1.342(3)	1.349(3)	**1.3455**	1.403(5)	1.398(5)	**1.4005**
$Yb(ap)_2(DMAP)_2$	1.341(8)	-	**1.341(8)**	1.393(6)	-	**1.393(6)**
$Yb(isq)_2(PFTet)$	1.289(5)	1.299(5)	**1.2940**	1.349(6)	1.349(6)	**1.349**
$Yb(isq)_2(pTolTet)$	1.286(3)	1.296(3)	**1.2895**	1.348(3)	1.344(3)	**1.346**

Investigating the crystal and bond distances of $Yb(N\text{-}ap)_2$ reveals that the initial ^{Dipp}ap ligands lose their planarity, but otherwise remain remarkably intact. Both ligands in the initial $Yb(ap)_2$ crown structure are reacted with consistently, with O-C bond distances of 1.32 Å and 1.31 Å, which falls almost exactly between the ^{Dipp}ap and ^{Dipp}isq bond distances. The conjugated C-C bond distances are consistent with both the ^{Dipp}ap bond distances found in the starting material, $Yb(ap)_2$ crown, as well as those of the aromatic carbon bonds in the diisopropyl aryl group on the ^{Dipp}ap nitrogen. The N-C bond distances, however, show some differences between the two inserted ligands, with N-C bond distances of 1.36 Å and 1.40 Å. The latter matches that of the single bonded N-C of the ^{Dipp}ap with the former being between that of the ^{Dipp}ap and ^{Dipp}isq ligands.

Despite their stark colors that change with reactivity, the UV-Vis of $Yb(ap)_2$ crown and its azide and DMAP products are featureless for most of the synthesized ytterbium compounds. This featuresless UV-Vis is indicative of a lack of charge transfer bands. With the copper bis(^{Dipp}ap) crown complex, the lone $d_{x^2-y^2}$ electron had no orbital into which to transfer within this energy range due to the orbitals spliting and closed shell nature of the amidophenolate ligands. Here, the lone 4f electron is unable to participate in charge transfer within this energy range due to the 4f orbitals lack of valence character and the clsoed shell nature of the amidophenolate ligands. The lack of valence character of the 4f orbitals of the lanthanides is known, and best exemplified by their extremely high redox potentials.[51]

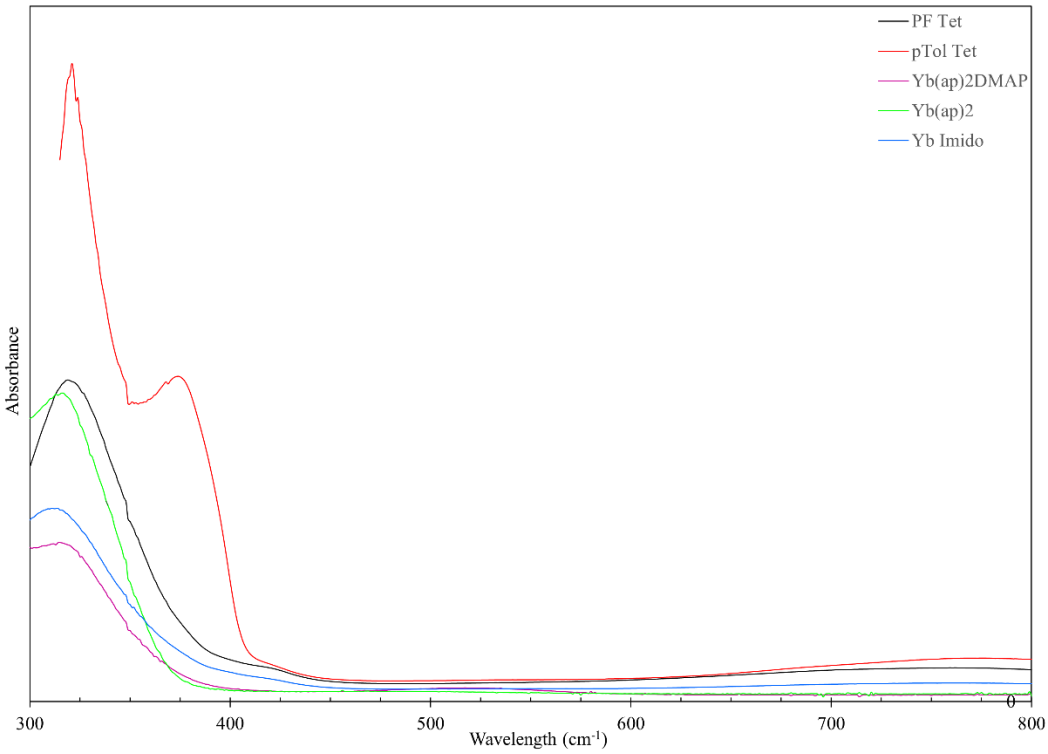

Figure 4: UV-Vis of the Yb ligand compounds.

Only $Yb(isq)_2(pTol\text{-}tet)$, has an absorbance above 350 nm with a peak at 374 nm. Absorbances of around 370 nm are most commonly associated with protein aromatic side groups, particularly tyrosine and its phenol at 375 nm, indicating the possible presence of ligand or imido inserted ligand impurity. [Yb(III) f-f- transitions at 900-1000 nm][55].

The character of the single unpaired 4f electron in Yb(III) was investigated via the magnetic susceptibility, μ_{eff}, of each compound. These were taken at room temperature following standard NMR methodology, the Evan's method.[52] Briefly, quantitative C_6D_6 solution of a compound with added ferrocene was take in a standard NMR tube in which was placed a sealed capillary external reference containing a C_6D_6 solution of ferrocene. The frequency shift (Hz) of ferrocene, $\Delta\nu$, caused by the paramagnetic Yb compound, can be used to calculate the mass susceptibility, χ_g ($\frac{cm^3}{g}$), using Equation 1[53] below:

$$\chi_{Molar} = \chi_g * M = \frac{3 * \Delta\upsilon}{4\pi * \upsilon * c} * M$$

where ν is the probe frequency (Hz) of the NMR, and c is the mass concentration ($\frac{g}{cm^3}$); this ignores solvent diamagnetism and the density correction since the concentration is under 10 mM.[53]

Multiplying the mass susceptibility by the molecular mass ($\frac{g}{mol}$) of the compound in solution, M, gives the molar susceptibility, χ_{Molar} ($\frac{cm^3}{mol}$),. Using Equations 2 and 3 allows for the calculation of the effective magnetic moment, μ_{eff}, from the molar susceptibility and accounting for the effect of paired electrons, via the diamagnetic correction, χ_D. This diamagnetic correction is unique to each system based on ligand and metal, and is here approximated with Equation 4[54] due to the redox non-innocent ligands themselves and the potential multiconfigurational oxidation state of these Yb(III) complexes of redox non-innocent ligands[44].

$$\mu_{eff} = 2.828\sqrt{(\chi_P T)}$$

$$\chi_P = \chi_{Molar} - \chi_D$$

$$\chi_D = -\frac{1}{2} MW * 10^{-6}$$

The predicted effective magnetic moment for Yb(III) is μ_{eff} = 4.5 μ_B.[55] The theoretical magnetic moments for a complex of Yb(III) spin coupled with an organic radical lies within the range of μ_{eff} = 3.4 - 5.6 μ_B, where a μ_{eff} = 3.4 μ_B is the theoretical spin of antiferromagnetically coupled spin and μ_{eff} = 5.6 μ_B being the theoretical magnetic moment of the ferromagnetically coupled spins.[55] Table 1 shows the effective magnetic moments for the compounds synthesized, which range from μ_{eff} = 3.95 - 4.93 μ_B. More, temperature dependent, data would be necessary to speculate about the prescence of a multiconfigurational ground state, i.e., intermediate valency where the ligand and metals orbitals are close in energy and therefore partially occupied and lowering of μ_{eff} at various temperatures, or redox isomerism, a temperature dependent charge transfer where the μ_{eff} abruptly changes at a particular temperature due to a larger gap in metal and ligand orbital energies.[42, 45, 56]

Table 2: Magnetic susceptibility and Evan's Method data

Compound	Δν (Hz)	χ_{Molar} ($10^3 \frac{cm^3}{mol}$)	μ_{eff} (μ_B)
$Yb(ap)_2$	54	6.01	3.95
$Yb(ap)_2$(DMAP)(THF)(K)	33	8.26	4.61
$Yb(isq)_2$(DMAP)(Imido)(K)	42	9.37	4.89
$Yb(isq)_2$(PFTet)	57	9.17	4.84
$Yb(isq)_2$(p tolTet)	54	9.51	4.93

The lower magnetic susceptibility of the bis(^{Dipp}ap) complex compared to the rest of the complexes synthesized, and that of the theoretical Yb(III) electron, suggests a antiferromagnetic

spin coupling. The consistent bond distances in the ^{Dipp}ap crystal structure that closely match those of the related neodymium complex, support a consistent Yb(III) oxidation state with two closed shell ligands and not a intervalence oxidation state. More data is required to speculate as to the reason behind the significantly (14%) lower μ_{eff} than theoretical. The magnetic susceptibility of Yb-^{Dipp}isq complexes fall within the range of 4.6-4.9 μ_B. Changes to the magnetic susceptibility seem dependent on the ligand bond angles, where a more planar O-Yb-O bond angle between the ^{Dipp}isq and ^{Dipp}ap ligands produces stronger ferromagnetic coupling, and the more acute O-Yb-O angle generating stronger antiferromagnetic coupling.

Table 3: Selected bond angles for Yb-^{Dipp}ap and Yb-^{Dipp}isq products.

	N_{ap}-Yb-N_{ap} angle	O_{ap}-Yb-O_{ap} angle
$Yb(ap)_2$ crown	170.91(9)	116.01(8)
$Yb(ap)_2$	166.0(2)	97.4(1)
$Yb(ap)_2(DMAP)_2$	176.3(2)	111.71(18)
$Yb(PF\text{-}tet)(isq)_2$	159.5(1)	92.4(1)
$Yb(pTol\text{-}tet)(isq)_2$	157.29(7)	85.30(6)

This implies the ligand-metal orbital overlap, dictated by geometry, is the major contributor to the Yb(III) coupling. This further supports the singular room temperature Yb(III) redox configuration of this system. As the ligands become more parallel, ^{Dipp}isq potentially couple more to each other, causing ferrocoupling with Yb(III), whereas the acute angle reduces intraligand coupling, producing stronger ferrocoupling.

Reactivities

To isolate a mono-imido kinetically, a frozen toluene solution of $Yb(ap)_2$ crown was a layered with 1 equivalent of PFN_3 in cold toluene, which was subsequently frozen with liquid nitrogen. These were then thawed at -94°C with a liquid nitrogen-acetone bath, with the initial red solution stable for 1.5 hours without reaction. Upon slight warming of solution, a color change to brown was observed and stable upon re-cooling to -94°C. The stabilized brown solution was stable stirring for over an hour, but upon further slight warming led to the completion of the tetrazene product with half of the starting material. No discernable difference by ^{1}H or ^{19}F NMR spectroscopy was observed between the reaction and one under normal conditions. The reaction was repeated with a controlled warming of a layered frozen solution of toluene from -89°C. Three layers of toluene were frozen in N_2(l) on top of each other with $Yb(ap)_2$ crown and PFN_3 dissolved in the bottom and top layer, respectively. The red solution was thawed at -89°C and stirred for an hour before being warmed to -84°C, stirring for a subsequent hour. Afterwards, the solution was

warmed to -78°C and then -72°C, each for an hour with no change in the red solution. Further warming to room temperature resulted in no visible change in reaction.

The stability of the Yb tetrazene compounds was investigated to determine the nature of the tetrazenes and to attempt to convert them into a mono or bis imido. Tetrazenes are frequently static metallocycles of transition metals, but have been known to be in equilibrium with an imide-azide complex.[47] Tetrazenes have also been shown to be redox active themselves.[47, 49] In light of this, the Yb tetrazenes were subjected to triphenylphosphine in an attempt to react with any metallocycle opened metallaazide-imide and alternatively with UV light as ruthenium tetrazenes have been shown to UV sensitive, reacting into bis imidos under UV irradiation.[48]

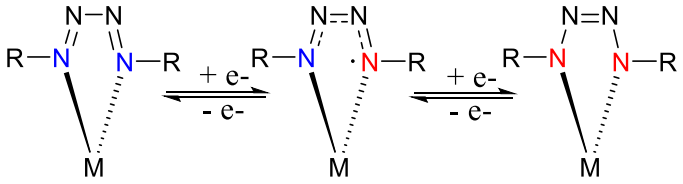

Figure 5: Potential electronic configurations for metal-tetrazene complexes.

$Yb(isq)_2$(pTol-tet) was found to have good thermal stability, with no visible change in ^1H NMR spectra after 20 hours at 75°C. Only after 48 hours at 90°C was full decomposition achieved, with only minor conversion to the arylazo. $Yb(isq)_2$(pTol-tet) was stable to UV light for over 18 hours at room temperature. The ytterbium tetrazene did react very slowly with PPh_3 in the presence of DMAP, added to stabilize any potential intermediate, with one new peak at -0.7 ppm in ^{31}P NMR spectroscopy. This did not match literature for pTolN=PPh_3, and the PPh3 remained largely unreactive so no further investigation was attempted.

It was noted that with rare earth imidos, particularly scandium, stable imido complexes could be formed using DMAP to induce sterically driven hydride abstraction between the scandium methyl and anilido, yielding the scandium DMAP imido and methane.[57] The tetrazene requires two open coordination spheres, initially occupied by two THF molecules in the starting material $Yb(ap)_2$ crown. An attempt to block those coordination spheres sterically could prevent the tetrazene formation, so the reactivity of $Yb(ap)_2$ crown was investigated with two consecutive equivalents of DMAP. Upon addition of one equivalent of DMAP, a room temperature red C_6D_6 solution of $Yb(ap)_2$ crown quickly turned orange as the DMAP slowly dissolved. ^1H NMR spectroscopic analysis of the crude product showed peak broadening of the DMAP protons, along with a small shifting of the starting material peaks, suggesting coordination with the paramagnetic

Yb. Another equivalent of DMAP was then added, turning the orange solution yellow, and showing an increase in the broadened DMAP peaks. To test the lability of the DMAP, one equivalent of PFN_3 was subsequently added at room temperature to the yellow, bis(DMAP) solution. After over an hour, conditions beyond which the azide would normally be fully consumed with $Yb(ap)_2$ crown, no color change was observed; both IR and ^{19}F NMR spectroscopy confirming the continued presence of the azide. With the hypothesis supported experimentally, the intermediate, mono DMAP product ($Yb(ap)_2(DMAP)$) was isolated and characterized for eventual reactivity with PFN_3.

A frozen solution of $Yb(ap)_2$ crown and DMAP in toluene was layered with a solution of PFN_3. The solutions were frozen before thawing and mixing at -35. The initial orange solution slowly turned dark green within 1.5 hours and let stir overnight. IR indicated the complete consumption of PFN_3, yielding a green solid upon solvent removal by hi-vac. The green compound was reacted at room temperature in toluene, as well as diethyl ether, with a second equivalent of PFN_3. The reaction slowly turned dark blue over two hours, producing $Yb(isq)_2$(PF-tet) as the major product and with pentafluoroaniline ($PFNH_2$) as a minor product within 16 hours of reaction, indicating the presence of the intermediate potential imido species. Attempts to synthesize a mixed tetrazene via addition of $pTolN_3$ to the green imido initially proved unsuccessful. The potential imido was unreactive to PPh3 in C_6D_6 at room temperature.

Interestingly, though, when the green solid, potential imido was later reacted with a second equivalent of PFN_3 in THF instead of toluene, in an attempt to more quickly and cleanly produce the tetrazene by DMAP exchange, $PFNH_2$ was the sole product by ^{19}F NMR spectroscopy with no indication of tetrazene formation by ^{1}H NMR spectroscopy. Lowering the temperature to -35°C yielded the same results, so the stability of the imido was tested in THF at room temperature overnight. The ^{19}F NMR spectra indicated the clean conversion of the potential DMAP imido to $PFNH_2$ in THF. The difference in reactivity between the imido in toluene and THF supports the necessity of the DMAP in stabilizing the compound: When it is removed via ligand exchange with THF the imido decomposes to the aniline before reacting with another equivalent of azide compared to the slow conversion to the tetrazene product. The initial inability to form a mixed imido with $pTolN_3$ is probably due to its reduced reactivity.

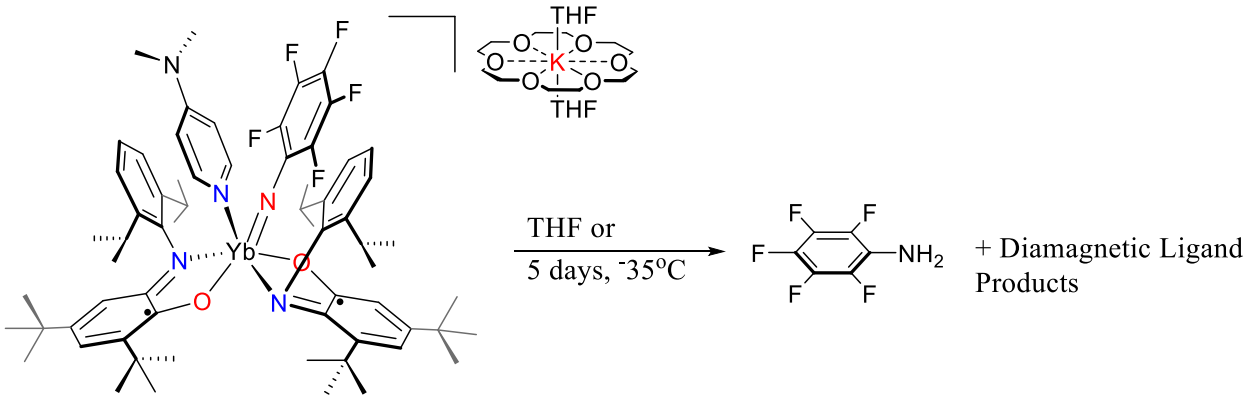

Figure 6: Decomposition pathways of Yb-imido complex.

Initial reactions to form the Yb(ptol-tet) formed small quantities of ligand inserted Yb(pTolNap)$_2$. Literature revealed this reaction was fairly unique, with only one similar reaction found, utilizing a copper oxide compound to insert ammonia into catechol, giving a 7 membered ring, cyclic N-acetyl acetamide in poor yield (48%) (Figure 7 below).[50] So, isolation of this product was attempted.

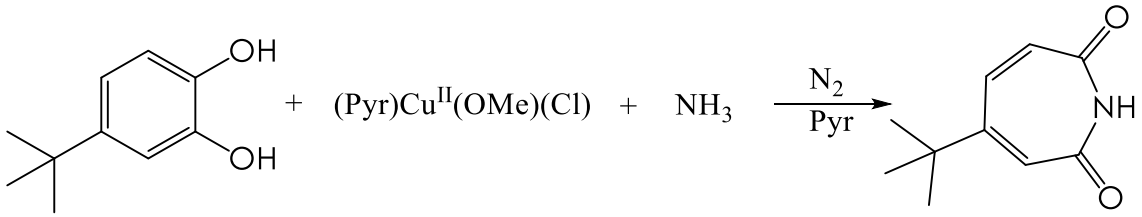

Figure 7: Catechol nitrogen ring insertion.

Unfortunately, the DMAP adduct was too unstable to yield crystals, decomposing as a pure solid at -35°C within days, and in solution even faster. With no efficient method to obtain all the desired characterization, a change of the DMAP was made, making use of lanthanide's high oxophilicity.[63] Two choices were chosen for ease of synthesis, with pyridine N-oxide and triphenylphosphine oxide used to replace DMAP in initial coordination to prevent tetrazene formation. Yb(ap)$_2$ was reacted with one equivalent of N or phosphine oxide then cooled to -35degC before azide addition. Upon reaction completion, the crude imidos showed acceptable crude stability as solids, so further studies were continued.

Conclusion

The first terminal ytterbium monoimido has been synthesized and characterized using redox non-innocent amidophenolate ligands. Initial reactivity with azides provided ytterbium tetrazene complexes that were remarkably stable to both heat and azide reactive conditions such

as UV light. This suggest the tetrazenes are fixed metallocycles with orbitals distant to the ^{Dipp}isq frontier molecular orbitals. Steric hinderance through DMAP coordination prohibited the formation of the tetrazene and facilitated the synthesis of the monoimido. The decomposition pathway of the imido, along with minor products produced in the tetrazene synthesis suggest the imido inserts into the ligand, producing a 7-membered ring structure for a unique synthetic route to this organic product.

1. Murugesu, M.; Schelter, E. J., Not Just Lewis Acids: Preface for the Forum on New Trends and Applications for Lanthanides. *Inorganic Chemistry* **2016,** *55* (20), 9951-9953.
2. Macdonald, M. R.; Bates, J. E.; Ziller, J. W.; Furche, F.; Evans, W. J., Completing the Series of +2 Ions for the Lanthanide Elements: Synthesis of Molecular Complexes of Pr2+, Gd2+, Tb2+, and Lu2+. *Journal of the American Chemical Society* **2013,** *135* (26), 9857-9868.
3. Fedushkin, I. L.; Yambulatov, D. S.; Skatova, A. A.; Baranov, E. V.; Demeshko, S.; Bogomyakov, A. S.; Ovcharenko, V. I.; Zueva, E. M., Ytterbium and Europium Complexes of Redox-Active Ligands: Searching for Redox Isomerism. *Inorganic Chemistry* **2017,** *56* (16), 9825-9833.
4. Fedushkin, I. L.; Maslova, O. V.; Morozov, A. G.; Dechert, S.; Demeshko, S.; Meyer, F., Genuine Redox Isomerism in a Rare-Earth-Metal Complex. *Angewandte Chemie International Edition* **2012,** *51* (42), 10584-10587.
5. Halbach, R. L.; Nocton, G.; Amaro-Estrada, J. I.; Maron, L.; Booth, C. H.; Andersen, R. A., Understanding the Multiconfigurational Ground and Excited States in Lanthanide Tetrakis Bipyridine Complexes from Experimental and CASSCF Computational Studies. *Inorganic Chemistry* **2019,** *58* (18), 12083-12098.
6. Booth, C. H.; Walter, M. D.; Kazhdan, D.; Hu, Y.-J.; Lukens, W. W.; Bauer, E. D.; Maron, L.; Eisenstein, O.; Andersen, R. A., Decamethylytterbocene Complexes of Bipyridines and Diazabutadienes: Multiconfigurational Ground States and Open-Shell Singlet Formation. *Journal of the American Chemical Society* **2009,** *131* (18), 6480-6491.
7. Coughlin, E. J. Facilitating Multi-Electron Chemsitry in the F-Block Using Iminoquinone Ligands. PhD. Dissertation, Purdue University, West Lafayette, 2019.
8. Coughlin, E. J.; Zeller, M.; Bart, S. C., Neodymium(III) Complexes Capable of Multi-Electron Redox Chemistry. *Angewandte Chemie International Edition* **2017,** *56* (40), 12142-12145.
9. Aldrich, K. E.; Odom, A. L., A photochemical route to a square planar, ruthenium(iv)-bis(imide). *Chemical Communications* **2019,** *55* (30), 4403-4406.
10. Yousif, M.; Wannipurage, D.; Huizenga, C. D.; Washnock-Schmid, E.; Peraino, N. J.; Ozarowski, A.; Stoian, S. A.; Lord, R. L.; Groysman, S., Catalytic Nitrene Homocoupling by an Iron(II) Bis(alkoxide) Complex: Bulking Up the Alkoxide Enables a Wider Range of Substrates and Provides Insight into the Reaction Mechanism. *Inorganic Chemistry* **2018,** *57* (15), 9425-9438.
11. Ng, W.-M.; Guo, X.; Cheung, W.-M.; So, Y.-M.; Chong, M.-C.; Sung, H. H. Y.; Williams, I. D.; Lin, Z.; Leung, W.-H., 4-Coordinated, 14-electron ruthenium(ii) chalcogenolate complexes: synthesis, electronic structure and reactions with PhICl2 and organic azides. *Dalton Transactions* **2019,** *48* (35), 13315-13325.
12. Lu, E.; Chu, J.; Chen, Y., Scandium Terminal Imido Chemistry. *Accounts of Chemical Research* **2018,** *51* (2), 557-566.
13. *CRC Handbook of Chemistry and Physics*. 87th ed.; CRC Press: Boca Raton, FL, 2006.
14. Schultz, M.; Boncella, J. M.; Berg, D. J.; Tilley, T. D.; Andersen, R. A., Coordination of 2,2‘-Bipyridyl and 1,10-Phenanthroline to Substituted Ytterbocenes: An Experimental Investigation of Spin Coupling in Lanthanide Complexes. *Organometallics* **2002,** *21* (3), 460-472.
15. Evans, D. F., 400. The determination of the paramagnetic susceptibility of substances in solution by nuclear magnetic resonance. *Journal of the Chemical Society (Resumed)* **1959**, 2003.
16. Bera, P.; Brandão, P.; Mondal, G.; Jana, H.; Jana, A.; Santra, A.; Bera, P., Synthesis of a new pyridinyl thiazole ligand with hydrazone moiety and its cobalt(III) complex: X-ray crystallography, in vitro evaluation of antibacterial activity. *Polyhedron* **2017,** *134*, 230-237.

17. Bain, G. A.; Berry, J. F., Diamagnetic Corrections and Pascal's Constants. *Journal of Chemical Education* **2008,** *85* (4), 532.
18. Lukens, W. W.; Magnani, N.; Booth, C. H., Application of the Hubbard Model to Cp*2Yb(bipy), a Model System for Strong Exchange Coupling in Lanthanide Systems. *Inorganic Chemistry* **2012,** *51* (19), 10105-10110.
19. Vaddypally, S.; McKendry, I. G.; Tomlinson, W.; Hooper, J. P.; Zdilla, M. J., Electronic Structure of Manganese Complexes of the Redox-Non-innocent Tetrazene Ligand and Evidence for the Metal-Azide/Imido Cycloaddition Intermediate. *Chemistry - A European Journal* **2016,** *22* (30), 10548-10557.
20. Hakey, B. M.; Darmon, J. M.; Akhmedov, N. G.; Petersen, J. L.; Milsmann, C., Reactivity of Pyridine Dipyrrolide Iron(II) Complexes with Organic Azides: C–H Amination and Iron Tetrazene Formation. *Inorganic Chemistry* **2019,** *58* (16), 11028-11042.
21. Demmin, T. R.; Swerdloff, M. D.; Rogic, M. M., Copper(II)-induced oxidations of aromatic substrates: catalytic conversion of catechols to o-benzoquinones. Copper phenoxides as intermediates in the oxidation of phenol, and a single-step conversion of phenol, ammonia, and oxygen into muconic acid mononi. *Journal of the American Chemical Society* **1981,** *103* (19), 5795-5804.
22. Kepp, K. P., A Quantitative Scale of Oxophilicity and Thiophilicity. *Inorganic Chemistry* **2016,** *55* (18), 9461-9470.